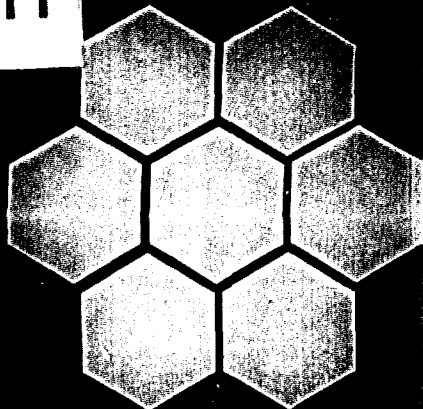


AD-A232 911



Materials Research Center  
Lehigh University

**DTIC FILE COPY**

FINAL REPORT

AFOSR-TR- 91 0164

2

**STRENGTH AND TOUGHNESS OF TAILORED CERAMIC MICROSTRUCTURES**

by

Professors M.P. Harmer (PI), H.M. Chan (Co-PI), G.A. Miller (Co-PI)

and graduate students J.D. French, C.J. Russo, M. Stuart, and N. Padture

sponsored by

U.S. Air Force - Office of Scientific Research,

contract number AFOSR-87-0396

Report Period: September 1, 1987 - October 31, 1990

**DTIC**  
**ELECTE**  
**MAR 13 1991**  
**S B D**

**DISTRIBUTION STATEMENT A**

Approved for public release;  
Distribution Unlimited

91 3 11 110

## REPORT DOCUMENTATION PAGE

Form Approved  
OMB No. 0704-0188

1a. REPORT SECURITY CLASSIFICATION <b>Unclassified</b>			1b. RESTRICTIVE MARKINGS		
2a. SECURITY CLASSIFICATION AUTHORITY			3. DISTRIBUTION/AVAILABILITY OF REPORT Approved for public release; distribution is unlimited.		
2b. DECLASSIFICATION/DOWNGRADING SCHEDULE					
4. PERFORMING ORGANIZATION REPORT NUMBER(S)			5. MONITORING ORGANIZATION REPORT NUMBER(S)		
6a. NAME OF PERFORMING ORGANIZATION <b>Lehigh University</b>		6b. OFFICE SYMBOL (if applicable)	7a. NAME OF MONITORING ORGANIZATION <b>Same as 89</b>		
6c. ADDRESS (City, State, and ZIP Code) <b>Materials Research Center Bethlehem, PA 18015</b>			7b. ADDRESS (City, State, and ZIP Code) <b>Same as 8c</b>		
8a. NAME OF FUNDING/SPONSORING ORGANIZATION <b>Air Force Office of Scientific Research</b>		8b. OFFICE SYMBOL (if applicable) <b>NE</b>	9. PROCUREMENT INSTRUMENT IDENTIFICATION NUMBER <b>AFOSR-87-0396</b>		
8c. ADDRESS (City, State, and ZIP Code) <b>Bolling Air Force Base Washington, DC 20322-6448</b>			10. SOURCE OF FUNDING NUMBERS		
			PROGRAM ELEMENT NO. <b>61102F</b>	PROJECT NO. <b>2306</b>	TASK NO. <b>A2</b>
11. TITLE (Include Security Classification) <b>Strength and Toughness of Tailored Ceramic Microstructures</b>					
12. PERSONAL AUTHOR(S) <b>Professors M.P. Harmer, H.M. Chan, and Gary A. Miller</b>					
13a. TYPE OF REPORT <b>Final</b>		13b. TIME COVERED FROM <b>9/1/87</b> TO <b>10/31/90</b>		14. DATE OF REPORT (Year, Month, Day) <b>December 30, 1990</b>	
15. PAGE COUNT					
16. SUPPLEMENTARY NOTATION					
17. COSATI CODES			18. SUBJECT TERMS (Continue on reverse if necessary and identify by block number)		
FIELD	GROUP	SUB-GROUP			
19. ABSTRACT (Continue on reverse if necessary and identify by block number)  <b>See separate sheet.</b>					
20. DISTRIBUTION/AVAILABILITY OF ABSTRACT <input type="checkbox"/> UNCLASSIFIED/UNLIMITED <input type="checkbox"/> SAME AS RPT. <input type="checkbox"/> DTIC USERS			21. ABSTRACT SECURITY CLASSIFICATION		
22a. NAME OF RESPONSIBLE INDIVIDUAL <b>S. Chatter</b>			22b. TELEPHONE (Include Area Code) <b>202-767-4433</b>		22c. OFFICE SYMBOL <b>NE</b>

UNCLASSIFIED

## ABSTRACT

AFOSR project 87-0396 was undertaken to develop a detailed understanding of the link between microstructural variables and the strength and toughness of ceramic materials. A major emphasis of this effort has been developing approaches for producing multiphase ceramic microstructures with enhanced reliability i.e. elevated temperature microstructural stability and damage tolerance and/or room temperature flaw tolerance.

Improvements in elevated temperature damage tolerance depend upon having a dual phase interconnected microstructure with more than 16 volume percent second phase. Our findings show that adding cubic zirconia to alumina improves damage tolerance in that  $\text{Al}_2\text{O}_3$  with 50% c- $\text{ZrO}_2$  (AZ50) shows the same hardness yet appreciably less indentation damage than alumina at 1200°C and is very resistant to grain coarsening for up to 100 hours at 1650°C. Also,  $\text{Al}_2\text{O}_3$  with 50% YAG (AY50) has twice the hardness of  $\text{Al}_2\text{O}_3$  at 1200°C. Future experiments will assess creep and stress rupture properties of these and other interconnected dual phase ceramics.

Improvements in room temperature flaw tolerance depend upon having a controlled inhomogeneous dual phase microstructure with phases of different thermal expansion coefficients. The thermal expansion mismatch promotes toughening by enhancing grain bridging at the sites of the inhomogeneity. Our findings show that adding  $\text{Al}_2\text{O}_3$  spray-dried agglomerates to homogeneous  $\text{Al}_2\text{O}_3/\text{Al}_2\text{TiO}_5$  or  $\text{Al}_2\text{O}_3/\text{c-ZrO}_2$  fine powders, and/or tape casting of alternating layers (35 microns thick) of  $\text{Al}_2\text{O}_3/\text{Al}_2\text{TiO}_5$  and undoped alumina enhances flaw tolerance considerably. Also, novel tape-cast trilaminate composites with strong outer layers and flaw tolerant interiors have been designed to optimize the dependence of strength on flaw size.

## CONTENTS

### Abstract

#### 1. Technical Report

- 1.1 Coarsening-Resistant Dual-Phase Interpenetrating Microstructures
- 1.2 Creep Resistant Fine Grained Monolithic Ceramics
- 1.3 Coarsening Resistance, Hot Hardness and Indentation Creep of  $\text{Al}_2\text{O}_3\text{:c-ZrO}_2$  and  $\text{Al}_2\text{O}_3\text{:YAG}$
- 1.4 Mechanical Properties and Grain Growth Inhibition in the System  $\text{Al}_2\text{O}_3\text{:c-ZrO}_2$
- 1.5 Mechanical Properties of Interpenetrating Microstructures: the  $\text{Al}_2\text{O}_3\text{:c-ZrO}_2$  System
- 1.6 Mechanical Behavior of the Alumina - Mullite System
- 1.7 Controlled Microstructural Inhomogeneity for Improved Flaw Tolerance
- 1.8 Flaw Tolerant  $\text{Al}_2\text{O}_3\text{-Al}_2\text{TiO}_5$  Composites
- 1.9 Optimization of Strength and Toughness Using Laminates
- 1.10 Influence of Grain Size and Degree of Crystallization of Intergranular Glassy Phase on the Mechanical Behavior of a Debased Alumina
- 1.11 Microstructural Evolution and Mechanical Properties in Dual-Phase, Interpenetrating Ceramic Microstructures: the  $\text{Al}_2\text{O}_3\text{:c-ZrO}_2$  System

#### 2. Publications and Presentations

#### 3. Awards and Accomplishments

#### 4. Personnel

Accession For	
NTIS GRA&I	<input checked="checked" type="checkbox"/>
DTIC TAB	<input type="checkbox"/>
Unannounced	<input type="checkbox"/>
Justification	
By _____	
Distribution/	
Availability Codes	
Dist	Avail and/or Special
A-1	



**COARSENING-RESISTANT DUAL-PHASE INTERPENETRATING  
MICROSTRUCTURES**

**J.D. French, M.P. Harmer, H.M. Chan, and G.A. Miller**

**Department of Materials Science and Engineering  
and the Materials Research Center  
Lehigh University, Bethlehem, PA 18015 USA**

**Published in the Journal of the American Ceramic Society 73[8] 2508, 1990**

## Coarsening-Resistant Dual-Phase Interpenetrating Microstructures

Jonathan D. French, Martin P. Harmer, Helen M. Chan and Gary A. Miller, Department of Materials Science and Engineering and The Materials Research Center, Lehigh University, Bethlehem, PA 18015.

### **Abstract**

Grain growth in a 50:50 (volume percent) dual phase mixture of  $\text{Al}_2\text{O}_3$  and c- $\text{ZrO}_2$  (cubic zirconia) is severely limited compared to that for either of the single phases. At 1650°C, the growth rate in the duplex composition was 160, and 3500 times lower than for single phase  $\text{Al}_2\text{O}_3$  and c- $\text{ZrO}_2$ , respectively. The restriction of the grain growth is attributed to the limited mutual solubility, and the physical constraint provided by the interpenetrating geometry of the two phases. Grain coordination number and dihedral angle are also considered as factors affecting grain stabilization in two-phase systems. A potentially important practical application of this work is the fabrication of grain-stabilized fibers for use as reinforcement in composite structures at elevated temperatures.

### **Introduction**

Conventionally, grain growth is controlled with the use of either solid solution or second phase additives. Solid solution additives can be very effective but they have limited applicability in that they are system specific<sup>1,2</sup> The use of second phase particles is also effective, however, particle mobility, particle-boundary unpinning and coarsening by Ostwald ripening can limit the usefulness of this approach<sup>3</sup> In both cases, homogeneity of the additive distribution is critical

for the prevention of abnormal grain growth<sup>2,3</sup>

An alternate method of restraining grain growth for the production of fine-grained ceramics is through the development of dual/multi-phase interpenetrating microstructures. By intimately mixing two (or more) phases with limited solid solubility the growth of the individual phases is inhibited since long range interdiffusion is limited. Interpenetrating phase mixtures have been used in the metals field for many years to develop microstructures suitable for superplastic forming of aluminum, copper and titanium alloys and duplex stainless steels<sup>4</sup>. However, there has been little exploitation of this effect for ceramic systems.

The ceramic system  $\text{Al}_2\text{O}_3$ :c- $\text{ZrO}_2$  is ideally suited for testing the grain growth limiting potential because it meets the criterion of limited mutual solubility. It should be noted that although limited work has been carried out with the 50:50 composition<sup>5</sup>, particle pinning has been clearly demonstrated in alumina-rich and zirconia-rich  $\text{Al}_2\text{O}_3$ - $\text{ZrO}_2$  composites<sup>6,7</sup>.

#### Experimental Procedure

High purity powders of  $\text{Al}_2\text{O}_3$ <sup>\*</sup> and c- $\text{ZrO}_2$ <sup>®</sup> (8 mol%  $\text{Y}_2\text{O}_3$ ) were mixed in equal portions (by volume) in 200-proof ethanol and ball milled for 16 hours. After milling, the slurry was magnetically stirred during drying to prevent differential settling. The dried cake was then crushed in a polyethylene bag with a rolling pin. Pellets were uniaxially pressed in a cylindrical die using a pressure of 55 MPa, then isostatically pressed at 350 MPa. The

<sup>\*</sup>Sumitomo AKP-HP, Osaka, Japan. <sup>®</sup>Tosoh 8Y  $\text{ZrO}_2$ , Japan.

pellets were calcined at 1000°C for 16 hours, then sintered at 1650°C for times ranging from 15 minutes to 100 hours. Pellets of single phase  $\text{Al}_2\text{O}_3$  and c- $\text{ZrO}_2$  were also prepared under similar conditions. All powder processing was performed in a clean-room environment to prevent contamination from impurities which could form liquid phases.

Cross-sections of each pellet were polished using standard metallographic techniques, and thermally etched at 1450°C for 90 minutes. Scanning electron microscopy (SEM) was used to observe the microstructures. Grain size was measured using a lineal intercept technique for the undoped samples. For the duplex specimens, the method developed by Wurst and Nelson<sup>8</sup> was adapted for measuring the individual grain sizes of the two phases.

## Results and Discussion

The grain growth data for the undoped  $\text{Al}_2\text{O}_3$ , undoped c- $\text{ZrO}_2$ , and both phases in the 50-50 composition (AZ50) can be seen in Figure 1. Note the severely limited growth, even after 100 hours at 1650°C, in the AZ50 composition. Typical microstructures can be seen in Figures 2a-c. The grain growth kinetics depicted in Figure 1 were analyzed in terms of the relation  $G^n - G_0^n = Kt$ , where  $G$  is the grain size at time  $t$ ,  $n$  is the grain growth kinetic exponent,  $G_0$  is the grain size after a short sintering time (defined as  $t = 0$ ), and  $K$  is a constant. Integer values for  $n$  ranging from 2 to 6 resulted in linear regressions which accounted for 90 to 99+ percent of the variation. In other words, any exponent in this range could be used to describe the



coarsening behavior and would provide a reasonable fit to the experimental data. With this in mind, the value of 3 was chosen for  $n$  to provide a comparison with published data for other additives.

K-values for the single phase compositions and both phases in the composite were:

	Phase	$(K \times 10^{23}), \text{ m}^3/\text{s}$	$(\text{Correlation Coefficient})^2$
single phase	$\text{Al}_2\text{O}_3$	1200	.943
	c- $\text{ZrO}_2$	27000	.984
AZ50	$\text{Al}_2\text{O}_3$	7.3	.938
	c- $\text{ZrO}_2$	7.6	.943

The limited grain growth of the AZ50 is attributed to the limited solid solubility, the increased diffusion path length relative to the single phases and the physical constraint of the two phases.<sup>9</sup> Since the two phases form two interpenetrating three-dimensional networks, it is expected that the grain growth of one phase will be coupled to that of the other. As a result, the coarsening rate of the slower phase will be rate-limiting.

At low volume fractions of an isolated second phase, particles can coarsen by coalescence as they are dragged by moving grain boundaries (assuming mobile particles). Another particle coarsening mechanism for low volume fractions of particles is Ostwald ripening, where large particles grow at the expense of small ones. If we consider, for example, the coarsening of precipitates of phase B in a matrix of phase A, then the driving force for Ostwald ripening is the reduction in the A/B interfacial area:<sup>10</sup>

$$d\bar{r}/dt = (D \gamma_{AB} V_m S / 2RT\bar{r}^2)$$

where  $d\bar{r}/dt$  is the precipitate coarsening rate,  $D$  is the bulk

diffusivity of B in A,  $\gamma_{AB}$  is the interfacial energy of an A/B interface,  $V_m$  is the molar volume of precipitates,  $S$  is the solubility of B in A,  $\bar{r}$  is the mean precipitate radius and  $T$  is the absolute temperature. Thus, coarsening is slow in systems which have relatively low values of  $\gamma_{AB}$ ,  $S$  and  $D$ .

At high volume fractions, such as AZ50, dragging of particles by moving boundaries is not likely to be so important. Due to the limited solubility of the phases, it is likely that grain boundary and interphase boundary diffusion will be controlling. Due to the high connectivity of each phase in AZ50, it is postulated that coarsening occurs mainly by diffusion of species along interphase boundaries, rather than grain boundaries.

It is important to note that for any two-phase system, the quantities  $\gamma_{AB}$  and  $D_{AB}$  (diffusivity along the interphase boundary) may be strongly interdependent. For example, in metallic systems, it has been shown that the diffusion coefficient of a species along an interphase boundary depends on the orientation difference across the boundary<sup>11</sup>, and hence the value of the boundary energy. Although the authors are unaware of similar detailed studies in ceramic systems, it is reasonable to suppose that boundaries having very low interfacial energies will exhibit good lattice matching, and will be poor diffusion paths.

At high volume fraction of second phase and/or large particle size it becomes important to consider the effects of dihedral angle and grain coordination number on the driving force for

coarsening.<sup>12</sup> For a given dihedral angle, particles with low coordination numbers have boundaries which are convex (see Figure 3, Case I). For a distribution of particle sizes, there is a net driving force for second phase atoms to move away from the smaller particles towards the larger ones (classic Ostwald ripening). At higher coordination numbers however, the tendency is for the boundary curvature to be concave and the driving force is reversed (see Figure 3, Case II). Matter would thus tend to move away from the larger particles and coarsen the smaller ones. Higher dihedral angles will tend to promote Case I, while low dihedral angles will promote case II. In this regard, the high coordination number promotes a self-stabilized microstructure.

It should be noted that because of residual porosity, the experimental conditions do not represent an ideal situation for model studies of grain growth. However, they do provide a quantitative basis for comparison of the presence of an interpenetrating second phase with the effect of other additives. For example, 250 ppm MgO lowered K for  $\text{Al}_2\text{O}_3$  by a factor of 50 at  $1600^\circ\text{C}$ .<sup>13</sup> In the present case for the AZ50 composite, K-values for  $\text{Al}_2\text{O}_3$  and c- $\text{ZrO}_2$  were reduced by factors of 160 and 3500, respectively at  $1650^\circ\text{C}$ . The results presented are consistent with previous experiments<sup>6,7</sup> in the  $\text{Al}_2\text{O}_3$ :c- $\text{ZrO}_2$  system which demonstrate that grain growth restraint increases with volume fraction of second phase. Specifically, previous work<sup>7</sup> showed that 20 volume percent  $\text{Al}_2\text{O}_3$  reduced the final grain size of c- $\text{ZrO}_2$ , after 2 hours at  $1650^\circ\text{C}$ , from 11 to 3  $\mu\text{m}$ . In the present case, for the same thermal treatment, 50 volume percent  $\text{Al}_2\text{O}_3$

decreased the c-ZrO<sub>2</sub> grain size from 13 to 1.4 μm. A direct comparison with previous results<sup>6</sup> for zirconia inclusions in alumina is not possible because the grain size of undoped alumina in the present study is significantly larger than that reported by Lange and Hirlinger<sup>6</sup> for a given thermal treatment. Finally, it would be useful to have a theoretical treatment of the relation between matrix grain size, time, temperature and volume fraction of second phase. Many analyses of particulate restraint of grain growth have been made.<sup>14</sup> However, these analyses typically involve low volume fractions of non-interacting (isolated) second phase particles. For AZ50, the conditions are vastly different, with large second phase particles filling 3- and 4-grain junctions, occupying whole grain edges and forming a continuous network. What is needed is a model capable of describing grain growth under these conditions. Such a model must properly account for the interaction of the interpenetrating phases, grain coordination and dihedral angle and might best be developed using computer simulation.<sup>14</sup>

The data presented in this communication represent part of a larger study of the system (1-x)Al<sub>2</sub>O<sub>3</sub>:(x)c-ZrO<sub>2</sub>. Preliminary results have shown the room temperature strength and toughness to follow a rule-of-mixtures of the single phases. The grain growth kinetics and the room and elevated temperature mechanical properties of other compositions in this system are currently being evaluated.

#### Acknowledgment

Financial support for this work was provided by the United

States Air Force Office of Scientific Research, Ceramics Program, under contract number AFOSR-87-0396. Also, helpful and stimulating discussions with W. Gust and F. Lange are gratefully acknowledged.

#### References

1. M. P. Harmer, "Use of Solid-Solution Additives in Ceramic Processing", Advances in Ceramics, Vol. 10, American Ceramic Society, Columbus OH, 1985, pp. 679 - 696.
2. J. E. Blendell and C. A. Handwerker, "Effect of Chemical Composition on Sintering of Ceramics", J. Cryst. Growth. 75 pp. 138 - 160 (1986).
3. B. Kibbel and A. H. Heuer, "Exaggerated Grain Growth in  $ZrO_2$ -Toughened  $Al_2O_3$ ", J. Am. Ceram. Soc., 69[3] 231-236 (1986)
4. J. Pilling and N. Ridley, Superplasticity in Crystalline Solids, The Institute of Metals, London, 1989, pp. 8 - 47.
5. F. J. Esper, K. H. Friese and H. Grier, "Mechanical, Thermal and Electrical Properties in the System of Stabilized  $ZrO_2(Y_2O_3)/\alpha-Al_2O_3$ ". Advances in Ceramics, Vol. 12, "The Science and Technology of Zirconia II", edited by N. Claussen, M. Ruhle and A. Heuer, American Ceramic Society, Columbus, OH (1984) pp. 528 - 536.
6. F. F. Lange and M. M. Hirlinger, "Hindrance of Grain Growth in  $Al_2O_3$  by  $ZrO_2$  Inclusions", J. Am. Ceram. Soc., 70[8] 243 - 249 (1987).
7. F. F. Lange and M. M. Hirlinger, "Grain Growth in Two-Phase Ceramics:  $Al_2O_3$  Inclusions in  $ZrO_2$ ", J. Am. Ceram. Soc., 70[11] 827-30 (1987).
8. J. C. Wurst and J. A. Nelson, "Lineal Intercept Technique for Measuring Grain Size in Two-Phase Polycrystalline Ceramics", J. Am. Ceram. Soc., 55[2] 109 (1972).
9. J. W. Cahn, "A Model for Connectivity in Multiphase Structures", Acta Met. 14 (1966) 477 - 480.
10. J. W. Martin and R. D. Doherty, Stability of Microstructure in Metallic Systems, Cambridge University Press, London, 1976, pp. 173-210.
11. B. B. Straumal, B. S. Bokstein, L. M. Klinger and L. S. Shvindlerman, "Indium Diffusion along Interphase Twist

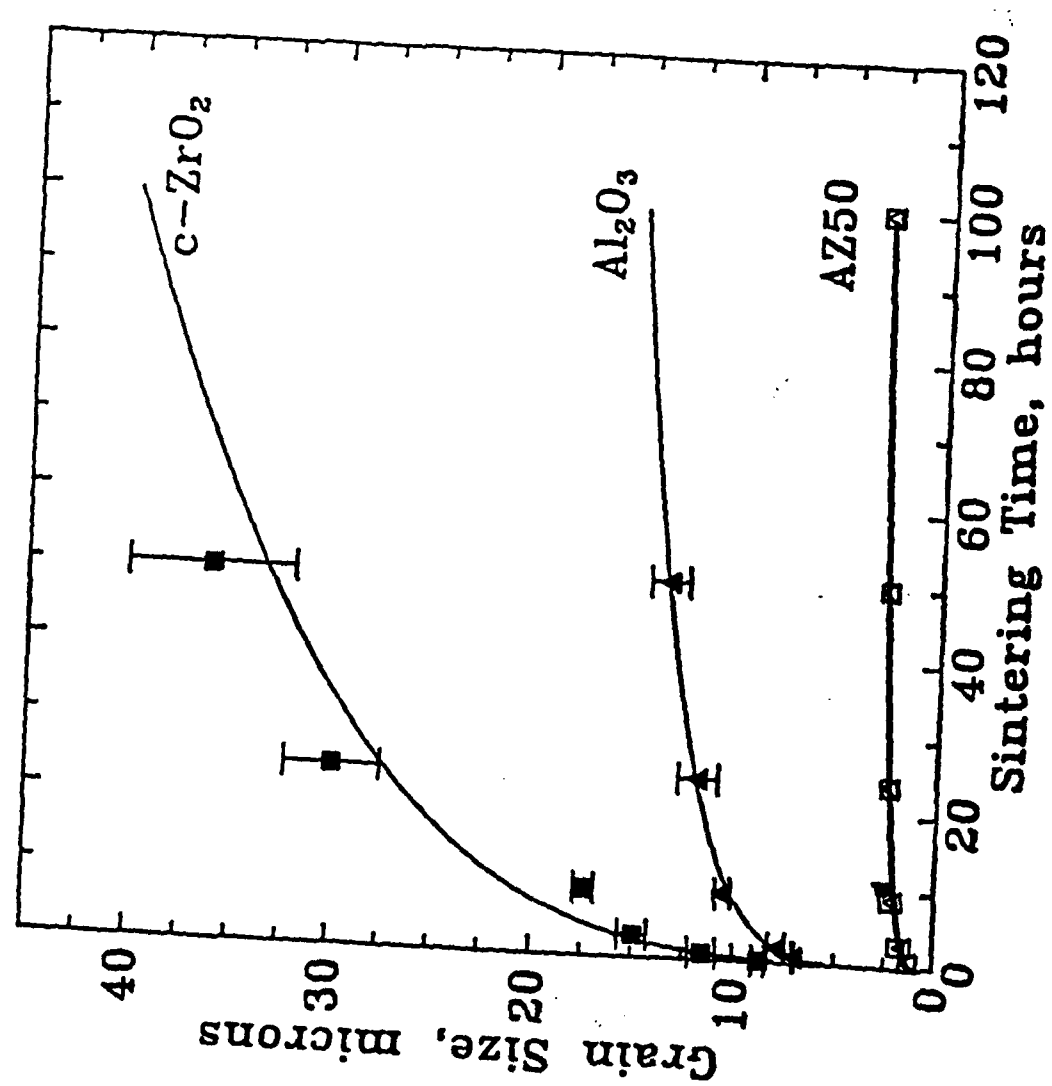
Boundaries Sn-Ge", Scripta Met., 15[11] 1197-1200 (1981).

12. W. D. Kingery and B. Francois, "Sintering of Crystalline oxides, I. Interactions Between Grain Boundaries and Pores"; pp. 471-98 in Sintering and Related Phenomena. Edited by G. C. Kuczynski, N. A. Hooton, and G. F. Gibbon. Gordon Breach, New York, 1967.
13. S. J. Bennison and M. P. Harmer, "Grain-Growth Kinetics for Alumina in the Absence of a Liquid Phase", J. Am. Ceram. Soc., 68[1] C22 - C24 (1985).
14. D. J. Srolovitz, M. P. Anderson, G. S. Grest and P. S. Sahni, "Computer Simulation of Grain Growth-III. Influence of a Particle Dispersion", Acta Met., 32 (1984) 1429-1438.

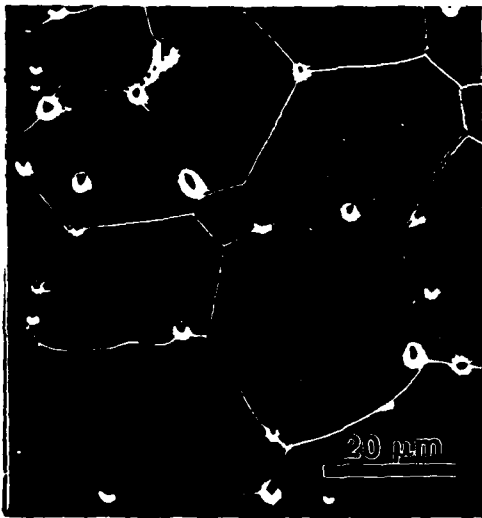
Figure 1. Dependence of average grain size on sintering time at 1650°C for single phase  $c\text{-ZrO}_2$  (■), single phase  $\text{Al}_2\text{O}_3$  (▲), and AZ50 -  $\text{Al}_2\text{O}_3$  (Δ) and  $c\text{-ZrO}_2$  (□).

Figure 2. Typical microstructures, after 24 hours at 1650°C, of (a) single phase  $c\text{-ZrO}_2$ , (b) single phase  $\text{Al}_2\text{O}_3$  and (c) AZ50 -  $\text{Al}_2\text{O}_3$ . The dark phase is  $\text{Al}_2\text{O}_3$ .

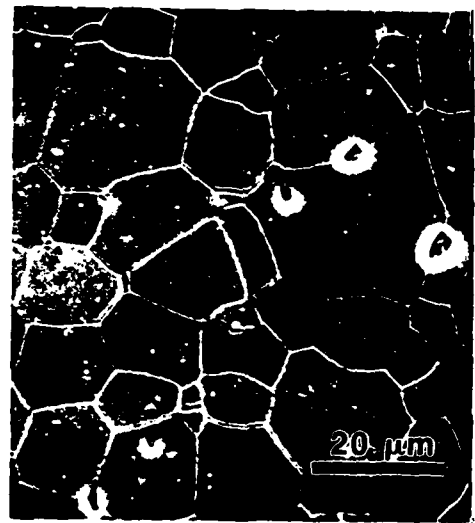
Figure 1.



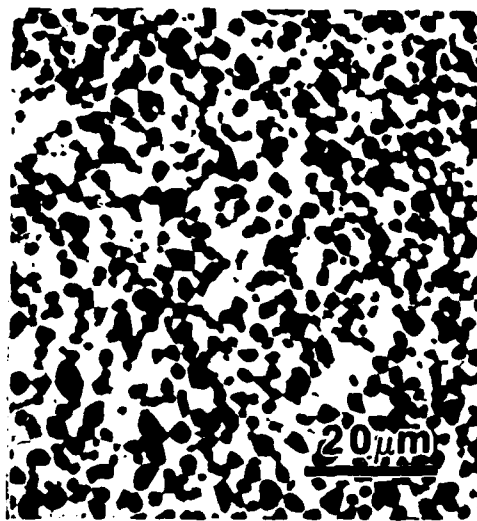




(a)

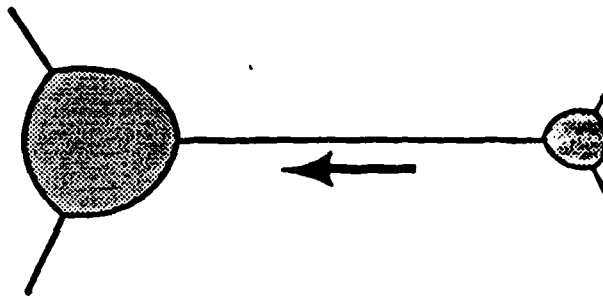


(b)

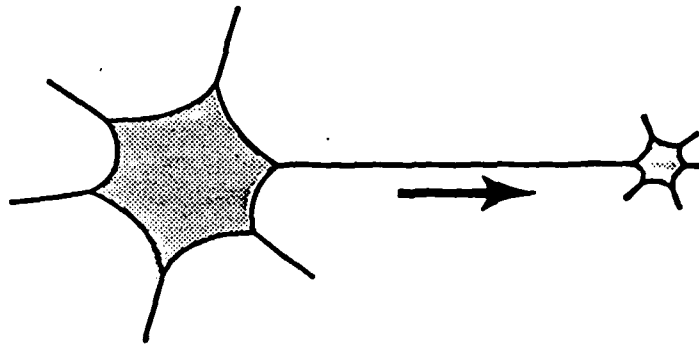


(c)

Figure 2.



Case I. Low coordination number



Case II. High coordination number

Figure 3. Illustration of the effect of grain coordination number on the driving force for coarsening.

**CREEP RESISTANT FINE GRAINED MONOLITHIC CERAMICS**

**Department of Materials Science and Engineering  
Lehigh University, Bethlehem, PA 18015 USA**

**To be published in the 1990 volume of Air Force Office  
of Scientific Research Accomplishments**

## ACCOMPLISHMENT

### CREEP RESISTANT FINE GRAINED MONOLITHIC CERAMICS

One of the main problems with the use of monolithic ceramic materials in advanced aerospace applications at elevated temperatures ( $T > 1200^{\circ}\text{C}$ ) is the degradation of mechanical properties. This is due to grain growth, where each individual particle making up the material enlarges after time at temperature. (Strength is inversely proportional to flaw size, which is usually related to the grain size, thus fine grained materials are stronger, in general, than coarse grained materials.) Another problem at high temperature, "creep", where the material will plastically deform under an applied load, can be especially severe in fine grained, stronger materials. Researchers at Lehigh University have developed a composition of 50% alumina - 50% cubic zirconia, which they call "AZ50", that exhibits essentially no grain growth after 100 hours at  $1650^{\circ}\text{C}$ , while the alumina and cubic zirconia grain size increased by a factor of 10 and 40, respectively (See Figure 1). The AZ50 composition retains its strength after 100 hours at  $1650^{\circ}\text{C}$ , while the strength of alumina degrades by 30%. Examination of the fracture surfaces of the AZ50 tested at  $1150^{\circ}\text{C}$  showed no evidence of creep. Comparison with creep data from other researchers suggests that the creep resistance of AZ50 is comparable (if not superior) to that of commercial alumina.

The high temperature hardness ( $1200^{\circ}\text{C}$ ) of the AZ50 was measured to be four times higher than cubic zirconia and twenty five percent higher than that of alumina. Indentation creep studies carried out at  $1200^{\circ}\text{C}$  showed that AZ50 maintains its superior hardness at long indentation times (See Figure 2). Furthermore, the damage that accumulated around the diamond indenter during hot hardness testing was much less noticeable in the AZ50 material in comparison to the alumina, which was found to be severely cracked (See Figure 3). This creep resistance and high hardness, coupled with the microstructural stability of AZ50, lead the researchers at Lehigh to believe that the high temperature mechanical properties of AZ50 are superior to those of both alumina and cubic zirconia.

These studies have widespread implications for the development of structural ceramics with superior high temperature mechanical properties. A potentially important practical application of this work is the fabrication of grain-stabilized fibers for uses as reinforcement in composite structures at elevated temperatures. Conventional ceramic fibers have ultra-fine grain size, and often suffer from grain growth during sintering or in service at elevated temperatures, resulting in strength and toughness degradation of the composite. Fibers containing suitable interpenetrating phase mixtures should have enhanced resistance to grain growth and property degradation at elevated temperatures.

While the current work has focused on 50% alumina - 50% cubic zirconia as a model system to study, the same benefits should be obtainable in many other mixed-phase systems whose high temperature properties may be exploited to a much greater extent than those of the alumina - cubic zirconia system.

### Figure Captions

1.   a.   Dependence of average grain size on sintering time at 1650°C.
- b.   Typical microstructures, after 24 hours at 1650°C; a) Single phase  $\text{Al}_2\text{O}_3$ ; b) single phase  $\text{c-ZrO}_2$ ; and c) AZ50.
3.   Indentation creep curves at 1200°C for AZ50 and  $\text{Al}_2\text{O}_3$ .
4.   SEM micrographs of indentation sites ( $3000\times^S$  at 1200°C); a) AZ50; b)  $\text{Al}_2\text{O}_3$ .

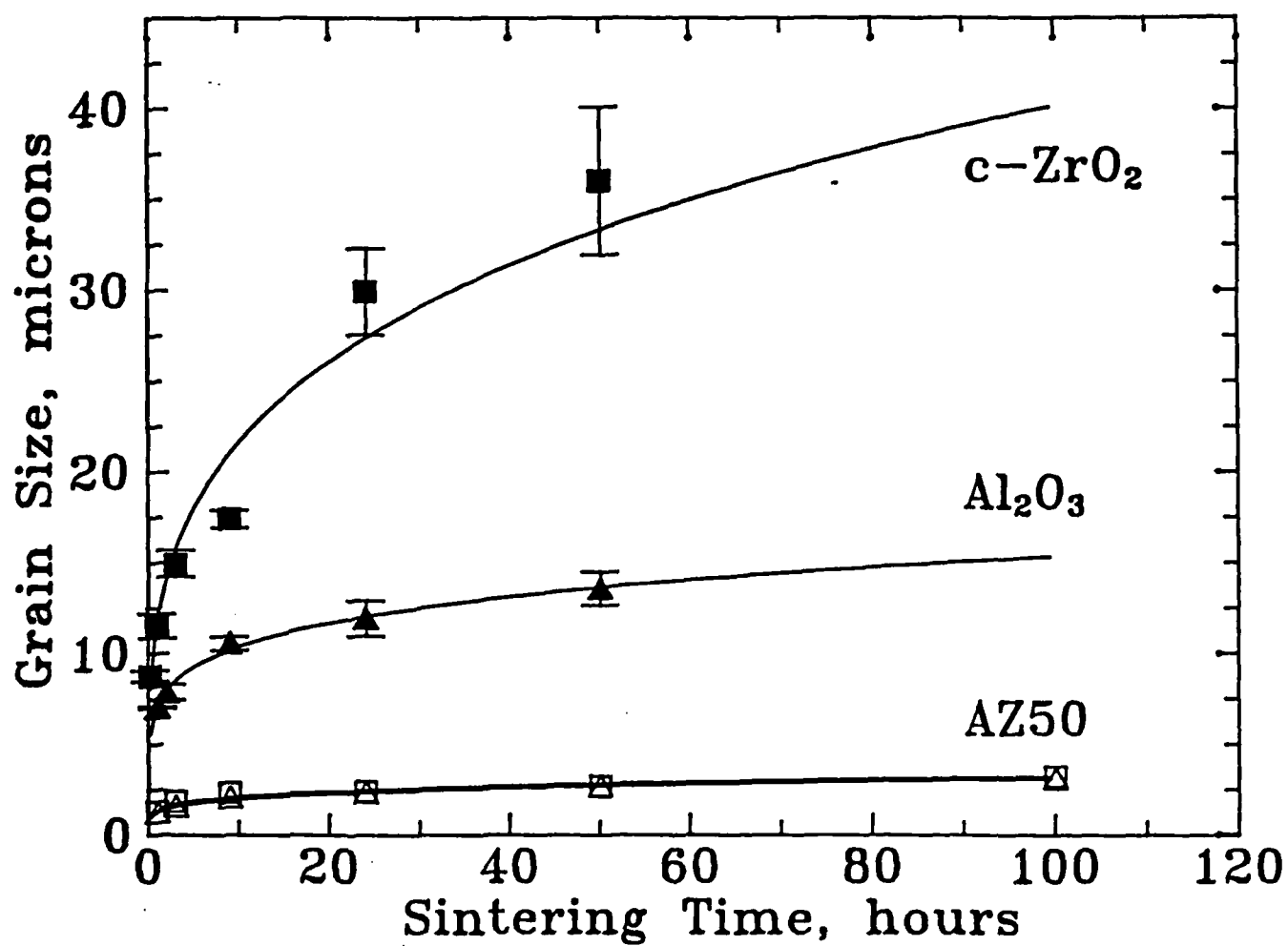


Figure 1. Average grain size as a function of sintering time at 1650°C for c-ZrO<sub>2</sub>, Al<sub>2</sub>O<sub>3</sub> and AZ50. Note the coarsening resistance of AZ50 compared to the single phase materials.



single phase  
 $\text{Al}_2\text{O}_3$

single phase  
c- $\text{ZrO}_2$

dual phase  
AZ50

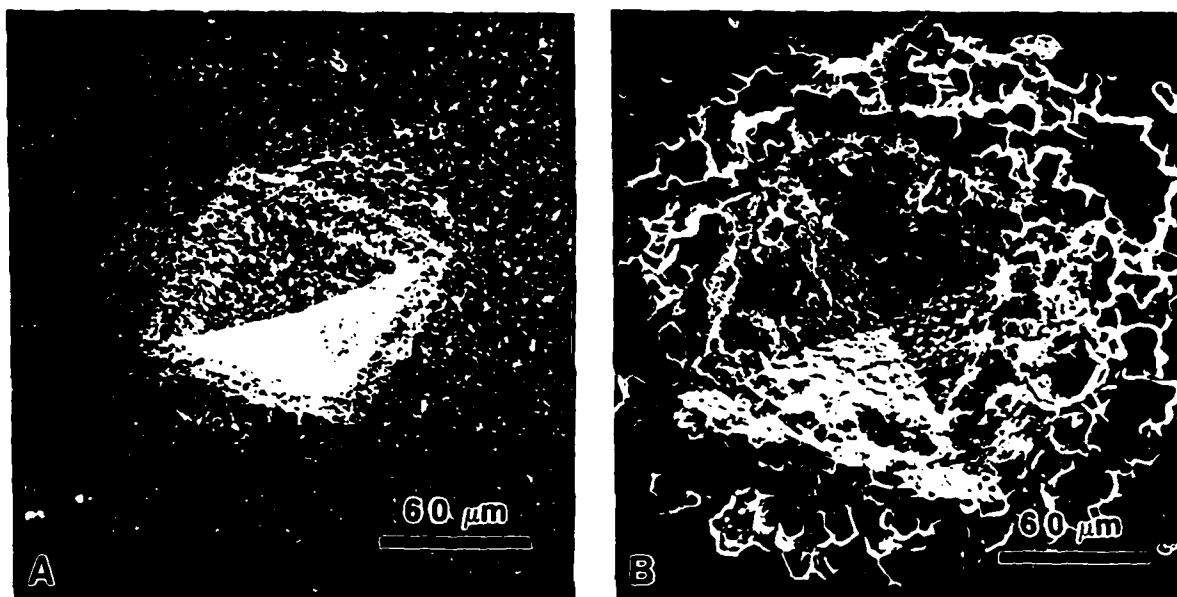


**Figure 2.** Indentation sites in (A) AZ50 and (B)  $\text{Al}_2\text{O}_3$  made at  $1200^\circ\text{C}$ , for 1000 seconds with a 10 N load. There is significantly less damage around the indentation site in AZ50 than  $\text{Al}_2\text{O}_3$ .



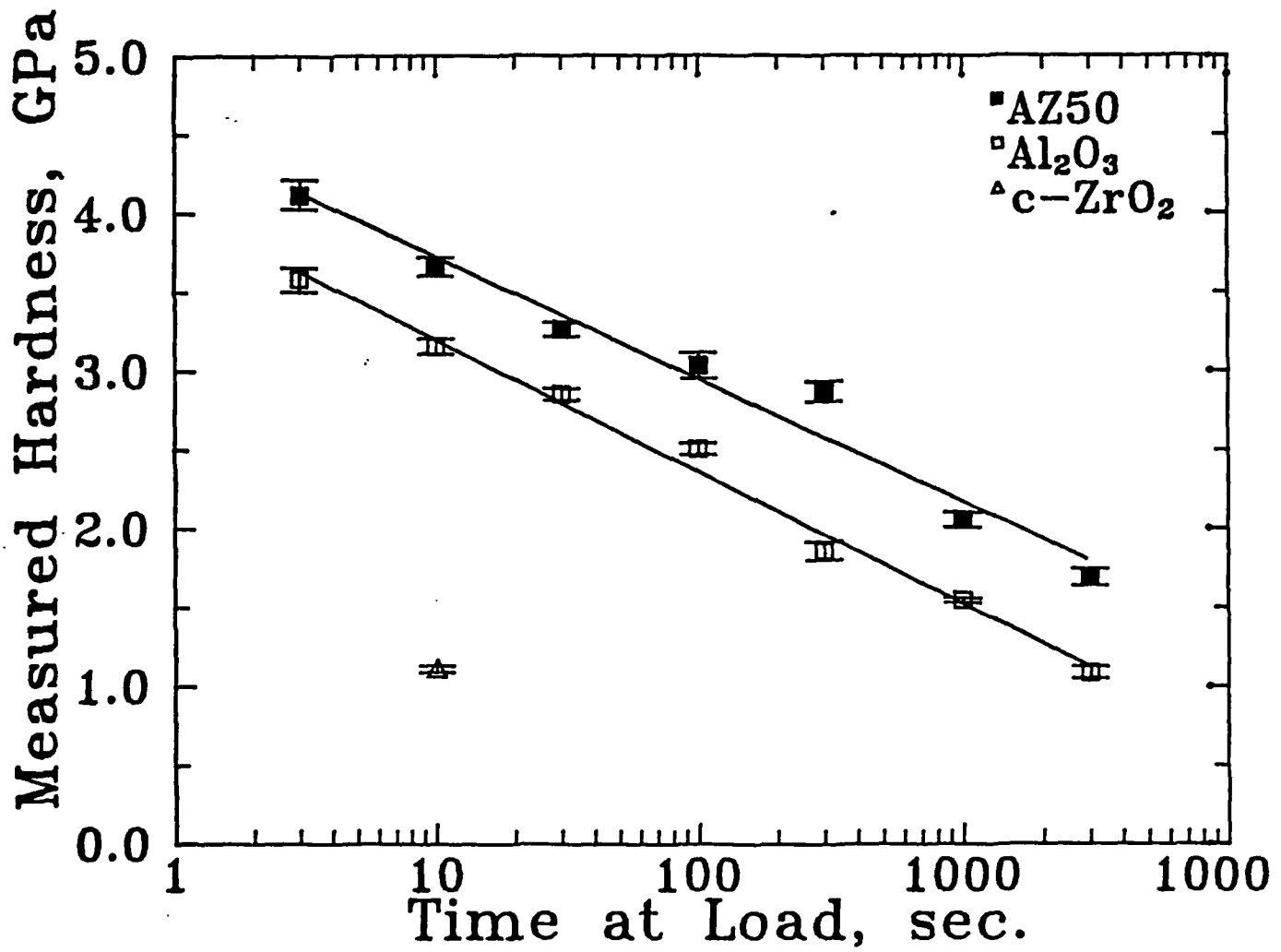


Figure 3. Indentation creep of AZ50 and Al<sub>2</sub>O<sub>3</sub> at 1200°C.

COARSENING RESISTANCE, HOT HARDNESS AND INDENTATION CREEP  
OF  $\text{Al}_2\text{O}_3$  and  $\text{Al}_2\text{O}_3\text{:YAG}$

J. D. French, M.P. Harmer, H.M. Chan, and G.A. Miller

Department of Materials Science and Engineering  
Lehigh University, Bethlehem, Pa 18015 USA

Technical update for final report

## Coarsening Resistance, Hot Hardness and Indentation Creep of Alumina:c-Zirconia and Alumina:YAG

It has been shown in our recent publication "Coarsening-Resistant Dual-Phase Interpenetrating Microstructures" (see section 1.1 of this report) that the AZ50 composition (50 vol%  $\text{Al}_2\text{O}_3$ , 50 vol% c- $\text{ZrO}_2$ ) exhibits pronounced resistance to grain coarsening at 1650°C. This is shown by the marked decrease in the grain growth rates ( $K_{\text{Al}_2\text{O}_3}$  and  $K_{\text{ZrO}_2}$ ) in the region where both phases are interconnected, Figure 1.

The system  $\text{Al}_2\text{O}_3:\text{Y}_3\text{Al}_5\text{O}_{12}$  (YAG) exhibits similar behavior as the  $\text{Al}_2\text{O}_3$ :c- $\text{ZrO}_2$  system. In addition, the hardness of the AY50 material is approximately twice that of the AZ50 material at 1200°C as shown in Figure 2. The indentation creep behavior at 1200°C for the AY50, AZ50 and single phase  $\text{Al}_2\text{O}_3$  and c- $\text{ZrO}_2$  are shown in Figure 3. It can be seen that the slope of the AY50 and AZ50 are comparable, but AY50 has a greater hardness than AZ50 (smaller indentations in AY50 than AZ50) for the same indentation conditions.

Our future work in this area is planned to include characterization of the elevated temperature properties of the  $\text{Al}_2\text{O}_3$ :YAG system (hardness and creep), and modelling of the coarsening behavior in these interpenetrating microstructures.

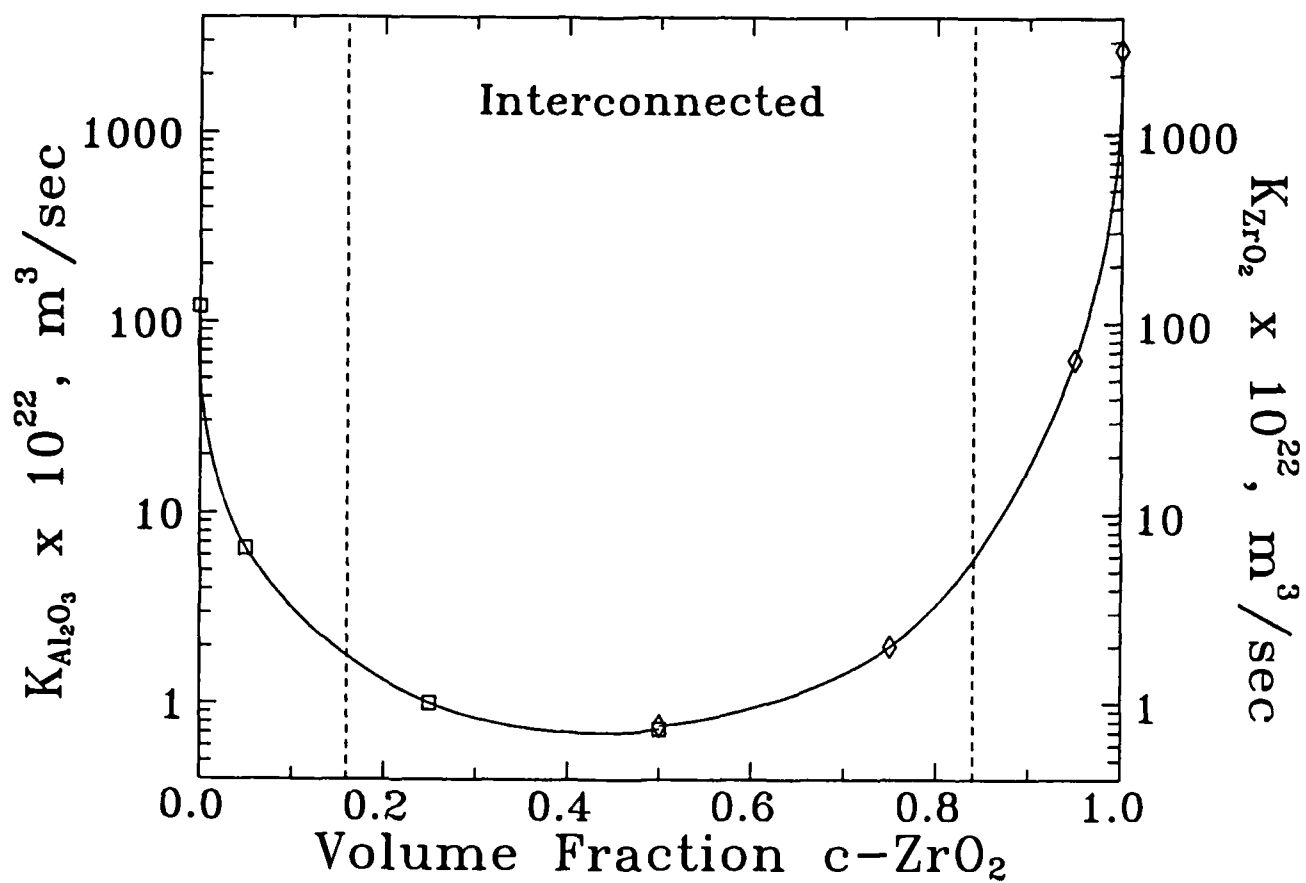


**Figure 1.** Grain growth rate constants for Al<sub>2</sub>O<sub>3</sub> and c-ZrO<sub>2</sub> as a function of c-ZrO<sub>2</sub> content.

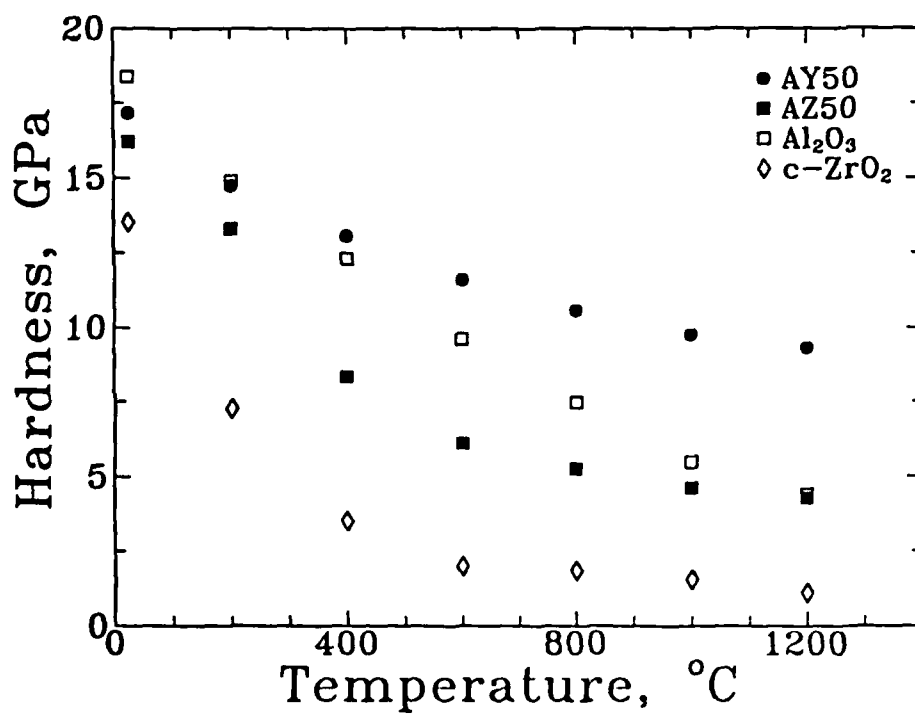


**Figure 2.** Hardness as a function of temperature for AY50, AZ50, Al<sub>2</sub>O<sub>3</sub> and c-ZrO<sub>2</sub>.

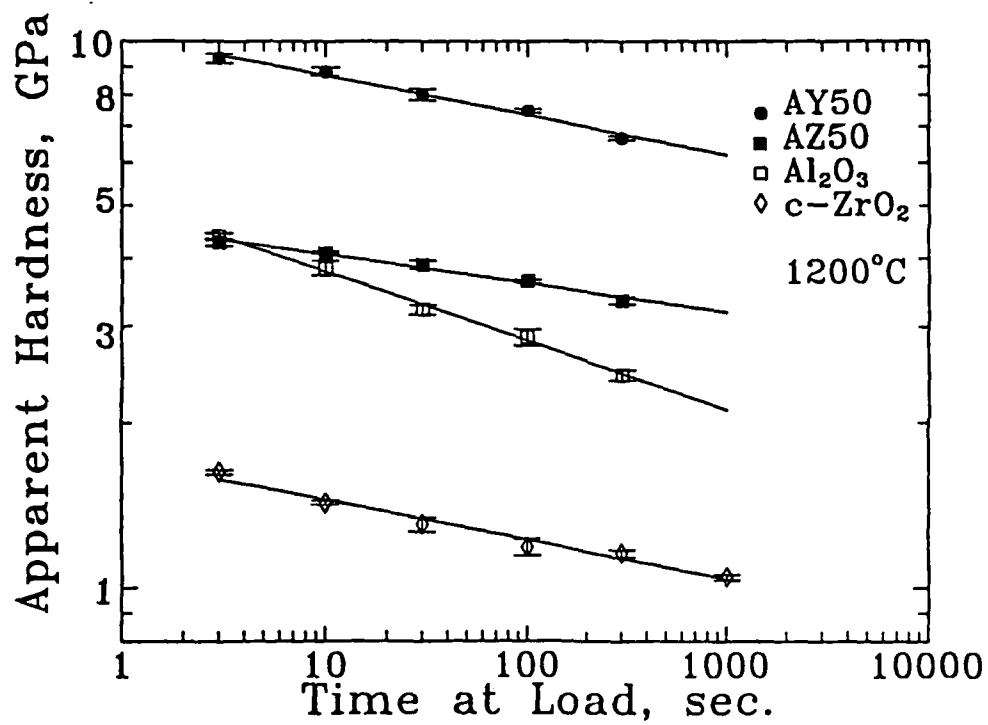


**Figure 3.** Indentation creep of AY50, AZ50, Al<sub>2</sub>O<sub>3</sub> and c-ZrO<sub>2</sub> at 1200°C.

**MECHANICAL PROPERTIES AND GRAIN GROWTH INHIBITION  
IN THE SYSTEM  $\text{Al}_2\text{O}_3\text{:c-ZrO}_2$**

**J.D. French, H.M. Chan, M.P. Harmer, and G.A. Miller**

**Department of Materials Science and Engineering  
Lehigh University, Bethlehem, Pa 18015 USA**

**Published in the Proceedings of the Materials Research  
Society Symposium, 170, 239, 1990.**

# MECHANICAL PROPERTIES AND GRAIN GROWTH INHIBITION IN THE SYSTEM $\text{Al}_2\text{O}_3\text{:c-ZrO}_2$

J. D. French, H. M. Chan, M. P. Harmer and G. A. Miller  
Department of Materials Science and Engineering, Lehigh  
University, Bethlehem, PA 18015.

## ABSTRACT

The grain coarsening in a 50:50 volume percent  $\text{Al}_2\text{O}_3\text{:c-ZrO}_2$  composite is shown to be severely limited even after long heat treatments at high temperatures (100 hours at 1650°C). The strength behavior, measured by an indentation-strength-in-bending (ISIB) method, shows a "rule-of-mixtures" type behavior. The microstructural stability at high temperatures yields reliability in the mechanical properties which has important implications with regard to fiber-reinforcement technology.

## INTRODUCTION

Duplex interconnected microstructures have been used for many years in the metals field for the generation of fine-grained materials suitable for superplastic forming.[1] However, this technique has not been exploited in the field of ceramics for producing microstructurally stable materials. Microstructural stability implies reliability of mechanical properties, since grain growth would be limited during high temperature service.

To study the microstructural development and mechanical properties of dual phase interconnected microstructures, a suitable system must be chosen in which there is (a) limited solid solubility of the two phases, and (b) no intermediate compounds between phases. The system  $\text{Al}_2\text{O}_3\text{:c-ZrO}_2$  was selected since it fulfils both these criteria. Although there has been a fair amount of previous work in this system [2,3], the emphasis has been on highly alumina-rich and zirconia-rich compositions. Very little study has been carried out with compositions near 50:50 volume percent.

## EXPERIMENTAL PROCEDURE

Commercial, high purity powders\* were mixed in 200-proof ethanol and ball milled for 24 hours then air dried on a hot plate. After crushing the dried cake, specimens for mechanical testing (25 mm diameter, 3 mm thickness) were produced by die pressing/isostatic pressing (30 MPa/350 MPa). Single-phase specimens were fabricated using the same pressing schedule. The pellets were calcined in air for 16 hours at 1000°C followed by sintering. Table I shows the sintering times and temperatures for the three compositions. The sintering schedule was chosen

\*Sumitomo AKP-HP  $\text{Al}_2\text{O}_3$ , Japan; Tosoh 8Y- $\text{ZrO}_2$ , Japan.



to produce a final average grain size of  $\sim 5 \mu\text{m}$ . Pellets 12 mm diameter, 5 mm thickness were also produced for microstructural development studies. Polished cross-sections were characterized using scanning electron microscopy (SEM), and average grain sizes were determined using a lineal intercept technique. Room temperature strength was measured using an indentation-strength-in-bending (ISIB) technique. [4,5]

TABLE I. Sintering schedule for single phase and dual-phase specimens for mechanical testing.

Composition	Temperature, °C	Time, hours
$\text{Al}_2\text{O}_3$	1650	3
AZ50	1650	9
c-ZrO <sub>2</sub>	1500	2

## RESULTS AND DISCUSSION

Figure 1 shows the grain growth behavior of single phase  $\text{Al}_2\text{O}_3$ , single phase  $\text{ZrO}_2$ , and the duplex AZ50 as a function of sintering time at 1650°C. The sintering kinetics were modelled using the relation:

$$G^n - G_0^n = Kt \quad (1)$$

where  $G$  is the average grain size at time  $t$ ,  $n$  is the grain growth kinetic exponent,  $G_0$  is the grain size at  $t = 0$  and  $K$  is a constant. The growth rate constants, for  $n = 3$ , appear in Table II.

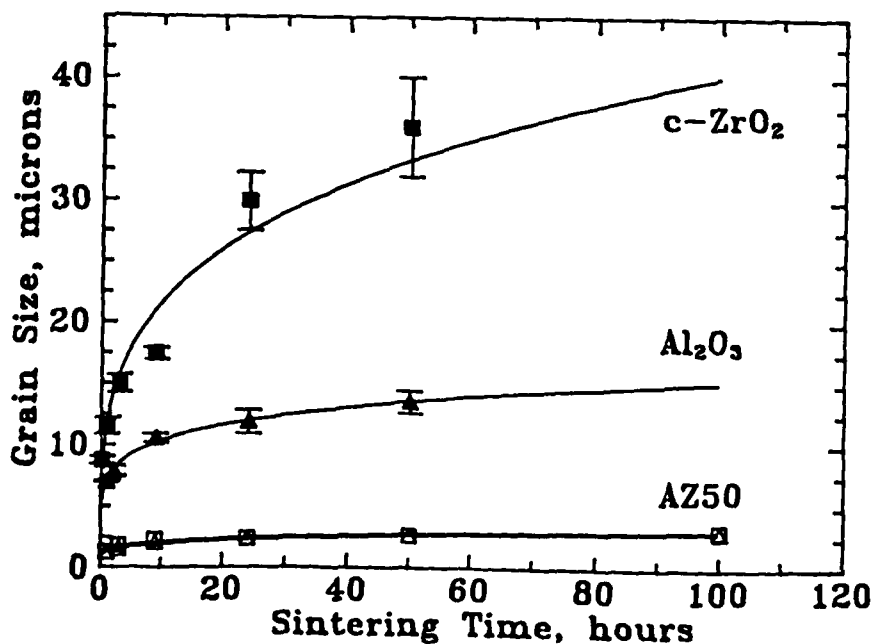


FIGURE 1. Effect of time, at 1650°C, on the average grain size of single phase c-ZrO<sub>2</sub> (■), single phase Al<sub>2</sub>O<sub>3</sub> (▲), and AZ50 - Al<sub>2</sub>O<sub>3</sub> phase (Δ) and c-ZrO<sub>2</sub> phase (□).

TABLE II. Grain growth constants, for  $n = 3$ , for single phase  $\text{Al}_2\text{O}_3$ , single phase  $c\text{-ZrO}_2$ , and each phase in AZ50.

<u>Composition</u>		<u><math>K \times 10^{23}</math>, <math>\text{m}^3/\text{s}</math></u>
single phase	$\text{Al}_2\text{O}_3$	1200
	$c\text{-ZrO}_2$	27000
AZ50	$\text{Al}_2\text{O}_3$	7.3
	$c\text{-ZrO}_2$	7.6

It can be seen that the presence of 50 vol%  $c\text{-ZrO}_2$  (AZ50), lowers the grain growth constant of  $\text{Al}_2\text{O}_3$  by a factor of 160. It should be noted that kinetic exponents from 2 to 6 all provided a reasonable fit (accounted for >90% of the variation) to the data. However  $n = 3$  was chosen to allow comparison with the effect of  $\text{MgO}$  on the grain growth of  $\text{Al}_2\text{O}_3$  [6], where  $K$  was observed to decrease by a factor of 50 at 1600 C. A typical microstructure of the AZ50 composition can be seen in Figure 2, where the dark phase is  $\text{Al}_2\text{O}_3$  and the light phase is  $c\text{-ZrO}_2$ .

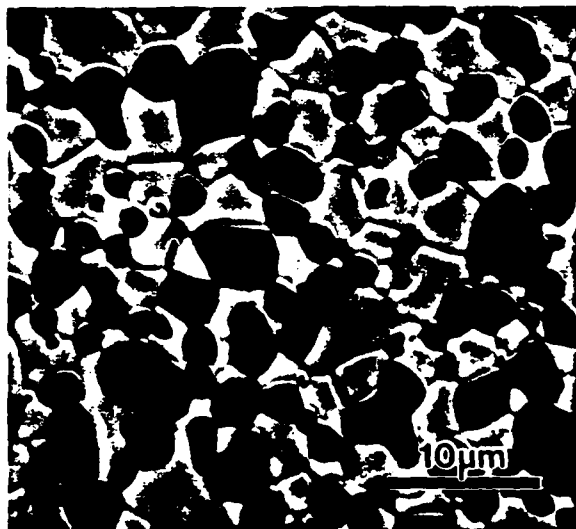


FIGURE 2. Typical microstructure of AZ50 after 100 hours at 1650°C.

Clearly the AZ50 duplex structure exhibits dramatic inhibition of grain coarsening relative to the constituent phases. The underlying physical mechanisms for this, together with grain growth data on other AZ compositions will be discussed in future work. [7]

The strength-indentation load results, Figure 3, show a "rule-of-mixtures" like behavior, i.e. the the AZ50 graph of  $\log \sigma - \log P$  is linear with a slope of  $-1/3$ , and falls midway between the single phase data. This result suggests that grain boundary stresses due to the thermal expansion mismatch between  $\text{Al}_2\text{O}_3$  and  $c\text{-ZrO}_2$  play a relatively minor role in the mechanical properties of the composite at these grain sizes.

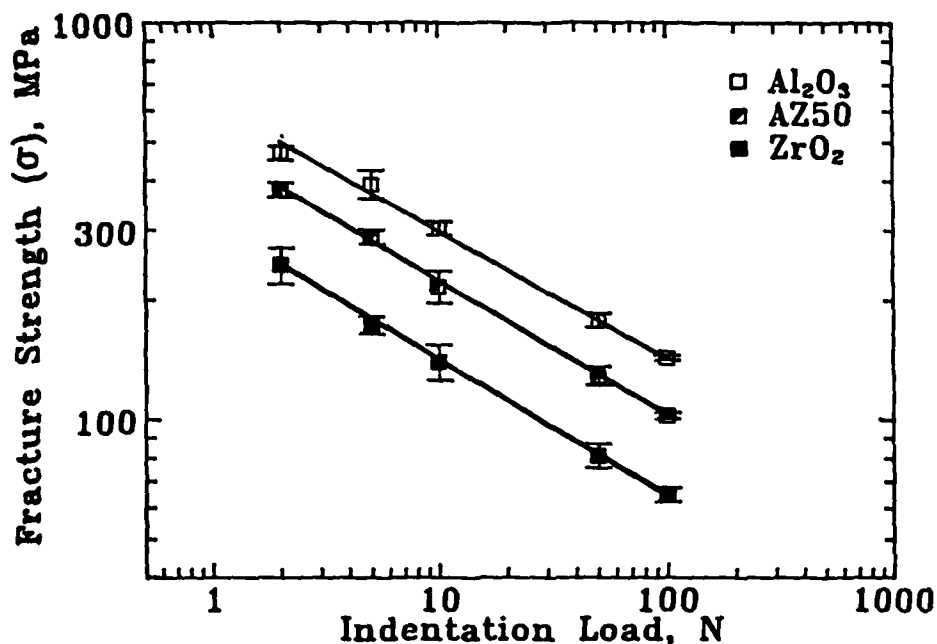


FIGURE 3. The effect of composition on the strength behavior of  $\text{Al}_2\text{O}_3\text{:c-ZrO}_2$  composites.

#### SUMMARY

- 1) AZ50 shows dramatic coarsening resistance even after 100 hours at 1650°C.
- 2) The strength data ( $\log \sigma - \log P$ ) shows a "rule-of-mixtures" type behavior with the strength of the AZ50 intermediate between that of the single phases.
- 3) The microstructural stability of a dual-phase microstructure, such as AZ50 could be applicable to fiber technology, where fiber coarsening could be controlled or possibly eliminated.

#### ACKNOWLEDGEMENTS

The authors would like to acknowledge W. Gust and F. Lange for their helpful discussions. Financial support for this project was provided by the Air Force Office of Scientific Research under contract number AFOSR-87-0396.

#### REFERENCES

1. J. Pilling and N. Ridley Superplasticity in Crystalline Solids, The Institute of Metals, London, 1989, pp.8-47.

2. F. F. Lange and M. Hirlinger, J. Am. Ceram. Soc. 70 (8) 243-249 (1987).
3. F. F. Lange and M. Hirlinger, J. Am. Ceram. Soc. 70 (11) 827-830 (1987).
4. J. B. Wachtman, Jr., W. Capps and J. Mandel, J. Mater., 7 (1972) 188-94.
5. G. de With and H. H. M. Wagemans, J. Am. Ceram. Soc., 72 (8) 1538-41 (1989).
6. S. J. Bennison and M. P. Harmer, J. Am. Ceram. Soc. 68 (1) C22-C24 (1985).
7. J. D. French, M. P. Harmer, H. M. Chan and G. A. Miller, Communication to be published in J. Am. Ceram. Soc.

**MECHANICAL PROPERTIES OF INTERPENETRATING MICROSTRUCTURES:**

**The  $\text{Al}_2\text{O}_3\text{:c-ZrO}_2$  SYSTEM**

**J.D. French, H.M. Chan, M.P. Harmer, and G.A. Miller**

**Department of Materials Science and Engineering  
Lehigh University, Bethlehem, PA 18015 USA**

**To be submitted to the Journal of the American Ceramic Society**

MECHANICAL PROPERTIES OF INTERPENETRATING MICROSTRUCTURES:  
THE  $\text{Al}_2\text{O}_3$ :c- $\text{ZrO}_2$  SYSTEM

Jonathan D. French, Helen M. Chan, Martin P. Harmer and Gary A. Miller, Materials Science and Engineering Department and the Materials Research Center, Lehigh University, Bethlehem, PA.

Abstract

Composites of  $\text{Al}_2\text{O}_3$ , A, and cubic  $\text{ZrO}_2$ , Z, (8 mol%  $\text{Y}_2\text{O}_3$ ), with c- $\text{ZrO}_2$  volume fractions ranging from zero to one, were fabricated by pressureless sintering of mechanically mixed powders. These AZ composites exhibit duplex microstructures (both phases are of similar size and shape) which at high volume fractions are very resistant to grain coarsening at elevated temperatures. Room temperature mechanical properties including elastic modulus (determined from elastic wave velocity measurements), strength, toughness (indentation-strength-in-bending) and Vickers hardness, all are linearly related to the volume fraction of second phase. Fracture toughness did not exhibit R-curve behavior since the strength of indented discs was proportional to (indentation load) $^{-1/3}$ . Fracture morphology changed from essentially intergranular for the tougher  $\text{Al}_2\text{O}_3$  to transgranular for c- $\text{ZrO}_2$  with AZ composites exhibiting mixed morphology.

## 1. Introduction

Much of the interest in duplex microstructures has focused on superplasticity and control of grain growth [1-10]. For many years, dual phase metallic microstructures have been found to be suitable for superplastic forming [10-12]. The intimate mixing of the phases provides a fine grain size which is stable at the forming temperature. Recently, superplasticity has also been found to be exhibited by fine-grained ceramics (both single phase and dual phase microstructures) [13]. In the case of non-transforming ceramics, there have been few systematic studies of the effects of volume fraction on the properties ceramic composites [14-16]. The present work was intended to provide such a data base for the  $\text{Al}_2\text{O}_3\text{:c-ZrO}_2$  system.

In a previous study [17] it was shown that an interconnected microstructure in the  $\text{Al}_2\text{O}_3\text{:c-ZrO}_2$  system resists coarsening at high temperatures. It is felt that the high volume fraction of second phase in these duplex microstructures is a key factor for the microstructural stability at high temperatures. The  $\text{Al}_2\text{O}_3\text{:c-ZrO}_2$  system is considered a model system in that both phases are mutually insoluble, there are no intermediate phases, pressureless sintering produces composites with near theoretical densities, and the phases are thermally and chemically stable over the entire temperature range below the eutectic temperature ( $1710^\circ\text{C}$ ).

The purpose of this study was to characterize the room temperature mechanical properties (elastic modulus, strength, toughness and hardness) of  $x\text{Al}_2\text{O}_3\text{:}(1-x)\text{c-ZrO}_2$  composites over the full range of compositions. High temperature mechanical properties will be presented elsewhere [18]. Although limited work exists

on duplex crystalline microstructures, there have been many studies of the mechanical properties of two-phase ceramic composites consisting of crystalline ceramic particles dispersed in glass matrices [19-30]. The results of this study will be compared with this body of literature.

## **2. Experimental Procedure**

### **2.1 Specimen Fabrication**

Commercial high-purity alumina (Sumitomo AKP-HP) and cubic zirconia (Tosoh 8Y-ZrO<sub>2</sub>) powders were mechanically mixed to generate (1-x)Al<sub>2</sub>O<sub>3</sub>:(x)C-ZrO<sub>2</sub> composites (where x is the volume fraction). Clean room processing was used throughout the powder preparation, details of which are outlined elsewhere [17]. Specimens were uniaxially pressed in a cylindrical die, 3.18 cm diameter, at a pressure of 30 MPa, followed by isostatic pressing at 350 MPa. The green pellets were placed in alumina crucibles packed with loose powder of the major phase composition. The specimens were calcined in air at 1000°C for 24 hours to burn off carbonaceous compounds present and prevent bloating during sintering. The sintering temperature and time were adjusted for each composition to generate a grain size of 3-6 microns for the major phase, Table I. After removal from the packing powder, the discs were polished to a 1 μm finish using standard metallographic techniques.

### **2.2 Mechanical Testing**

#### **1) Elastic Properties**

The elastic properties (modulus of elasticity and Poisson's ratio) were measured by the elastic wave velocity technique on



discs of each composition. Single phase discs were hot pressed to eliminate the typical 2% residual porosity which would significantly reduce the elastic properties.

#### ii) Hardness

For each composition, 8 to 10 room temperature hardness measurements were made using a Vickers indenter with 10 N load and 10 second dwell time. Hardness values were determined from the equation:

$$H = 2P \sin(\theta/2) / d^2 \quad (1).$$

where H is the hardness in GPa, P is the indentation load,  $\theta$  is the angle between opposite faces of the indenter (for Vickers,  $\theta=136^\circ$ ) and d is the indentation diagonal length. An indentation load of 10 N was chosen to provide impressions significantly larger than the grain size.

#### iii) Indentation-Strength-In-Bending

The introduction of controlled flaws to test the intrinsic strength of ceramics is well established [30,31]. The introduction of a well-defined flaw, such as that produced with a Vickers indentation, can minimize variability in the strength. This type of flaw simulates the contact damage which is likely to occur during machining and in service.

The center of each disc was indented using a Vickers indenter loaded to various levels (2, 5, 10, 50 and 100 N) for a dwell time of 15 seconds. A drop of silicone oil covered the indentation site to minimize subcritical crack growth from water vapor. The discs were then broken in biaxial flexure (punch-on-three-ball-support), in an Instron servo-hydraulic testing machine in 7

- 15 milliseconds to eliminate possible environmental effects. Typically, 4 to 5 discs of each composition were tested at each indentation load.

### **2.3 Characterization - SEM Observations**

Broken pieces from mechanical testing were thermally etched in air (1450°C - 90 minutes) to reveal the crack path through the microstructure. An indentation load of 100 N was used to generate the cracks. Scanning Electron Microscopy (SEM) was used to observe the indentation cracks. The specimens were sputter coated with Au-Pd to prevent charging in the SEM (ETEC Corporation). Thermally etched surfaces provided a better indication of the nature of the crack propagation behavior (inter- or trans-granular) than as-polished surfaces.

## **3. Results**

### **3.1 Elastic Modulus and Poisson's Ratio**

Figure 1 shows the behavior of the modulus of elasticity for the composites. It can be seen that the modulus decreases linearly with increasing c-ZrO<sub>2</sub> content. Also plotted in Figure 1 are the predicted curves (dashed) from series and parallel models for composite elastic behavior. Poisson's ratio for the seven compositions appear in Table II.

### **3.2 Hardness**

As was true for the elastic modulus, the room temperature hardness, Figure 2, decreases linearly with increasing c-ZrO<sub>2</sub> content. The single phase materials had to be hot-pressed to achieve full density. Without hot-pressing, these materials contained approximately 2% residual porosity which lowered the hardness by about 10%.

### 3.3 Strength

Figure 3a shows the room temperature fracture strength-indentation load behavior of the AZ composites. The equations used for calculating the strength, based on the load at failure and specimen geometry, appear in Appendix I. The strength-indentation load behavior of materials which do not exhibit R-curve behavior (increasing fracture resistance with increasing crack length) will follow the relation [31,32]:

$$\sigma \propto P^{-1/3} \quad (2).$$

where  $\sigma$  is the fracture strength for a given indentation load  $P$ . It can clearly be seen that the strength data in Figure 1a follow such a  $P^{-1/3}$  relation for all compositions. The same data (when plotted as fracture strength verses volume fraction c-ZrO<sub>2</sub>) also shows that for all indentation loads the composite strength decreases linearly with increasing c-ZrO<sub>2</sub> content (Figure 3b).

### 3.4 Toughness

Since the strength-indentation load behavior follows a  $P^{-1/3}$  relation, the fracture toughness can be calculated from the strength data with the equation [32]:

$$K_C = n(E/H)^{1/8}(\sigma P^{1/3})^{3/4} \quad (3).$$

where  $n$  is a material-independent geometrical constant, which was experimentally determined by Chantikul et al. [32] to be  $0.59 \pm 0.12$ ,  $E$  is the elastic modulus and  $H$  is the hardness and  $\sigma$  is the strength for a given indentation load  $P$ .

The fracture toughness ( $K_C$ ) of the AZ composites also exhibits a linear decrease in toughness with increasing c-ZrO<sub>2</sub> content, Figure 4. Since the strength and toughness values for the

composites were not determined independently, and the relation between them is nonlinear ( $K_C \propto \sigma^{3/4}$ ) both properties cannot strictly follow a linear behavior. Apparently, the 3/4 exponent is not sufficiently different from unity to cause significant curvature in Figure 4. The plotted error bars represent + and - one standard deviation about the average strength at the various indentation loads. The error in  $K_C$  does not include the variation in the constant  $n$ , since the trend of the data is of primary interest, rather than the absolute toughness values.

Since the strength values follow a  $P^{-1/3}$  dependence, these composites do not show R-curve behavior (rising fracture resistance with crack size). A possible explanation is that grain bridging behind the crack tip is not as important for these fine-grained AZ composites as for coarser grained ceramics [33,34].

Figure 5 shows that cracks propagate mostly intergranularly in single phase  $Al_2O_3$ . As the c- $ZrO_2$  content increases the amount of transgranular fracture increases. In single phase c- $ZrO_2$ , the fracture path is all transgranular. Indentation cracks were observed on polished (and thermally etched) surfaces rather than fracture surfaces because the relative amounts of inter- and transgranular fracture are more clearly discernable.

#### 4. Discussion

##### 4.1 Elastic Modulus, Strength and Toughness

The trend of the room temperature mechanical properties for these composites is simple, the composite properties follow a linear behavior between the single phases. From the fracture toughness,  $K_C$ , and the modulus of elasticity,  $E_C$ , the fracture surface energy,  $2\delta_C$ , (or  $G_C$ ) of each composition can be calculated.

ed with the relation:

$$2\gamma_c = K_c^2/E_c \quad (4).$$

Figure 6 shows  $2\gamma_c$  as a function of c-ZrO<sub>2</sub> content. We see here that the behavior is slightly non-linear; specifically,  $2\gamma_c$  does not change appreciably below 25 vol% c-ZrO<sub>2</sub>. The fracture surface energy of an two-phase composite per unit crack area,  $G_c$ , can be written as follows:

$$G_c = G_1A_1 + G_2A_2 + G_{12}A_{12} \quad (5).$$

where  $G_1$ ,  $G_2$ ,  $A_1$ ,  $A_2$  are the fracture surface energies and area fractions of the two phases,  $G_{12}$  is the interfacial energy between the two phases, and  $A_{12}$  represents the interfacial area fraction. If we make some simplifying assumptions, such as the interaction term being negligible and the area fraction equal to the volume fraction, we arrive at a linear behavior between the two phases. However, from the indentation crack behavior of the composites (Figure 5) it can be seen that the interaction term and the mode of failure cannot be ignored. Significant portions of the cracks are transgranular Al<sub>2</sub>O<sub>3</sub> fracture (little of which is seen in the single phase Al<sub>2</sub>O<sub>3</sub>) and interphase fracture. Since the Al<sub>2</sub>O<sub>3</sub> exhibits two types of fracture behavior in the composites, a fourth term would be needed which accounts for both failure morphologies. That is:

$$G_c = G_{AA}^{iA} + G_{AA}^{tA} + G_ZA_Z + G_{AZ}A_{AZ} \quad (6).$$

where the superscripts designate the inter- and transgranular fracture of Al<sub>2</sub>O<sub>3</sub>. It is believed that the interaction term in equation (6) and the dual nature of the Al<sub>2</sub>O<sub>3</sub> fracture behavior lead to the nonlinearity of the fracture surface energy behavior

as a function of volume fraction in these composites.

Since the mechanical properties all decrease linearly with increasing c-ZrO<sub>2</sub> content, one might consider a mixing rule to describe the behavior. However, for the AZ system the difference between the series and parallel mixing models is so small that either model could be used to represent the data.

It is pertinent to show how the present findings for the AZ system compare with those of other studies of duplex microstructures. The linear change of mechanical properties with volume fraction can be seen as a common thread in nontransforming particulate ceramic composites. It should be noted that the linear behavior seems to occur in the simplest cases (such as fine grain sizes and homogeneous microstructures of theoretical density). Complications occur when the microstructure becomes more complex, such as large grain sizes, particlulated with large aspect ratios, etc..

Lange [14] reported fairly linear behavior for the toughness variation of Al<sub>2</sub>O<sub>3</sub>:c-ZrO<sub>2</sub> composites with volume fraction of second phase. Differences with present findings are that his values are somewhat higher and exhibited a minimum toughness at 80 vol% c-ZrO<sub>2</sub> (the toughness of single phase c-ZrO<sub>2</sub> was significantly higher than expected). The systematic error in the constant  $n$  in Equation (3) and the fact that Lange's data was measured from indentation crack length measurements, preclude direct comparison of the toughness values with present findings. Lange postulated that the toughness minimum was due to unfavorable residual stresses arising from the thermal expansion mismatch (cf.  $-8.4 \times 10^{-6}/^{\circ}\text{C}$  for Al<sub>2</sub>O<sub>3</sub> and  $-10 \times 10^{-6}/^{\circ}\text{C}$  for c-ZrO<sub>2</sub>). Howev-

er, no effect was seen at the low c-ZrO<sub>2</sub> end (where favorable residual stresses would be expected) of his toughness data. From the present results, it is believed that the toughness of the composite is simply related to the volume fraction of each phase, and residual stresses have little effect at the fine grain sizes tested. Lange also showed a linear behavior for the modulus of as a function volume fraction of t-ZrO<sub>2</sub> (2.5 mol% Y<sub>2</sub>O<sub>3</sub>) in Al<sub>2</sub>O<sub>3</sub>.

Yuan et al. [15] showed a linear increase in fracture strength of MgO with ZrO<sub>2</sub> additions. At 40 vol% ZrO<sub>2</sub>, they reported a fracture strength of 300 MPa and toughness of 3.0 MPa√m (8 mol% CaO was added to produce c-ZrO<sub>2</sub>). The extrapolated value of strength for c-ZrO<sub>2</sub> from the CaO doped samples was 450 MPa. These values were determined from four-point bend specimens (unindented). Based on the low indentation load value of fracture strength of c-ZrO<sub>2</sub> (250 MPa) in the present data set, the extrapolated value from the Yuan et al. data is not unreasonable. Kang and Kim [16] reported an increase in toughness with increasing B<sub>4</sub>C additions to TiB<sub>2</sub> up to 20 vol%, but toughness decreased slightly at 30 vol% due to increased porosity. Fracture strength of polished bars showed a maximum at the 10 vol% B<sub>4</sub>C composition. The strength reduction above 10 vol% was attributed to abnormally large B<sub>4</sub>C grains present in the higher volume fraction compositions.

Linear changes in strength and/or toughness with volume fraction of second phase have also been reported for glass matrices reinforced with crystalline particulates. Swearingen et al. [19] showed that for 25 μm Al<sub>2</sub>O<sub>3</sub> spheres in a sodium borosilicate

glass,  $K_{IC}$  increased linearly with increasing  $Al_2O_3$  content regardless of the thermal expansion difference ( $\alpha_{Al_2O_3} - \alpha_{glass}$ ) which was adjusted to vary from  $-3.7 \times 10^{-6}$  to  $+4 \times 10^{-6}/^{\circ}C$ . Extrapolation of the toughness to single phase  $Al_2O_3$  gives a toughness value of approximately 5 MPa/m which is a reasonable value based on literature values [14,33]. Lange [20] reported a linear increase in fracture strength of composites with fine (3.5  $\mu m$ )  $Al_2O_3$  additions to glass. Larger  $Al_2O_3$  spheres (11 and 44  $\mu m$ ) showed non-linear behavior, due to the larger flaws introduced by larger particles. Fracture energy as a function of volume fraction was nonlinear; remaining constant beyond 20 vol%  $Al_2O_3$ . However, this finding was confounded by fact that the amount of porosity increased with increasing  $Al_2O_3$  content. Lange discussed the conflicting processes of increased crack-front pinning and introduction of larger flaws due to the addition of large (higher modulus) particles. Others have also published similar linear increases of fracture strength of glass with increasing crystalline particulate additions [21,22].

Much of the fracture strength data reported [23-29] for glass-crystalline composites could not be compared with the present results due to the differences in the testing techniques. In previous data [23-29], based on flaw size criteria where the flaw population in the glass is controlled by the particle spacing (or particle size), failure is controlled by flaws induced by the presence of large inclusions. In the case of indentation-strength-in-bending, one well defined flaw is introduced as the source of failure, regardless of the surface flaw population.

#### 4.2 Hardness



Miyata and Jinno [30] provided data for the glass system  $\text{PbO} - \text{B}_2\text{O}_3$ , corroborating their theoretical model to predict the hardness behavior of glass-crystalline composites based on the stress intensity surrounding a spherical inclusion and a simplifying equation which relates hardness to the modulus and the yield stress. However, when their hardness data is replotted as a function of volume fraction (from 0 to 100%  $\text{PbO}$  phase), the data approximate to a linear behavior between the two single phases with hardness increasing with increasing  $\text{PbO}$  content. Lange [14] also reported a linear decrease in hardness of  $\text{Al}_2\text{O}_3\text{:t-ZrO}_2$  (2.5 mol%  $\text{Y}_2\text{O}_3$ ) as a function of  $\text{t-ZrO}_2$  content.

### Conclusions

Based on the present study of the mechanical behavior of the  $\text{Al}_2\text{O}_3\text{:c-ZrO}_2$  (AZ) ceramic composite system, the following conclusions can be made:

1. Room temperature properties including elastic modulus, strength, toughness and hardness decrease linearly with increasing volume fraction  $\text{c-ZrO}_2$ .
2. The AZ composites showed no R-curve behavior - fracture strength was proportional to  $(\text{indentation load})^{-1/3}$ . The fine grain size of the composites may have inhibited toughening mechanisms such as grain bridging behind the crack tip.
3. Fracture morphology changed progressively with volume fraction of second phase, from intergranular for the tougher  $\text{Al}_2\text{O}_3$  to transgranular for the  $\text{c-ZrO}_2$  with composites exhibiting a mixed behavior.

### Acknowledgements

The authors would like to thank R. Dill and K. P. Reddy at Corning for measuring the elastic moduli in this study. Helpful discussions with B. Lawn and N. Padture are also acknowledged.

#### Appendix I.

The fracture stress,  $\sigma$ , was calculated using the equation proposed by Watchman et al. [35], which states:

$$\sigma = -3P/(4\pi d^2)(X-Y) \quad (5).$$

with:

$$X = (1+\nu)\ln(B/C)^2 + ((1-\nu)/2)(B/C)^2 \quad (5.1).$$

$$Y = (1+\nu)(1+\ln(A/C)^2) + (1-\nu)(A/C)^2 \quad (5.2).$$

where  $P$  is the load at failure,  $d$  is the specimen thickness,  $\nu$  is Poisson's ratio,  $A$  is the radius of the support circle,  $B$  is the radius of the loaded area and  $C$  is the specimen radius.

A correction proposed by de With and Wagemans [36] was applied due to the thickness of the specimens relative to the punch radius. The correction was:

$$b = (1.6z^2+t^2)^{1/2} - 0.675t \quad (6).$$

where  $b$  is the radius of uniform loading (which was assumed by Watchman et al. to be equal to the punch radius  $z$ ), and  $t$  is the specimen thickness. This corrected value,  $b$ , was then substituted into equations 10.1 and 10.2 for the variable  $B$ . This correction is necessary for thinner specimens due to the greater amount of flexing of the specimen under the applied load [36]. As the amount of bending of the sample (prior to failure) changes, the area under constant loading changes.

#### References

1. F. F. Lange and M. M. Hirlinger, "Hindrane of Grain Growth in  $Al_2O_3$  By  $ZrO_2$  Inclusions", J. Am. Ceram. Soc. 67[3]164-68 (1984).

2. F. F. Lange and M. M. Hirlinger, "Grain Growth in Two-Phase Ceramics:  $\text{Al}_2\text{O}_3$  Inclusions in  $\text{ZrO}_2$ ", J. Am. Ceram. Soc. 70[11] 827-30 (1987).
3. S. Hori, R. Kurita, M. Yoshimura and S. Somiya, "Supressed Grain Growth in Final-Stage Sintering of  $\text{Al}_2\text{O}_3$  with Dispersed  $\text{ZrO}_2$  Particles", J. Mater. Sci. Lett. 4 1067-70 (1985).
4. D. J. Green, "Transformation Toughening and Grain Size Control in  $\beta$ "- $\text{Al}_2\text{O}_3$ / $\text{ZrO}_2$  Composites" J. Mater. Sci. 20 2639-46 (1985).
5. Y. Sheng and P. S. Nicholson, "Microstructure Development of a  $\text{ZrO}_2$  -  $\text{Na}\beta$ "- $\text{Al}_2\text{O}_3$  Composite", J. Mater. Sci. 24 982-86 (1987).
6. J. Kim, T. Kimura and T. Yamaguchi, "Microstructure Development in  $\text{Sb}_2\text{O}_3$ -doped  $\text{ZnO}$ " J. Mater. Sci. 24 2581-86 (1989).
7. J. B. Baldo and R. C. Bradt, "Grain Growth of the Lime and Periclase Phases in a Synthetic Doloma", J. Am. Ceram. Soc. 71[9] 720-25 (1988).
8. J. Pilling and N. Ridley, Superplasticity in Crystalline Solids, London, The Institute of Metals, 1989, pp. 8-47.
9. J. W. Edington, "Microstructural Aspects of Superplasticity", Met. Trans. A 13A[5] 703-15 (1982).
10. M. T. Cope, D. R. Evetts and N. Ridley, "Superplastic Deformation Characteristics of Two Microduplex Titanium Alloys", J. Mater. Sci. 21 4003-8 (1986).
11. M. W. Mahoney and A. K. Ghosh, "Superplasticity in a High Strength Powder Aluminum Alloy With and Without SiC Reinforcement", Met. Trans. A 18A[4] 653-61 (1987).
12. Y. Maehara and Y. Ohmori, "Microstructural Change During Superplastic Deformation of  $\delta$ -Ferrite/Austenite Duplex Stainless Steel", Met. Trans. A 18A[4] 663-72 (1987).
13. I-W Chen and L. A. Xue, "Development of Superplastic Structural Ceramics", J. Am. Ceram. Soc. 73[9] 2585-2609.
14. F. F. Lange, "Transformation Toughening: Part 4, Fabrication, Fracture Toughness and Strength of  $\text{Al}_2\text{O}_3$ - $\text{ZrO}_2$  Composites", J. Mater. Sci. 17 247-54 (1982).
15. T. C. Yuan, G. V. Srinivasan, J. F. Jue and A. V. Virkar, "Dual-Phase Magnesia-Zirconia Ceramics with Strength Retention at Elevated Temperatures", J. Mater. Sci. 24 3855-64 (1989).
16. E. S. Kang and C. H. Kim, "Improvements in Mechanical Properties of  $\text{TiB}_2$  by Dispersion of  $\text{B}_4\text{C}$  Particles", J. Mater. Sci. 25 580-84 (1990).

17. J. D. French, M. P. Harmer, H. M. Chan and G. A. Miller, "Coarsening-Resistant Dual-Phase Interpenetrating Microstructures", J. Am. Ceram. Soc. 73[8] 2508-10 (1990).
18. J. D. French, M. P. Harmer, H. M. Chan and G. A. Miller, Unpublished Work.
19. J. C. Swearingen, E. K. Beauchamp and R. J. Eagan, "Fracture Toughness of Reinforced Glasses", pp. 973-987 in Fracture Mechanics of Ceramics, Vol. 4, Edited by R. C. Bradt, D. P. H. Hasselman and F. F. Lange, Plenum Press, New York, 1978.
20. F. F. Lange, "Fracture Energy and Strength Behavior of a Sodium Borosilicate Glass- $\text{Al}_2\text{O}_3$  Composite System", J. Am. Ceram. Soc. 54[12] 614-20 (1971).
21. D. B. Binns, "Some Physical Properties of Two-Phase Crystal-Glass Solids", pp. 315-333 in Science of Ceramics, Edited by G. H. Steward, Academic Press, New York (1962).
22. W. J. Frey and J. D. MacKenzie, "Mechanical Properties of Selected Glass-Crystal Composites", J. Mater. Sci. 2 124-30 (1967).
23. J. S. Nedeau and R. C. Bennett, "Some Effects of Dispersed Phases on the Fracture Behavior of Glass", pp. 961-972 in Fracture Mechanics of Ceramics, Vol. 4, Edited by R. C. Bradt, D. P. H. Hasselman and F. F. Lange, Plenum Press, New York, 1978.
24. R. W. Davidge and T. J. Green, "The Strength of Two-Phase Ceramic/Glass Materials", J. Mater. Sci. 3 629-34 (1968).
25. D. P. H. Hasselman and R. M. Fulrath, "Proposed Fracture Theory of a Dispersion-Strengthened Glass Matrix", J. Am. Ceram. Soc. 49[2] 68-72 (1966).
26. D. P. H. Hasselman and R. M. Fulrath, "Micromechanical Stress Concentrations in Two-Phase Brittle-Matrix Ceramic Composites", J. Am. Ceram. Soc. 50[8] 399-404 (1967).
27. M. P. Borom, "Dispersion-Strengthened Glass Matrices- Glass-Ceramics, A Case in Point", J. Am. Ceram. Soc. 60[1-2] 17-21 (1977).
28. N. Miyata and H. Jinno, "Theoretical Approach to the Fracture of Two-Phase Glass-Crystal Composites", J. Mater. Sci. 7 973-82 (1972).
29. A.G. Evans, "The Role of Inclusions in the Fracture of Ceramic Materials", J. Mater. Sci. 9 1145-52 (1974).
30. N. Miyata and H. Jinno, "Micromechanics Approach to the Indentation Hardness of Glass Matrix Particulate Composites", J. Mater. Sci. 17 547-57 (1982).

31. R. F. Cook, B. R. Lawn and C. J. Fairbanks, "Microstructure-Strength Properties in Ceramics: I, Effect of Crack Size on Toughness", J. Am. Ceram. Soc. 68[11] 604-615 (1985).
32. P. Chantikul, G. R. Anstis, B. R. Lawn, and D. B. Marshall, "A Critical Evaluation of Indentation Techniques for Measuring Fracture Toughness: II, Strength Method", J. Am. Ceram. Soc. 64[9] 539-43 (1981).
33. P. Chantikul, S. J. Bennison and B. R. Lawn, "Role of Grain Size in the Strength and R-Curve Properties of Alumina", J. Am. Ceram. Soc. 73[8] 2419-27 (1990).
34. S. J. Bennison and B. R. Lawn, "Role of Interfacial Grain-Bridging Sliding Friction in Crack-Resistance and Strength Properties of Nontransforming Ceramics", Acta Metall. 37[10] 2659-71 (1989).
35. J. B. Watchman, W. Capps and J. Mandell, "Biaxial Flexure Tests of Ceramic Substrates", J. Mat., JMLSA, 7[2] 188-94 (1972).
36. G. de With and H. M. Wagemans, "Ball-on-Ring Test Revisited", J. Am. Ceram. Soc. 72[8] 1538-41 (1989).

Table I. Sintering conditions for the  $\text{Al}_2\text{O}_3\text{:c-ZrO}_2$  composites.  
All specimens were fired in air.

<u>Composition</u>	<u>Temperature, °C</u>	<u>Time, hours</u>
$\text{Al}_2\text{O}_3$	1650	3
AZ5, AZ25 AZ50, AZ75	1650	9
AZ95	1550	6
c-ZrO <sub>2</sub>	1500	2

Table II. Poisson's ratio for the  $\text{Al}_2\text{O}_3\text{:c-ZrO}_2$  composites

<u>Composition</u>	<u>Poisson's Ratio</u>
$\text{Al}_2\text{O}_3$	0.197
AZ5	0.210
AZ25	0.249
AZ50	0.268
AZ75	0.286
AZ95	0.312
c-ZrO <sub>2</sub>	0.310

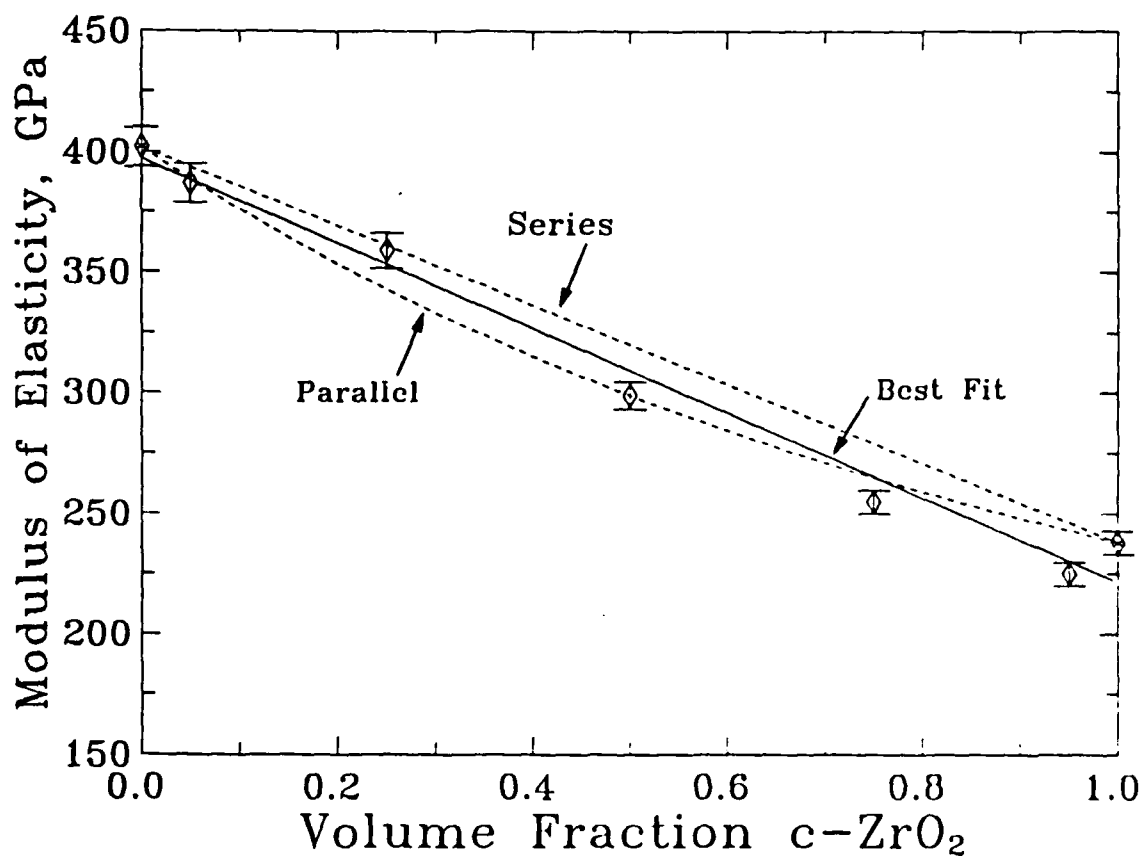


Figure 1. Elastic modulus as a function of volume fraction c-ZrO<sub>2</sub> for the Al<sub>2</sub>O<sub>3</sub>:c-ZrO<sub>2</sub> composites, measured by elastic wave velocity. Series and parallel mixing models (dashed curves) are presented for comparison. Solid curve represents the best fit line.

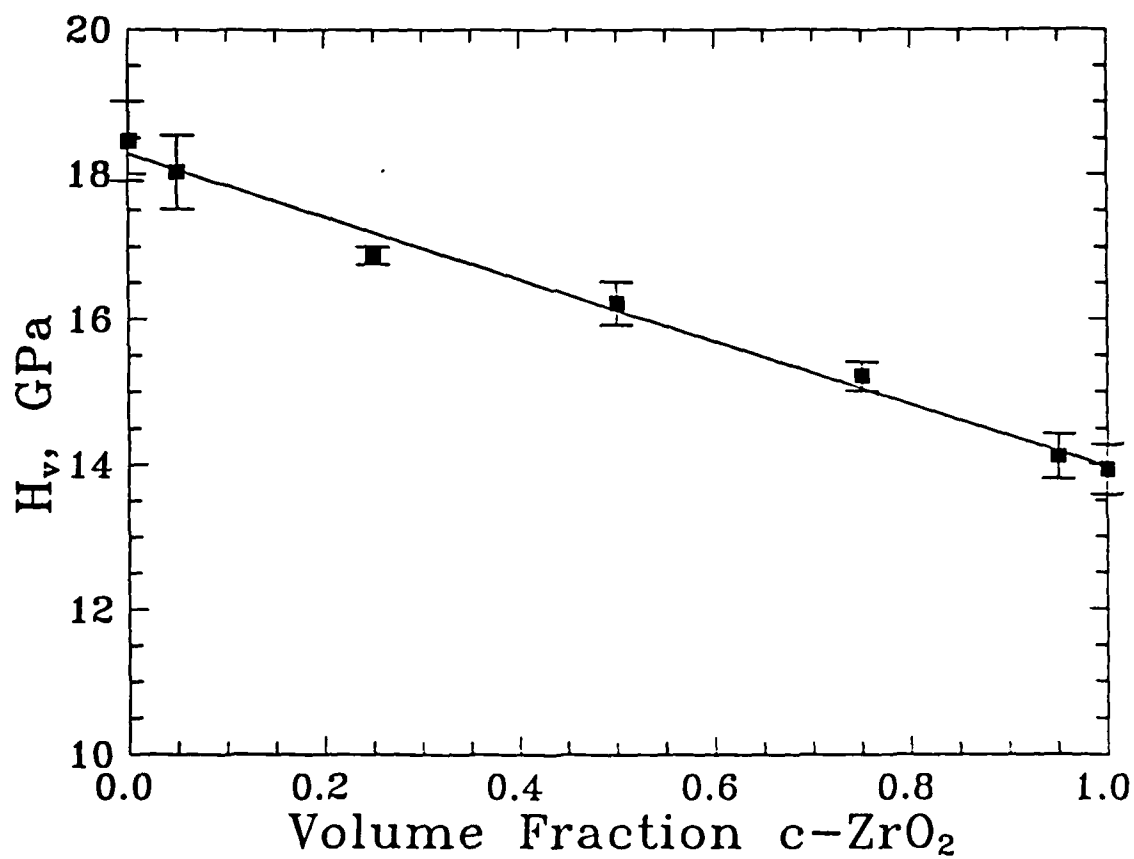
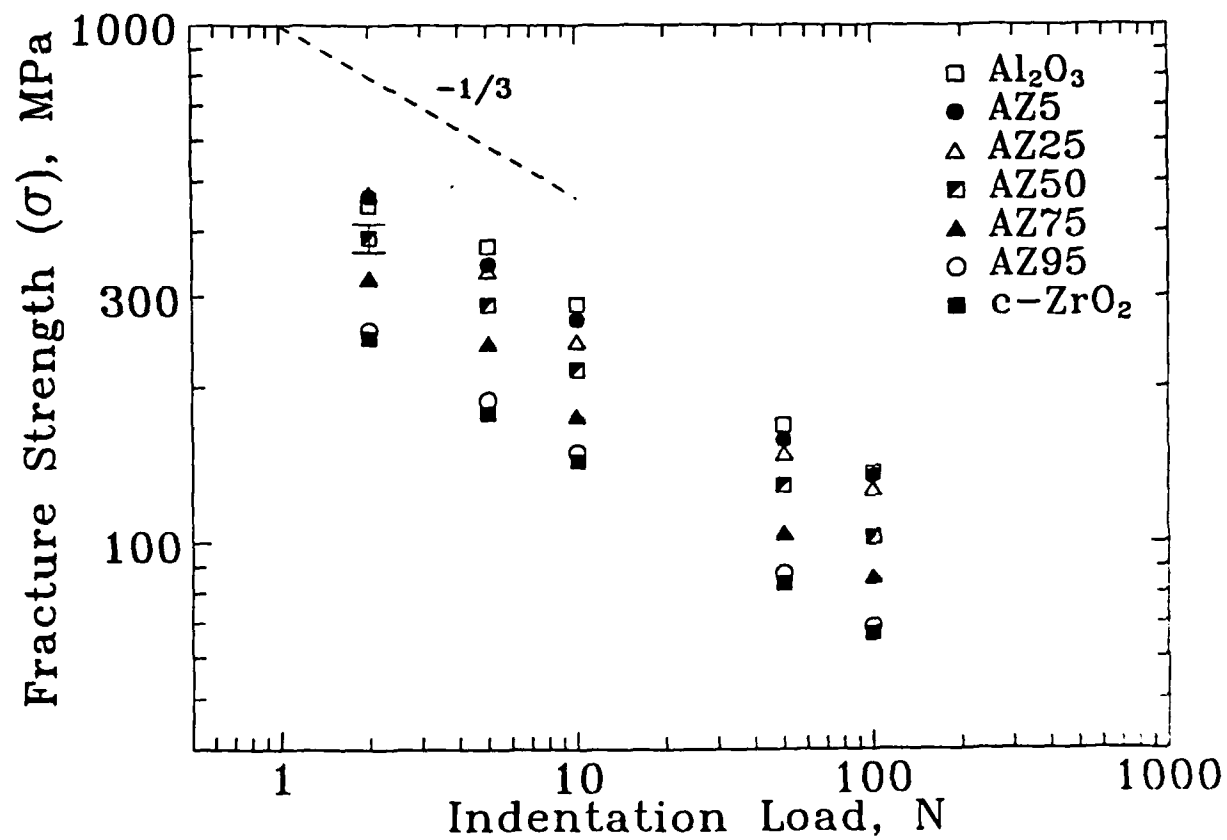


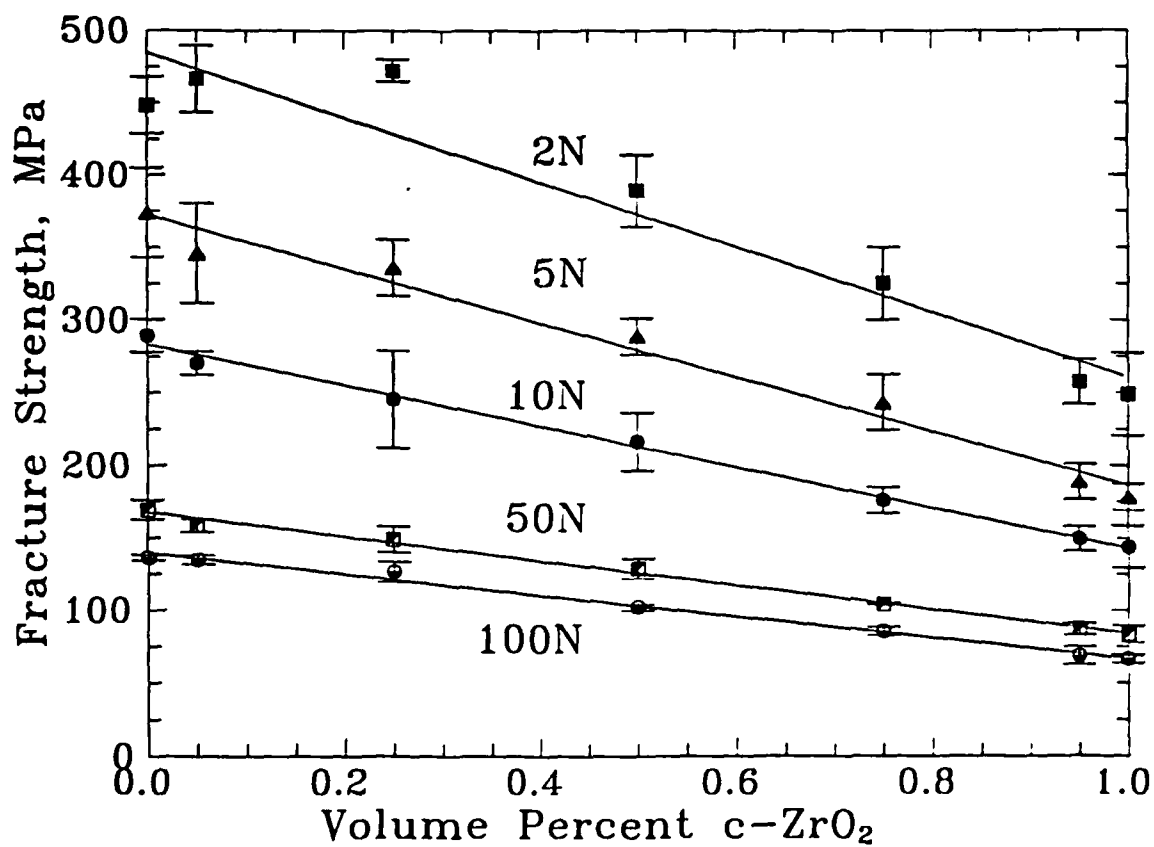
Figure 2. Vickers hardness as a function of c-ZrO<sub>2</sub> content for the AZ composites.





(a)

Figure 3. Fracture strength plotted as a function of (a) indentation load and (b) volume fraction c-ZrO<sub>2</sub> for the AZ composites.



(b)

Figure 3. Fracture strength plotted as a function of (a) indentation load and (b) volume fraction c-ZrO<sub>2</sub> for the AZ composites.

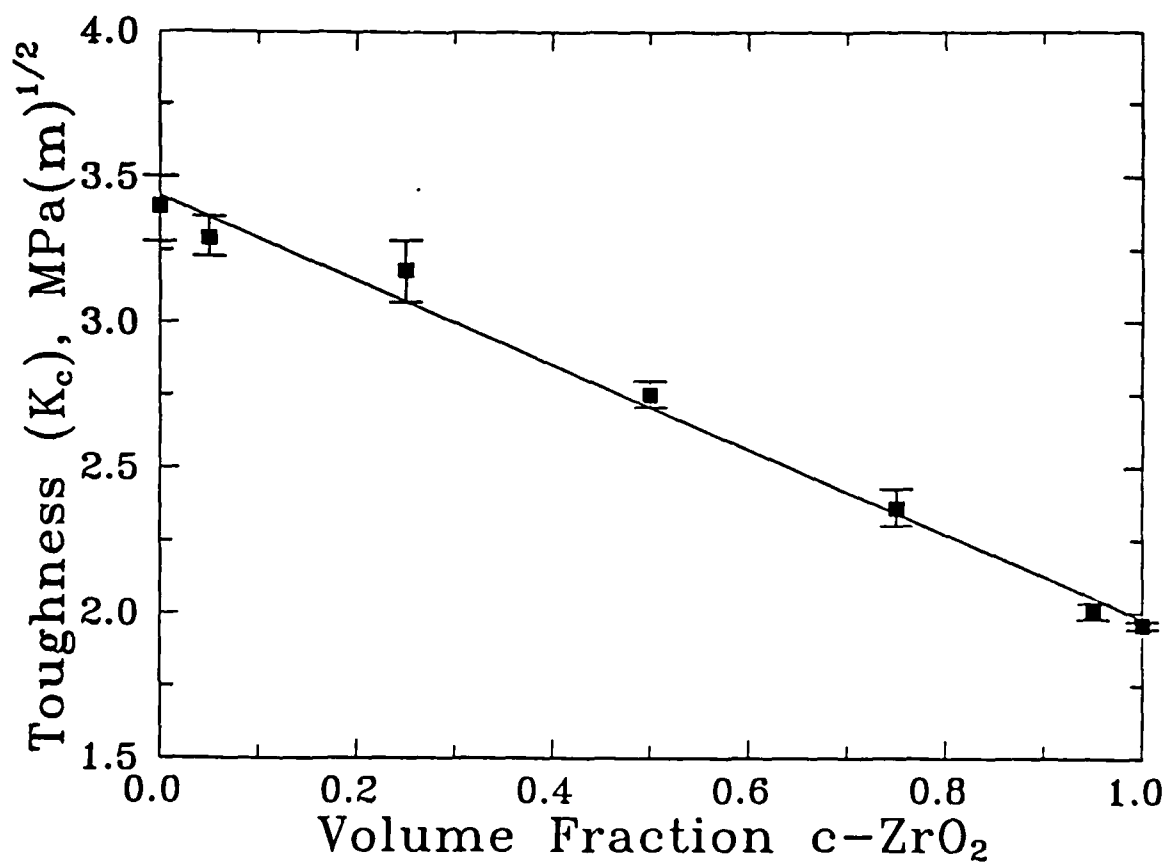


Figure 4. Fracture toughness as a function of  $c\text{-ZrO}_2$  content for the AZ composites, measured from the strength-indentation load data presented in Figure 3.

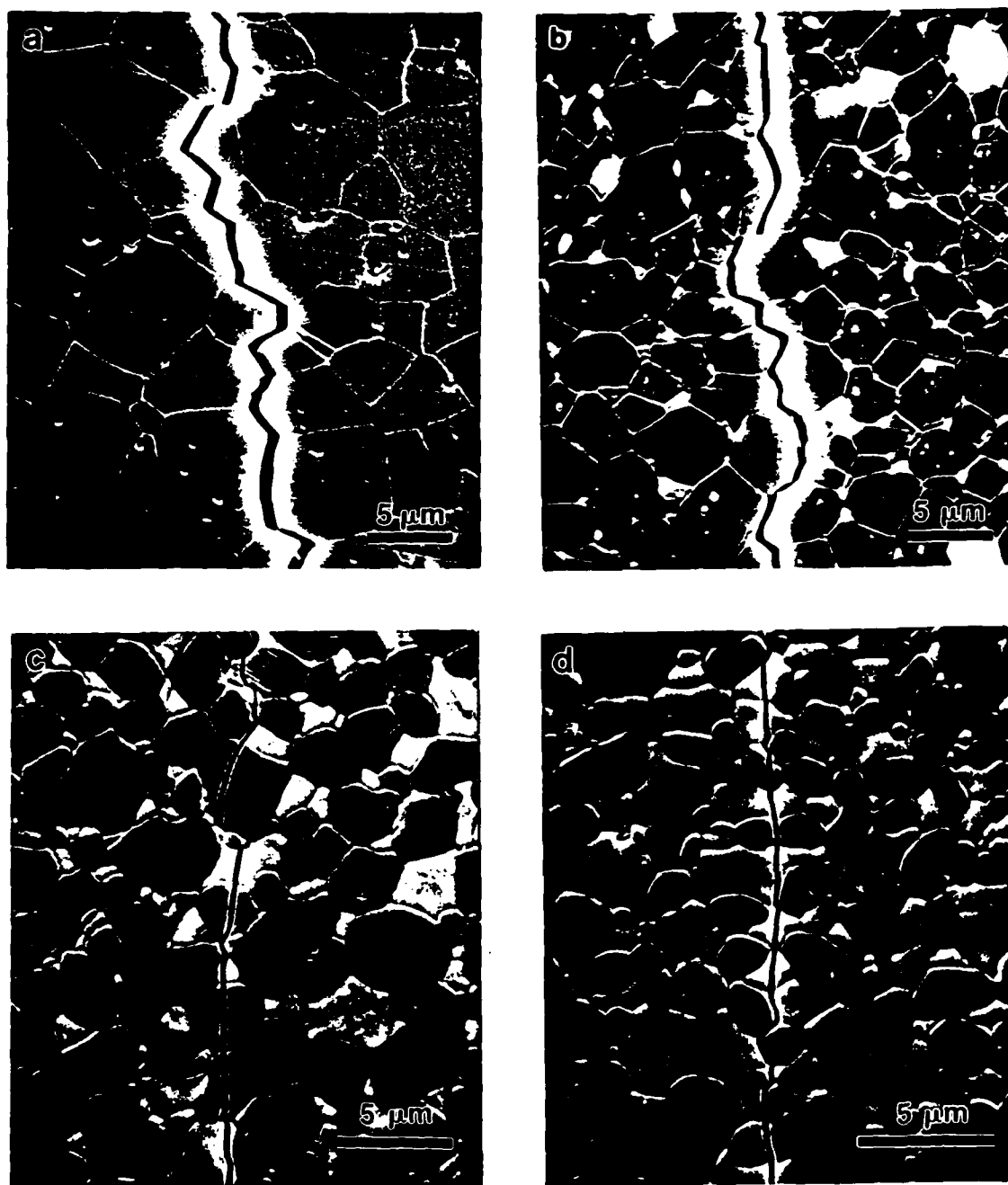


Figure 5. Typical indentation crack behavior for (a) single phase  $\text{Al}_2\text{O}_3$ , (b) AZ5, (c) AZ25, (d) AZ50, (e) AZ75, (f) AZ95 and (g) single phase c- $\text{ZrO}_2$ .

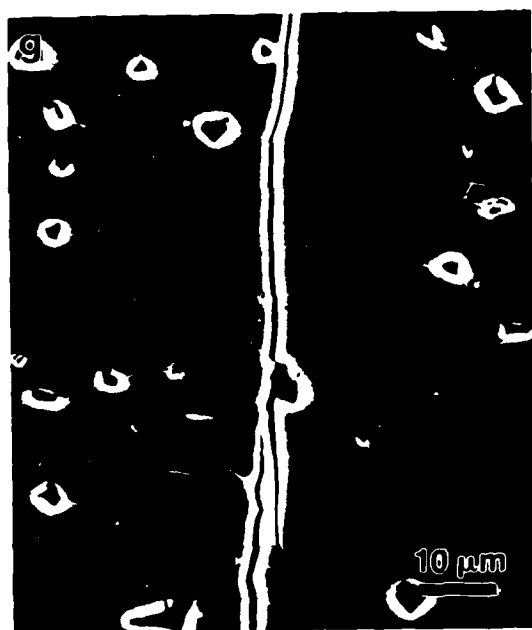
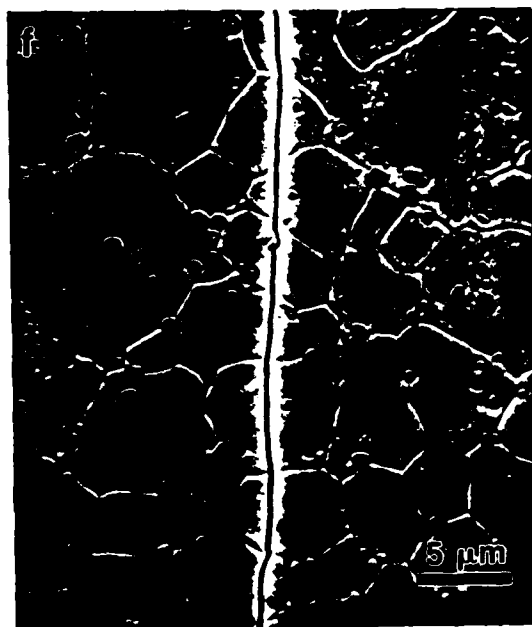


Figure 5. Typical indentation crack behavior for (a) single phase  $\text{Al}_2\text{O}_3$ , (b) AZ5, (c) AZ25, (d) AZ50, (e) AZ75, (f) AZ95 and (g) single phase c- $\text{ZrO}_2$ .

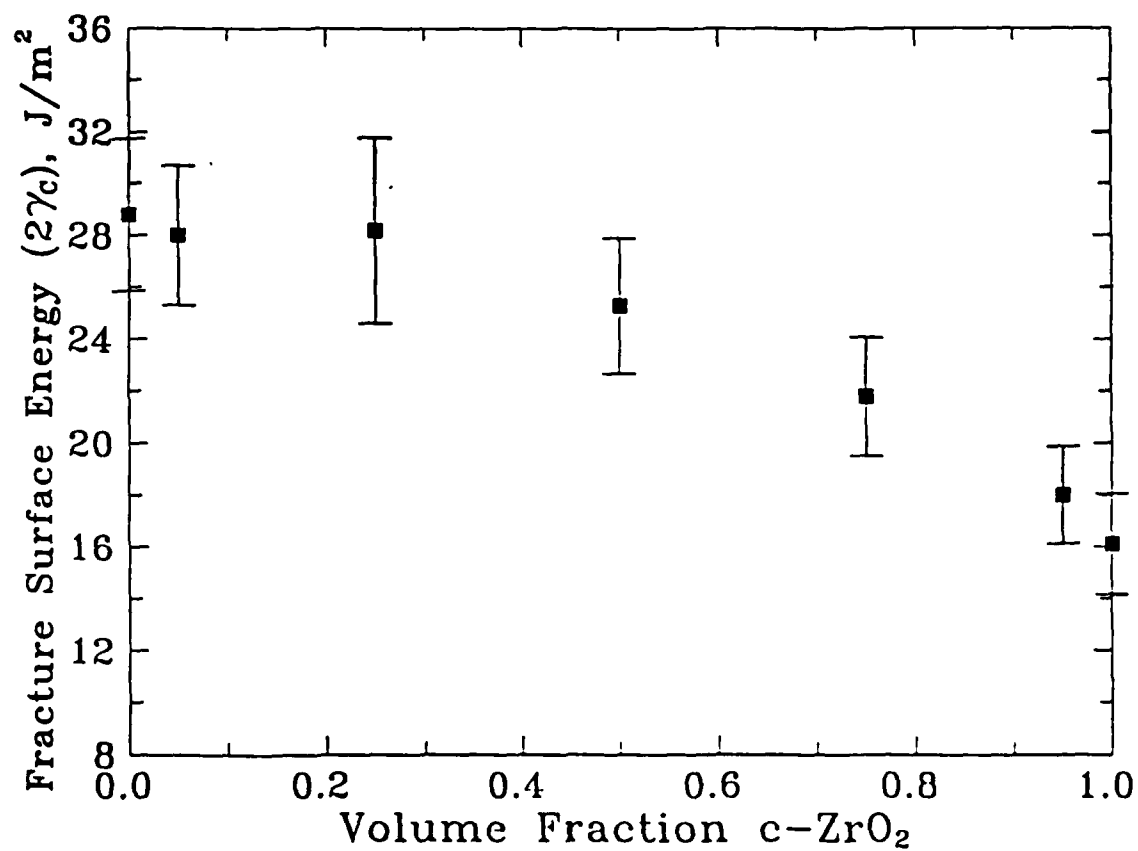


Figure 6. Fracture surface energy,  $2\gamma_c$ , as a function of c-ZrO<sub>2</sub> content for the AZ composites.

**MECHANICAL BEHAVIOR OF THE ALUMINA - MULLITE SYSTEM**

**M.D. Stuart, M.P. Harmer, H.M. Chan, and G.A. Miller**

**Materials Research Center  
Department of Materials Science and Engineering  
Lehigh University, Bethlehem, PA 18015 USA**

***Technical update for final report.***

## 1.6 Mechanical Behavior of the Alumina-Mullite System

One of the major toughening mechanisms responsible for R-curve behavior in non-transforming ceramics is grain localized bridging. Individual bridging grains in the wake of the crack tip act in a similar manner to reinforcing fibers in composite materials. They support a proportion of the applied load, thereby reducing the effective stress level at the crack tip. As the crack extends more ligamentary grains become available to help support the load and the apparent toughness continues to increase until a steady state value is acquired.

In order for such load shielding to occur the bridging grains must be held in place across the opposing crack faces. Several researchers have proposed that this takes place in non-cubic, monolithic materials by clamping stresses which result in frictional traction sites. These localized compressive stresses are generated due to differing amounts of thermal contraction on cooling of the anisotropic, crystalline grains. They play an important role in promoting flaw tolerant behavior.

The addition of mullite ( $3\text{Al}_2\text{O}_3 \cdot 2\text{SiO}_2$ ) to alumina provides a means of augmenting these residual stresses in a controlled manner. The combination of substantial thermal expansion mismatch between mullite and alumina and the thermal expansion anisotropy of the two phases is estimated to yield a residual grain boundary stress of



approximately 1 GPa. This is greater than 4 times that for single phase alumina and is intermediate to that achievable by aluminum titanate additions.

Another key microstructural element required for bridging type R-curve behavior is sufficient ligament size to span the crack opening. This is where the alumina-mullite system may have a significant advantage over other dual phase systems. The homogeneous microstructure may be coarsened, or scaled up, substantially by heat treatment above 1800°C. This is not the case for alumina-zirconia because of grain growth inhibition, and the inability to heat treat the structure above 1710°C due to the alumina-zirconia eutectoid reaction. For alumina-aluminum titanate the limitation on grain size is about 8 $\mu$ m because of spontaneous microcracking due to the magnitude of thermal expansion residual stress. Bridges in this case must be provided by heterogeneous agglomerates. The limit for grain size due to microcracking in the alumina-mullite system is predicted to be 64 $\mu$ m which would enable grains to bridge the wake of a crack for several millimeters.

The recent availability of high purity mullite powders have made it possible to produce dense alumina-mullite microstructures via conventional powder processing routes. Cleanliness was ensured by use of a class A-100 laminar flowhood for each powder preparation step. Powder combinations were mixed in a wet ball milling operation, dried, and deagglomerated by crushing. Pellets were uniaxially pressed and then wet-bag isostatically pressed,

before calcining and final sintering. Dual phase alumina-mullite ceramics have been produced in a full range of compositions; 5, 25, 50, 75, and 95 vol.%, with densities in excess of 98.5% (Fig.1). Coarsening of these homogeneous microstructures has produced grains of up to approximately 20 $\mu$ m.

The mechanical behavior of these structures is being assessed by the indentation-strength-in-bending technique. This test is particularly suited to determining a material's response to real flaws, such as those resulting from processing defects or in-service damage. Fine grained (3 $\mu$ m) alumina-50wt.% mullite was found to exhibit close to classical  $P^{-1/3}$  behavior without a significant plateau region (Fig.2). However, flaw tolerant R-curve behavior is anticipated for the coarser microstructures.

The effect of heterogeneity may also be investigated for this system by producing agglomerated phases, dispersed within a homogeneous duplex matrix. Such a study would then parallel the work done on the alumina-aluminum titanate system which displays significant R-curve behavior.

Mullite is also known for its creep resistance and high-temperature strength so that the alumina-mullite duplex system may exhibit advantageous high temperature mechanical properties. Thus, this system has the potential to complement the research performed on the alumina-zirconia duplex materials.

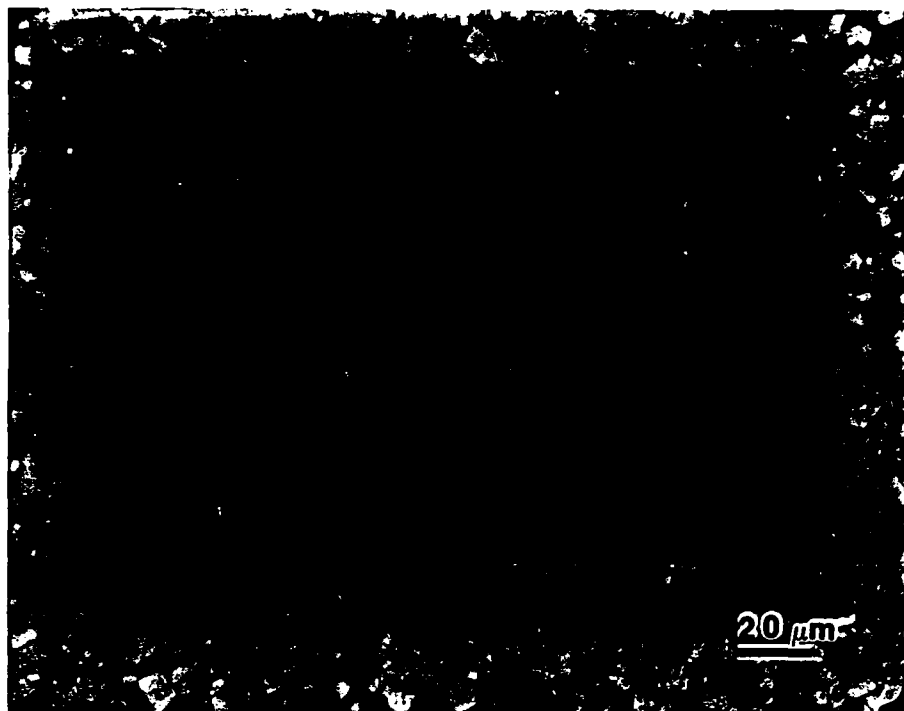


Fig. 1. Optical micrograph of alumina-50 wt.% mullite composite. The lighter phase is alumina.

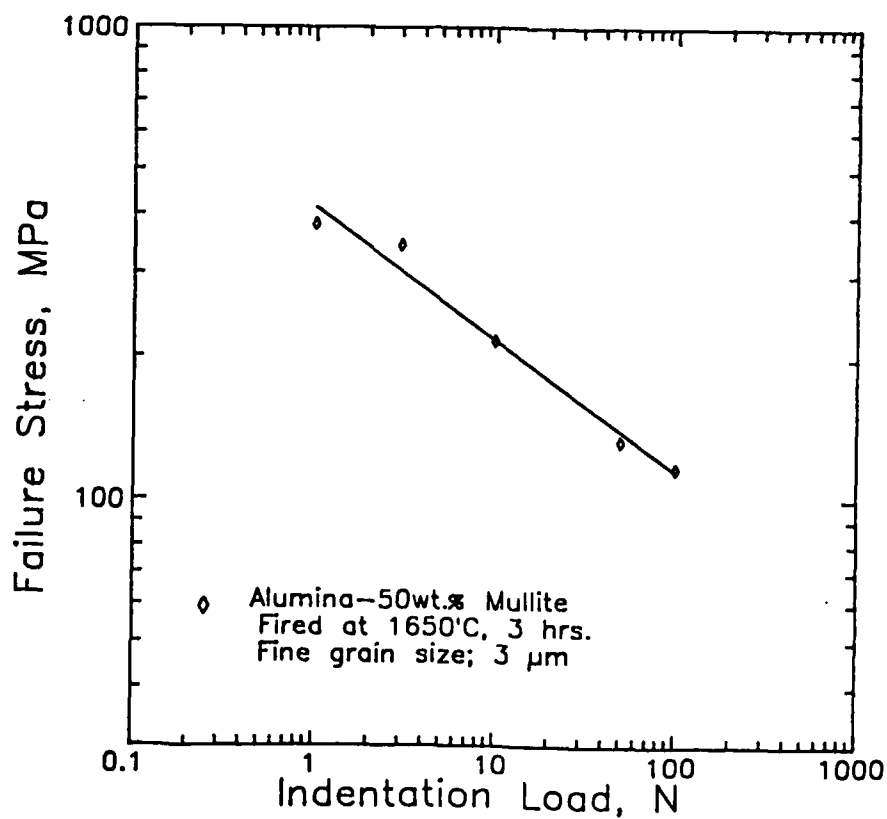


Fig. 2. Biaxial flexure strength versus Vickers indentation load for fine grained (3 $\mu$ m) alumina-50 wt.% mullite.

**CONTROLLED MICROSTRUCTURAL INHOMOGENEITY FOR  
IMPROVED FLAW TOLERANCE**

**J.D. French, N.P. Padture, M.P. Harmer, H.M. Chan, and G.A. Miller**

**Department of Materials Science and Engineering  
Lehigh University, Bethlehem, PA 18015 USA**

**Technical update for final report.**

### Controlled Microstructural Inhomogeneity for Improved Flaw Tolerance

It has been found that room temperature flaw tolerance can be enhanced in a dual-phase ceramic through the addition of controlled inhomogeneities. Due to the differential thermal expansion between the two phases, these inhomogeneous sites can act as crack bridging sites during fracture, thus improving flaw tolerance. This was accomplished in the  $\text{Al}_2\text{O}_3\text{:c-ZrO}_2$  system through the addition of 50 vol% of 50 micron spray-dried  $\text{Al}_2\text{O}_3$  agglomerates to conventional c- $\text{ZrO}_2$  powder. Typical microstructures of homogeneous and inhomogeneous AZ50 can be seen in Figure 1. The strength-indentation load response for the inhomogeneous AZ50 material shows a slight improvement in flaw tolerance, Figure 2. This effect is even more pronounced in the system  $\text{Al}_2\text{O}_3\text{:Al}_2\text{TiO}_5$ , where the differential thermal expansion between the two phases is larger than  $\text{Al}_2\text{O}_3\text{:c-ZrO}_2$ , Figure 3.

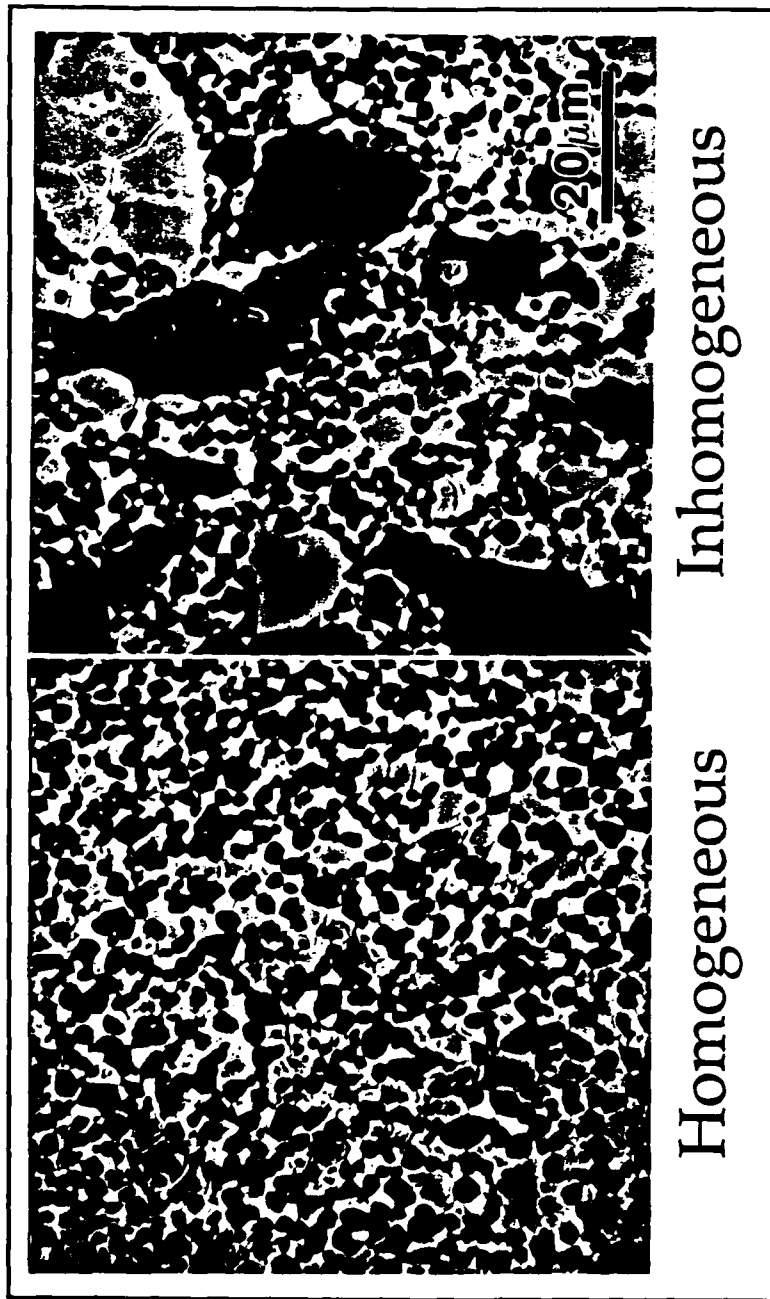


**Figure 1.** Comparison of homogeneous and inhomogeneous microstructures of AZ50 (50 vol%  $\text{Al}_2\text{O}_3$ , 50 vol% c-ZrO<sub>2</sub>).

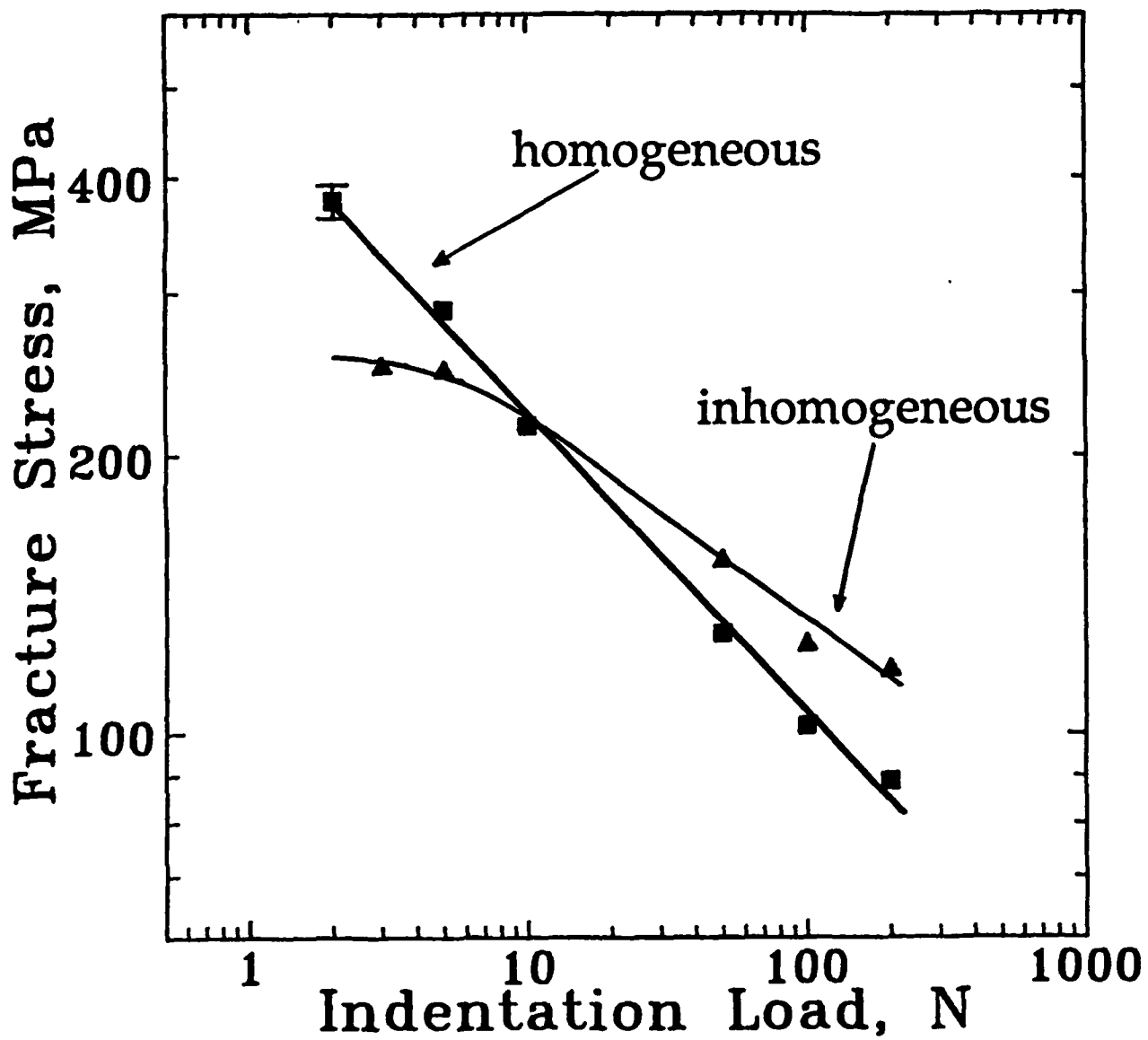
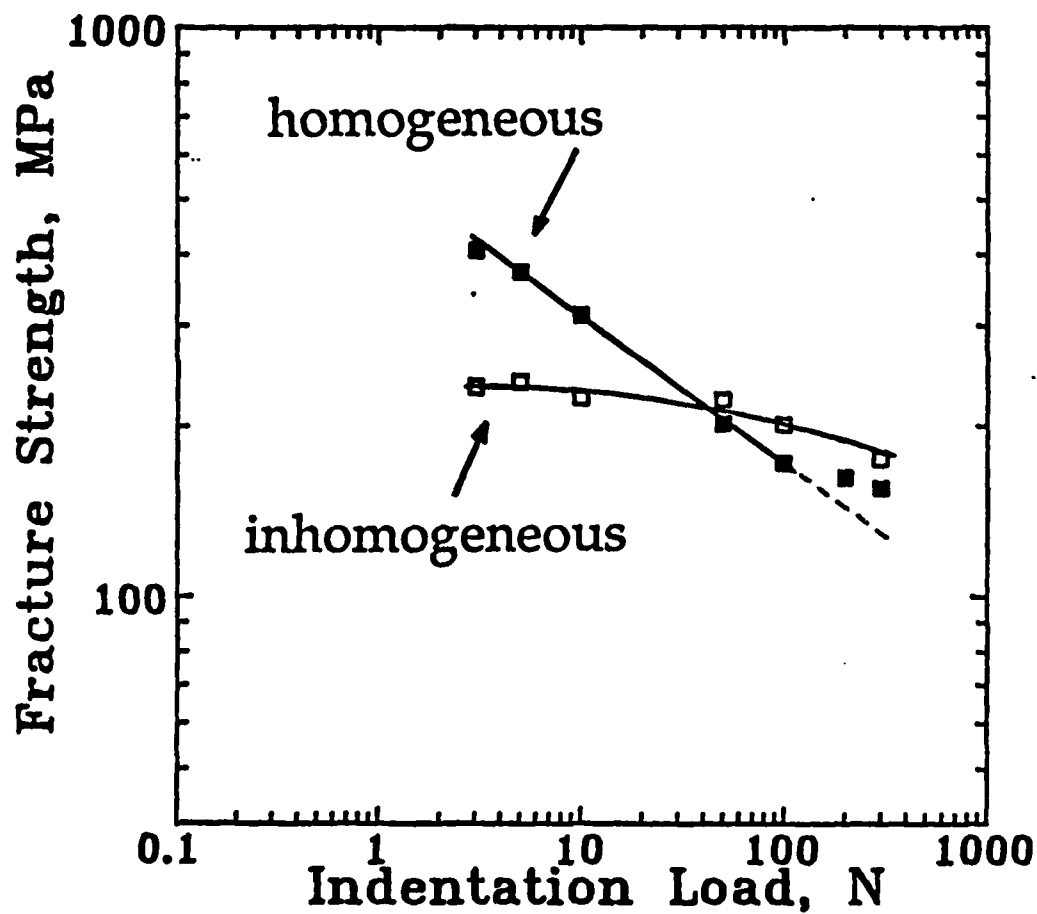


Figure 2. Strength-indentation load responses for homogeneous and inhomogeneous AZ50.



**Figure 3.** Strength-indentation load responses for homogeneous and inhomogeneous AAT20 (80 vol%  $\text{Al}_2\text{O}_3$ , 20 vol%  $\text{Al}_2\text{TiO}_5$ ). Note the severe flaw tolerance of the inhomogeneous microstructure.



FLAW TOLERANT  $\text{Al}_2\text{O}_3$ - $\text{Al}_2\text{TiO}_5$  COMPOSITES

N.P. Padture,<sup>1</sup> S.J. Bennison,<sup>2</sup> J.L. Runyan,<sup>2</sup>  
J. Rodel,<sup>2</sup> H.M. Chan,<sup>1</sup> and B.R. Lawn<sup>2</sup>

<sup>1</sup> Department of Materials Science and Engineering  
Lehigh University, Bethlehem, PA 18015 USA

<sup>2</sup> Ceramics Division  
National Institute of Standards and Technology  
Gaithersburg, MD 20899 USA

October 1990

For proceedings of symposium on composites: Processing, Microstructures  
and Properties, Orlando, FL, November 1990.

## FLAW TOLERANT $\text{Al}_2\text{O}_3$ - $\text{Al}_2\text{TiO}_5$ COMPOSITES

Nitin P. Padture,<sup>1</sup> Stephen J. Bennison,<sup>2</sup> Julie L. Runyan,<sup>2</sup> Jürgen Rödel,<sup>2</sup> Helen M. Chan,<sup>1</sup> Brian R. Lawn<sup>2</sup>

<sup>1</sup> Department of Materials Science & Engineering, Lehigh University  
Bethlehem, PA 18015

<sup>2</sup> Ceramics Division, National Institute of Standards & Technology  
Gaithersburg, MD 20899

### ABSTRACT

Fabrication of particulate-reinforced  $\text{Al}_2\text{O}_3$ - $\text{Al}_2\text{TiO}_5$  composites, with controlled homogeneous and heterogeneous microstructures, is described. The degree of flaw-tolerance in these composites, as determined by indentation-strength testing, is enhanced by the strong thermal expansion anisotropy stresses associated with the  $\text{Al}_2\text{TiO}_5$  particles and by the scale of the microstructure. In situ scanning electron microscope observations of bridging grains at propagating cracks in the microstructure are analyzed. The role of key microstructural elements in the underlying toughness-curve behavior responsible for the flaw-tolerance is discussed.

### INTRODUCTION

Researchers in recent years have demonstrated R-curves, i.e. an increasing crack resistance with crack size, in  $\text{Al}_2\text{O}_3$ -based ceramics [1-3]. A most important manifestation of this property is "flaw tolerance", i.e. near-invariance in strength over a broad range of flaw sizes. The major toughening mechanism responsible for R-curve behavior in  $\text{Al}_2\text{O}_3$  ceramics has been identified as grain-localized bridging of the crack-wake interface [2,4]. The bridging grains are "clamped" in the matrix by internal compressive stresses from thermal expansion anisotropy (TEA), which augment frictional closure tractions from pullout during crack propagation [5]. Further to internal stresses, microstructural scaling parameters appear as important variables in the ensuing toughness equation [5].

The present paper reports on processing strategies to

optimize the effect of TEA stresses and microstructural scaling on the R-curve. TEA in monophase  $\text{Al}_2\text{O}_3$  is relatively small, but can be enhanced by the incorporation of a suitable second phase.  $\text{Al}_2\text{TiO}_5$  was chosen in this study because it has large TEA; it also has low solubility in  $\text{Al}_2\text{O}_3$ , and does not form intermediate phases [6-8]. Estimates of the internal stress in  $\text{Al}_2\text{O}_3$ - $\text{Al}_2\text{TiO}_5$  yield  $\approx 3$  GPa [8], greater than in  $\text{Al}_2\text{O}_3$  by a factor  $\approx 10$ .

The simplest way to scale up ceramic microstructures is by heat treatments [8,9,11]. However, coarsening of ceramics containing  $\text{Al}_2\text{TiO}_5$  is severely restricted by an enhanced tendency to spontaneous microcracking [8]. To circumvent this problem scaling was achieved through controlled additions of large  $\text{Al}_2\text{O}_3$  grains within an otherwise fine-grained  $\text{Al}_2\text{O}_3$ - $\text{Al}_2\text{TiO}_5$  matrix.

It will be seen in the subsequent sections that the tailored  $\text{Al}_2\text{O}_3$ - $\text{Al}_2\text{TiO}_5$  composites show profoundly enhanced flaw tolerance, hence stronger R-curves.

## EXPERIMENTAL

Conventional ceramic processing routes were used to fabricate 80/20 vol%  $\text{Al}_2\text{O}_3$ / $\text{Al}_2\text{TiO}_5$  composites. Powders of high purity  $\alpha$ - $\text{Al}_2\text{O}_3$  (Sumitomo AKP-HP, 0.5  $\mu\text{m}$ ) and  $\beta$ - $\text{Al}_2\text{TiO}_5$  (Trans-Tech, crystallites 1-5  $\mu\text{m}$ , agglomerates 10-20  $\mu\text{m}$ ) were mixed under class A-100 clean-room conditions, dispersed in methanol and stir-dried. Three batches were prepared: A, homogeneous, with a pre-drying ball-milling stage to remove the agglomerates; B, heterogeneous, with spray-dried  $\text{Al}_2\text{O}_3$  agglomerates (25  $\mu\text{m}$ ) added to the ball-milled mix before drying; C, heterogeneous, similar to A but without ball milling, to retain  $\text{Al}_2\text{TiO}_5$  agglomerates (10-20  $\mu\text{m}$ ).

Disks 4 mm thick were uniaxially pressed at 50-60 MPa followed by wet-bag isostatic pressing at 350 MPa. These disks were calcined at 1050°C for 12 hr, then sintered at 1550-1600°C for 1-17 hr. Microstructures were examined in the SEM and characterized using routine ceramographic procedures.

Prospective tensile sides of 20 mm diam. disks were polished to 1  $\mu\text{m}$ , followed by indentation at the face center with a Vickers diamond at loads from 3 to 300 N. The indented specimens were then broken in biaxial flexure and the strengths determined. Details of this method are described elsewhere [3].

Compact-tension geometry fracture specimens were machined from 50 mm diameter disks for crack-interface examinations. These examinations were made in situ using a mechanical loading fixture housed in an SEM [10].

## RESULTS

Figure 1 shows the microstructures of materials A, B and C. The base size of the matrix  $\text{Al}_2\text{O}_3$  grains is consistently  $\approx 6$   $\mu\text{m}$ .

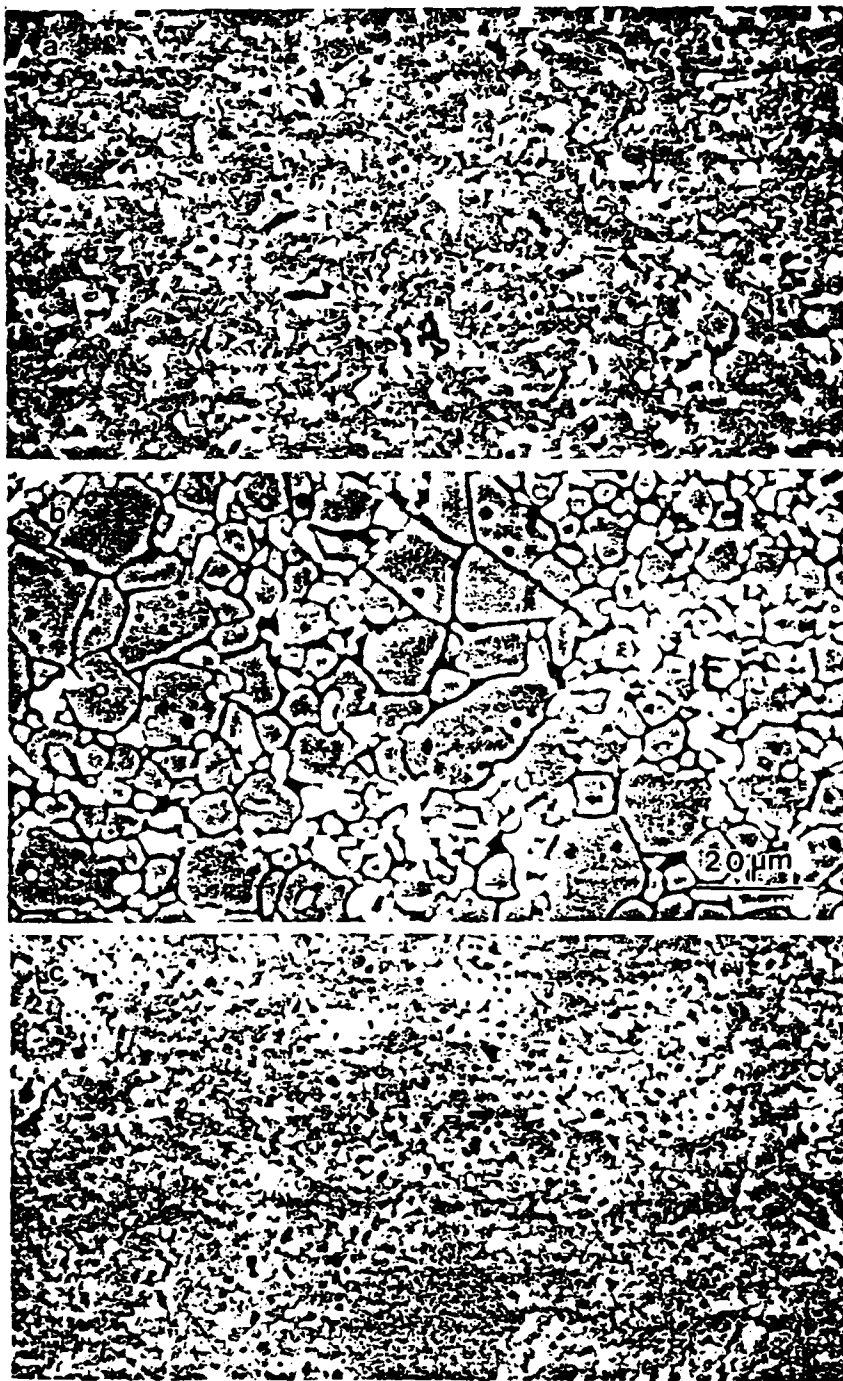


Figure 1. SEM microstructures of composites of 80% Al<sub>2</sub>O<sub>3</sub> (dark grains) and 20% Al<sub>2</sub>TiO<sub>5</sub> (light grains): (a) homogeneous material A, (b) heterogeneous material B; (c) heterogeneous material C. Samples polished to 1 μm and thermally etched.

In material A, fig. 1a, the  $\text{Al}_2\text{TiO}_5$  grains are homogeneously distributed, but are about half the size of the  $\text{Al}_2\text{O}_3$  grains. In material B and C, figs. 1b and 1c, distributions of relatively large heterogeneities are evident:  $\text{Al}_2\text{O}_3$  agglomerates in B;  $\text{Al}_2\text{O}_3$  and  $\text{Al}_2\text{TiO}_5$  agglomerates in C. Densities in all cases exceed 98% of the theoretical limit.

Figure 2 shows data for strength against indentation load for the three composites, together with a comparative curve computed for 6  $\mu\text{m}$  pure  $\text{Al}_2\text{O}_3$  from an earlier study [11]. The composites show significantly lower strength sensitivity to starter flaw size, i.e. greater flaw tolerance, than the base  $\text{Al}_2\text{O}_3$ . Further, the sensitivity decreases in the composite sequence A→B→C, i.e. with more pronounced heterogeneity.

Figure 3 shows SEM micrographs of a bridging site taken at two stages of monotonic loading, in material B. Grain-facet frictional contacts at points P and Q act on the large (alumina) grain. (The frictional tractions were sufficient to eject this grain totally from the matrix at a later stage in the crack opening.) Highly active bridge sites of this kind were significantly more prevalent in the composites than in the base  $\text{Al}_2\text{O}_3$ .

## DISCUSSION AND CONCLUSION

We conclude from the above results that  $\text{Al}_2\text{O}_3$ -based composites can show considerably enhanced flaw tolerance relative to base  $\text{Al}_2\text{O}_3$ . This enhanced tolerance is a manifestation of a more pronounced R-curve [4], resulting in turn from stronger grain-interlock bridging.

Specifically, it is evident that high residual TEA stresses and heterogeneity are key factors in the increased flaw tolerance. Simplistically, internal stresses contribute by augmenting the frictional tractions at sliding grain facets during pullout [5]. Heterogeneity increases the pullout distance at the larger individual grains. Predictive modelling of the resultant enhanced bridging in two-phase ceramics should provide useful guidelines for improved microstructural design of structural ceramics [5,12].

We note finally that the approach advocated here of including controlled heterogeneous stress centers to augment bridging is in strong violation of conventional ceramics processing wisdom, where one seeks to produce ultra-fine, defect-free microstructures. Ours is a philosophy of containing cracks, not of eliminating them. In the same context, it may be pointed out that those very same internal stress sources that enhance long-crack toughness also may lead to deleterious short-crack properties like wear, spontaneous microcracking and fatigue [12].

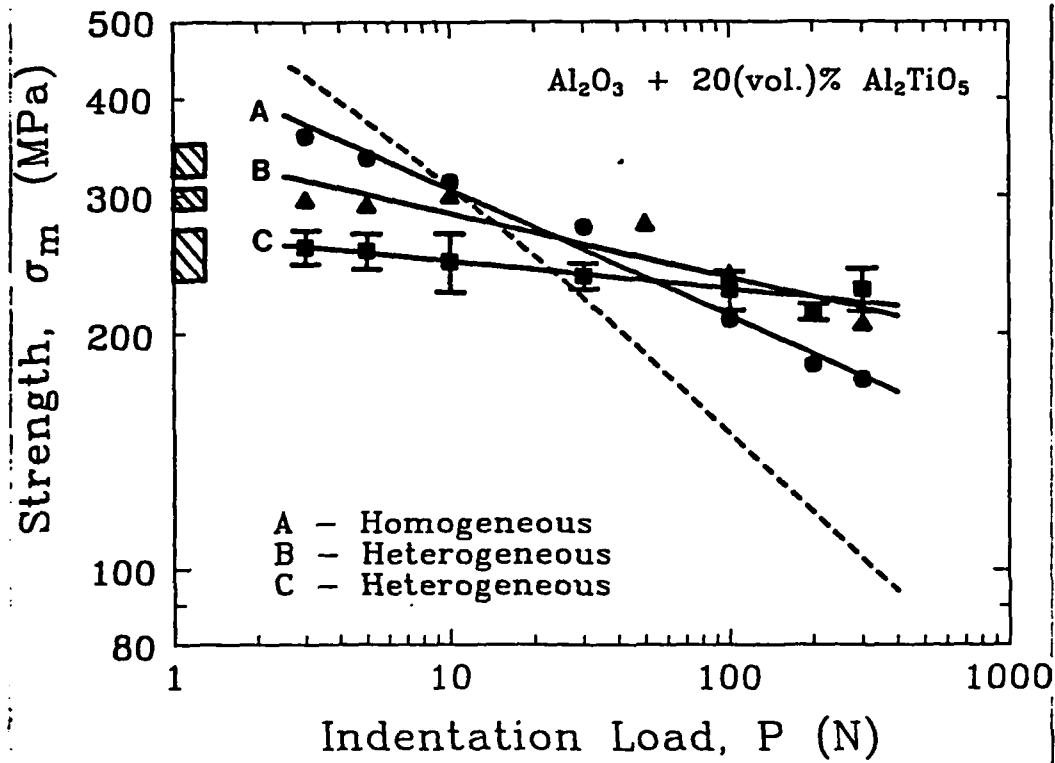


Figure 2. Indentation load versus strength plots. Data with solid curves for composite materials A, B and C. Error bars omitted from A and B data for clarity. Shaded area to left represents failures from natural flaws. Comparative dashed curve for  $\text{Al}_2\text{O}_3$  of same grain size.

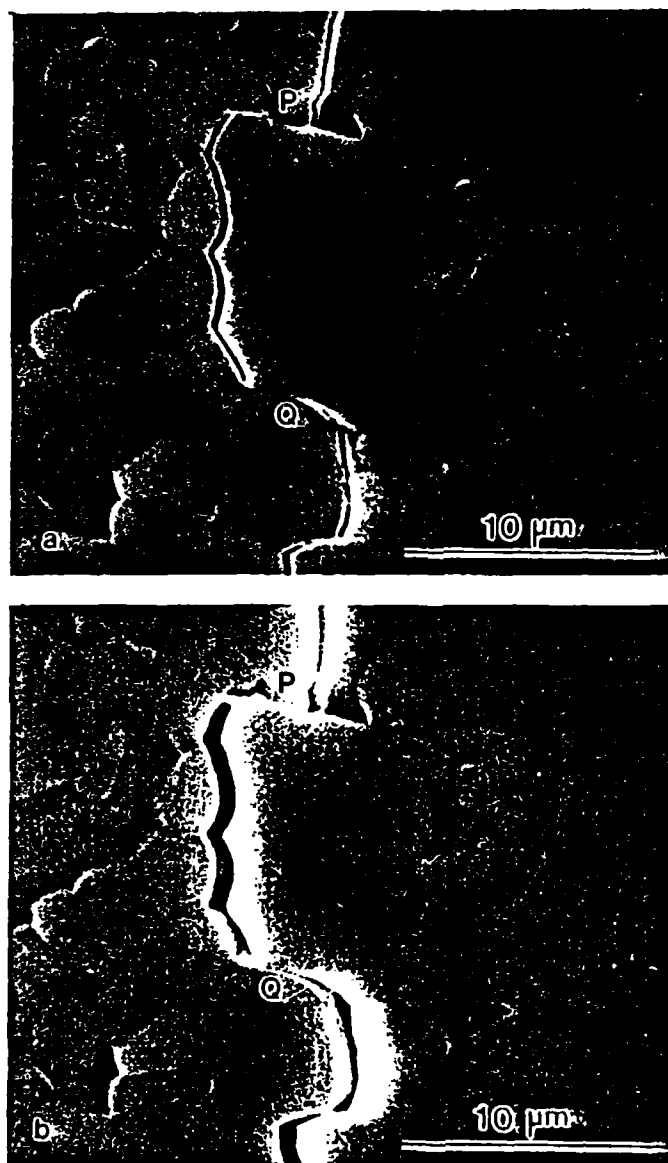


Figure 3. Bridging site at large alumina grain in composite B, showing frictional contact points at P and Q. Micrographs taken in situ with load applied in SEM.

## ACKNOWLEDGEMENTS

Funding for this work was provided by the Air Force Office of Scientific Research and E.I. duPont de Nemours and Co. Inc.

## REFERENCES

1. H. Hübner and W. Jillek, "Sub-Critical Crack Extension and Crack Resistance in Polycrystalline Alumina", *J. Mater. Sci.* 12[1] 117-25 (1977).
2. R. Knehans and R.W. Steinbrech, "Memory Effect of Crack Resistance During Slow Crack Growth in Notched  $Al_2O_3$  Bend Specimens," *J. Mater. Sci. Lett.* 1[8] 327-29 (1982).
3. R.F. Cook, B.R. Lawn and C.J. Fairbanks, "Microstructure-Strength Properties in Ceramics: I. Effect of Crack Size on Toughness," *J. Amer. Ceram. Soc.* 68[11] 604-15 (1985).
4. P.L. Swanson, C.J. Fairbanks, B.R. Lawn, Y-W. Mai and B.J. Hockey, "Crack-Interface Bridging as a Fracture Resistance Mechanism in Ceramics: I. Experimental Study on Alumina," *J. Amer. Ceram. Soc.* 70[4] 279-89 (1987).
5. S.J. Bennison and B.R. Lawn, "Role of Interfacial Grain-Bridging Sliding Friction in the Crack-Resistance and Strength Properties of Non-transforming Ceramics," *Acta Metall.* 37[10] 2659-71 (1989).
6. G. Bayer, "Thermal Expansion Anisotropy of Oxide Compounds," *Proc. Br. Ceram. Soc.* [22] 39-53 (1973).
7. S. M. Lange, C. L. Fillmore and L. H. Maxwell, "The System Beryllia-Alumina-Titania: Phase Relations and General Properties of Three-Component Porcelains," *J. Res. Natl. Bur. Stds.* 48[4] 298-301 (1952).
8. J.L. Runyan and S.J. Bennison, "Flaw Tolerance Properties of Aluminum Titanate reinforced Alumina Ceramics," *J. Europ. Ceram. Soc.*, in press.
9. S.J. Bennison, H.M. Chan and B.R. Lawn, "Effect of Heat Treatment on Crack-Resistance Curves in Liquid-Phase-Sintered Alumina," *J. Amer. Ceram. Soc.* 72[4] 677-79 (1989).
10. J. Rödel, J.F. Kelly and B.R. Lawn, *J. Amer. Ceram. Soc.* "In Situ Measurements of Bridged Crack Interfaces in the SEM," *J. Amer. Ceram. Soc.*, in press.
11. P. Chantikul, S.J. Bennison and B.R. Lawn, *J. Amer. Ceram. Soc.*, "Role of Grain Size in the Strength and R-curve Properties of Alumina," *J. Amer. Ceram. Soc.* 73[8] 2419-27 (1990).
12. S.J. Bennison, J. Rödel, S. Lathabai, P. Chantikul, B.R. Lawn "Microstructure, Toughness Curves and Mechanical Properties of Alumina Ceramics," *Toughening Mechanisms in Quasi-Brittle Materials*, Kluwer Academic Publishers, Dordrecht, The Netherlands, in press.



**OPTIMIZATION OF STRENGTH AND TOUGHNESS USING LAMINATES**

**C.J. Russo, M.P. Harmer, H.M. Chan, and G.A. Miller**

**Materials Research Center  
Department of Materials Science and Engineering  
Lehigh University, Bethlehem, PA 18015 USA**

**Technical update for final report.**

## 1.9 OPTIMIZATION OF STRENGTH AND TOUGHNESS USING LAMINATES

### I. Trilayer Composites.

Our objective is to create a laminated composite which has high strength over a large range of flaw sizes. Many conventional fine-grained ceramics have high strength, but only when the initial flaw size is small. Their low strength for larger flaws can be increased if an R-curve-inducing toughening mechanism is activated (such as grain bridging), but then the small flaw strength usually decreases. This illustrates a significant disadvantage associated with some R-curve phenomena. The improvement in toughness brought about by the R-curve mechanism is typically achieved at the expense of strength, a fact which has often been cited in criticism of flaw tolerant ceramics. We have been trying to improve the strength of such materials in the small flaw regime, while maintaining their high strength for larger flaws, by using a composite design.

Our approach has been to place a material which shows a  $\sigma - P$  response on the surface of a more flaw tolerant material having a flat  $\sigma - P$  response. Such a composite could, in principle, exhibit high strength over the entire range of starting flaw sizes (see Fig. 1). A key variable influencing the strength of the composite is the thickness of the surface layer. If this layer is too thick, the composite behaves as if it were made of the surface material alone (Figs. 2 & 3). On the other hand, when the surface layer is too thin, the composite ignores this layer

and takes on the strength of the underlying material (Fig. 4). We are presently varying the thickness of the surface material (between 30 and 250  $\mu\text{m}$ ) to see whether the desired composite can be produced.

Originally, we tried to make these composites using a fine grained alumina surface and a coarse, agglomerated alumina + 20 vol% aluminum titanate (A-AT20) body. Thus far, we have been unable to produce this microstructure, apparently because of titanium interdiffusion from the body material. A variety of surface materials were tried, including undoped alumina, 5 vol%  $\text{ZrO}_2$ -doped alumina, 500 ppm MgO-doped alumina, and 3 wt% MgO-doped alumina. In all cases, diffusion of titanium from the interior promoted grain growth in the surface layer, often resulting in huge, elongated grains (see Figs. 5 & 6). This abnormal grain growth can be prevented by firing at reduced temperatures (e.g. 1500C rather than 1600C); however, the body material then loses its coarseness and consequently, its flaw tolerance. If a longer sintering time at the lower temperature is used to regain the flaw tolerance of the body material, then the surface material once again exhibits the coarse, elongated grain structure seen at higher temperatures. It should be noted that although the MgO doping has not worked so far, we have not exhausted the possibilities, and are continuing to explore its use in controlling the microstructure of the surface layer.

For now, we have altered our strategy. Previous work has shown a significant difference between the indentation-strength

response of homogeneous and inhomogeneous A-AT20 (Fig. 7). The homogeneous material shows nearly a  $-1/3 \sigma - P$  response; while the inhomogeneous material shows the flaw tolerant, flat  $\sigma - P$  response (Fig. 7). The difference in their small flaw strengths is not as great as the difference between alumina and inhomogeneous A-AT20; but it is appreciable nonetheless. Making the surface layer out of homogeneous A-AT20 affords the opportunity to produce the desired composite without any composition gradients between the surface and the body, which eliminates the interdiffusion problem. Homogeneous A-AT20 is produced by thoroughly mixing the tape casting slurry in a 48 hour ball milling step. The inhomogeneous material is made by cutting the milling step down to about 6 hours, which results in poor mixing and a severely agglomerated tape. When sintered, such a tape produces a fine-grained matrix of fairly well dispersed  $Al_2O_3 + Al_2TiO_5$ , which contains coarse, polycrystalline islands of both alumina and aluminum titanate. We are presently varying the thickness of the homogeneous surface layer.

An abstract covering this work has been submitted to the Symposium on Ceramic Matrix Composites at the 93rd Annual Meeting of the American Ceramic Society in Cincinnati, and is included in the publications section of this report.

## II. Multilayer Composites.

The work described in this section represents our attempt to take advantage of some of the microstructures produced in the

surfaces of the trilayers. The multilayer composites consist of many thin ( 35um), alternating layers of A-AT20 and undoped alumina (See Fig. 8). The material is considered to be essentially A-AT20, and the alumina layers are considered to modify this A-AT20 by providing large, elongated grains of alumina to act as bridges. The A-AT20 is homogeneous, and forms a fine grained matrix. The alumina layers are initially undoped; but, during sintering, some titanium from the A-AT20 layers diffuses into the alumina layers, producing elongated grains (See Fig. 9). It was desired to have each alumina layer completely made up of large elongated grains, so that wherever a crack intersected an alumina layer, it would encounter a bridge.

These composites are similar to the materials being produced with controlled inhomogeneity by N. Padture and J.D. French (see attached publications). In their materials, a fine grained matrix of A-AT30 is modified by the addition of large alumina agglomerates, which are distributed uniformly throughout the body. During sintering, those alumina agglomerates evolve into coarse polycrystalline islands consisting of several alumina grains, which act as bridges during fracture. With this technique, however, no prior control can be exerted over the spacing between the bridging grains. The bridge spacing was an uncontrolled parameter whose value was determined through numerical analysis of  $\sigma - P$  data. In the laminated composites, it is expected that the bridge spacing can be directly controlled by varying the thickness of the alumina and A-AT20 layers. In this way, we can study the

effect of bridge spacing on toughness and strength.

Four of these laminated composites have been produced, and the indentation-strength (at 100N indent load) was measured to be 207 MPa. This result was encouraging, because the strength of the composites was about 30% greater than the strengths of the two constituent materials (at same indent load). In addition, the microstructure of these composites can be further improved, so further increases in strength and toughness are expected. For example, the number density of large, elongated alumina grains in the undoped alumina layers can be increased by modifying the sintering schedule (see Fig. 10), and this should provide more bridging sites.

In order to more fully characterize the toughness and R-curve behavior, and thus to better study the effect of bridge spacing on toughness, we plan to begin testing these composites in the Single Edge Notched Beam (SENB) geometry.

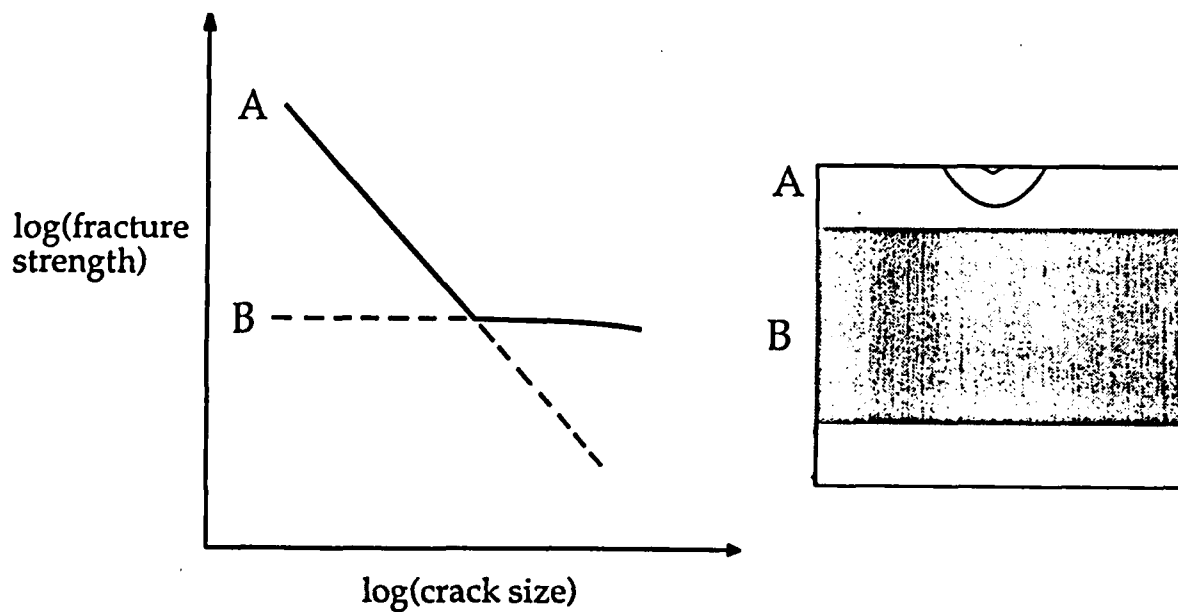


Figure 1. Desired trilayer composite material will show strength behavior indicated by solid line. Material A is a high strength, non-R-curve material; material B is a high toughness, R-curve material. By optimizing the thickness of material A, the composite will have highest possible strength over the entire range of starting flaw sizes.

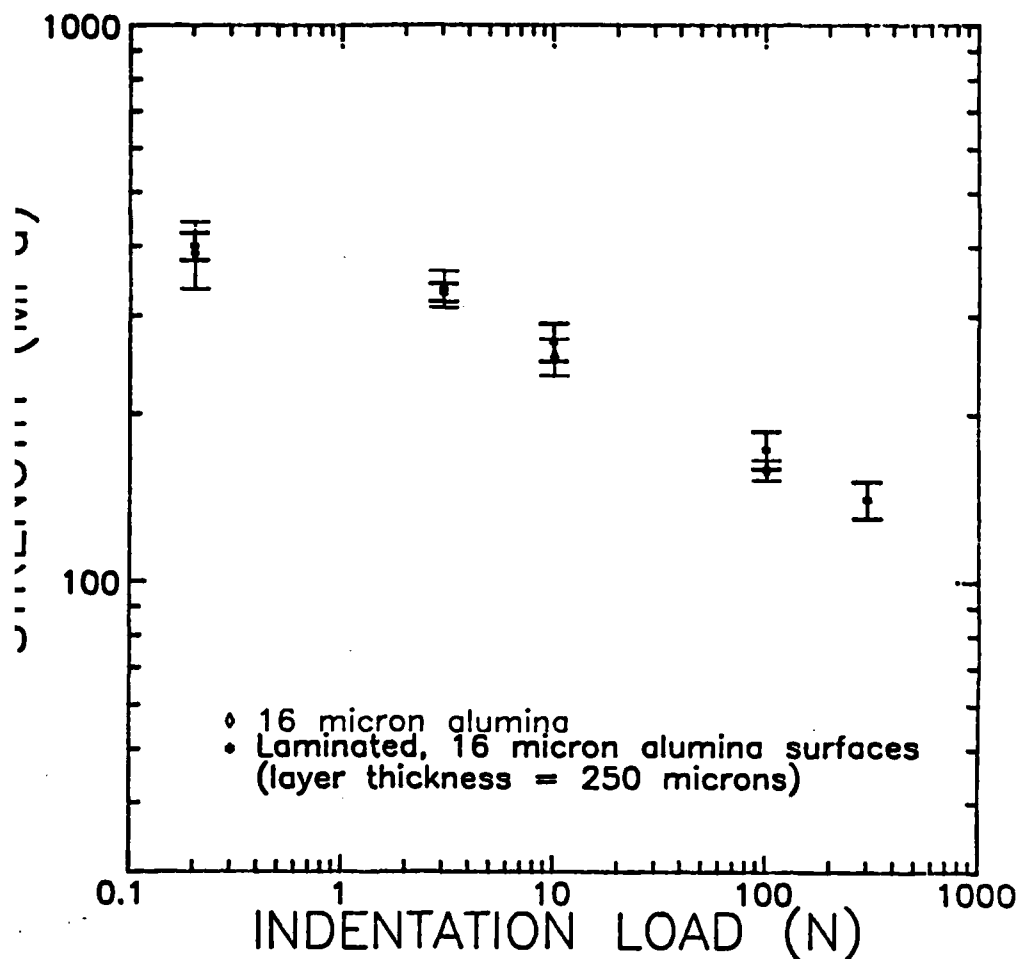


Figure 2. Indentation strengths of monolithic 16  $\mu$ m grained alumina and laminated 16 $\mu$ m/2 $\mu$ m alumina composite having 16 $\mu$ m alumina on surfaces. Note that the laminate strength is same as the strength of the surface material alone.

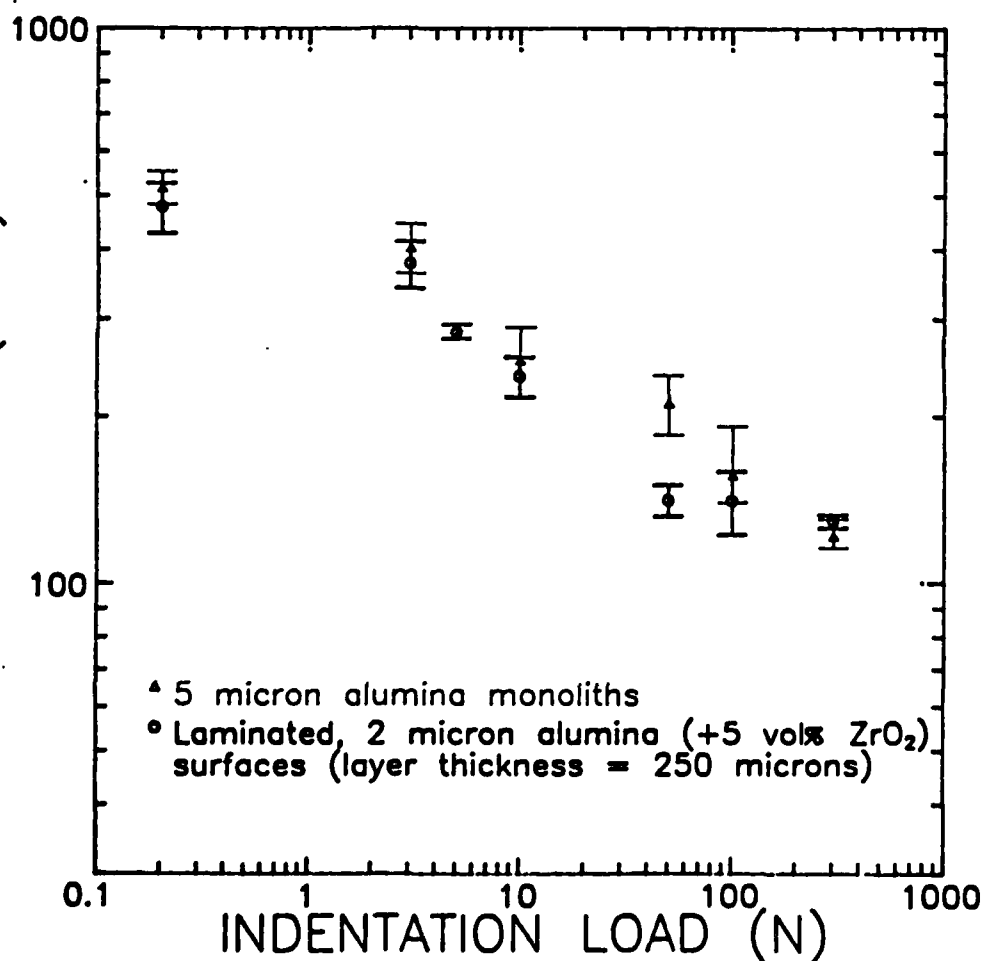


Figure 3. Indentation strengths of monolithic fine grained alumina and laminated 16 $\mu$ m/2 $\mu$ m alumina composite having 2 $\mu$ m alumina on surface. Note again that laminate strength is same as strength of surface material alone.



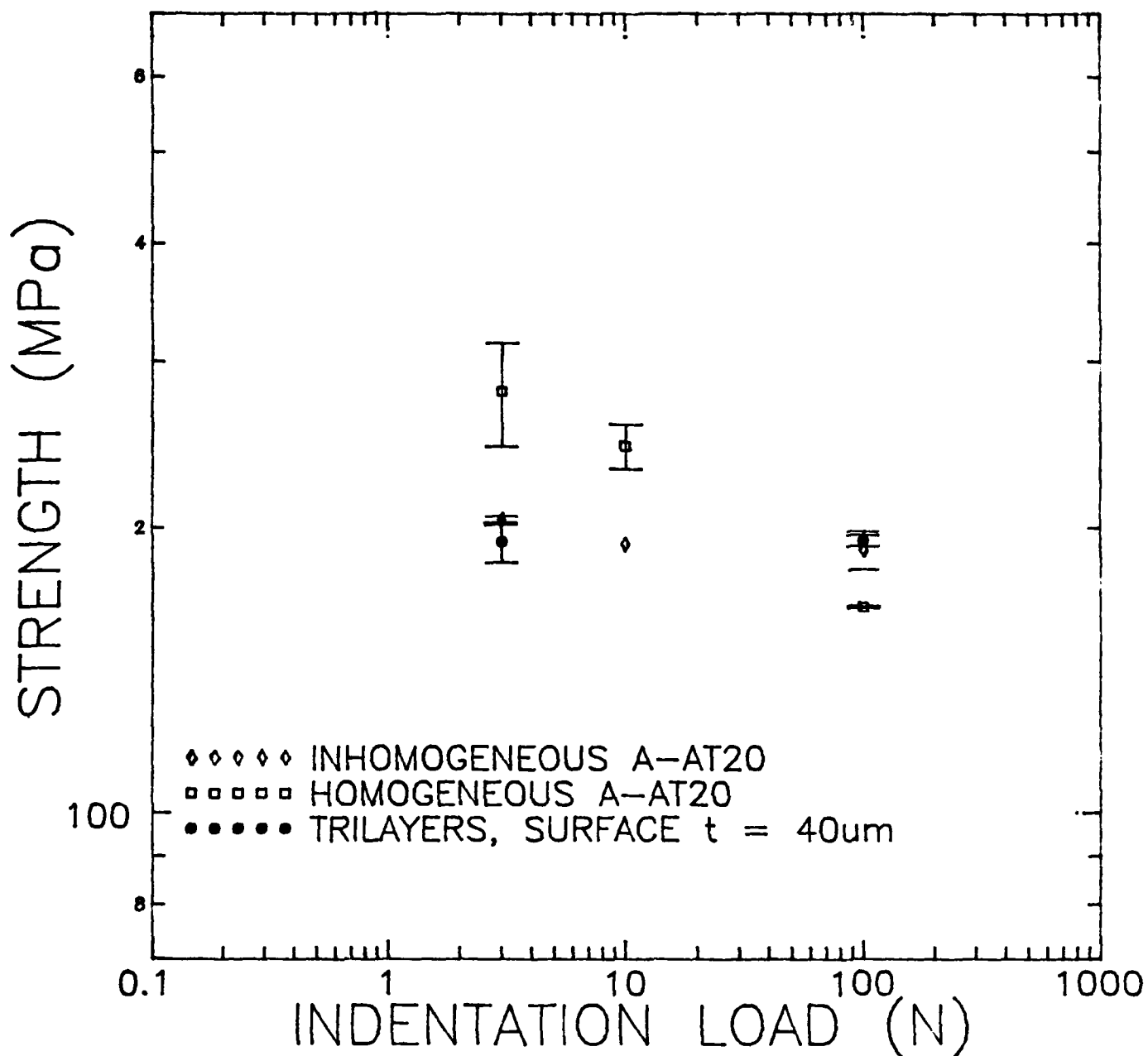


Figure 4. Indentation strength of homogeneous/inhomogeneous A-AT20 trilayer composite. Homogeneous surface layer is  $40\mu\text{m}$  thick. Note that the strength of the composite is same as the strength of the inhomogeneous body material alone.



Figure 5. As-fired surface of trilayer composite. Surface material was 500ppm MgO-doped alumina, which normally should have a fine grained, equiaxed microstructure. Titanium diffusion into the surface from the body during sintering has promoted the elongated grain structures seen here. (bar = 50  $\mu$ m)

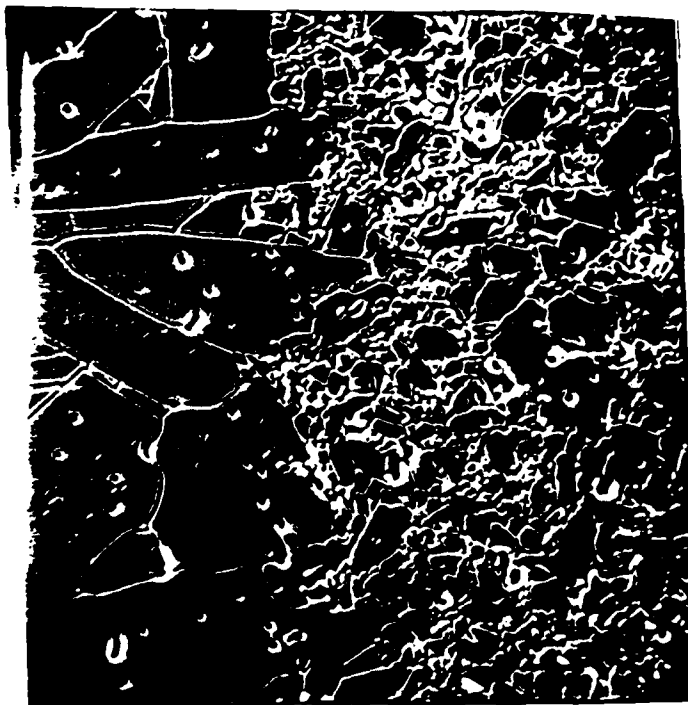


Figure 6. Polished and thermally etched cross-section of undoped alumina/ A-AT20 trilayer composite, near surface (at left). This again shows the effect of titanium from the A-AT20 body producing abnormal grain growth in the alumina surface layer. (bar = 25  $\mu$ m)

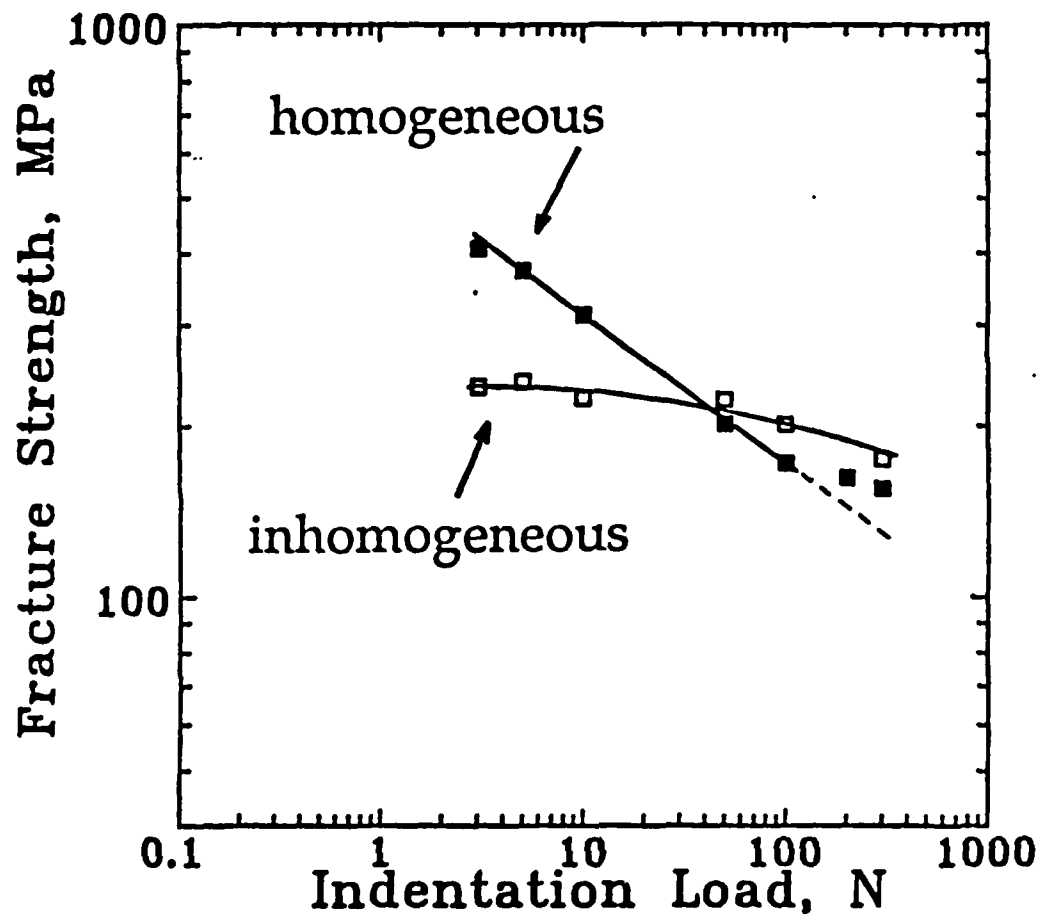


Figure 7. Indentation strengths of homogeneous and inhomogeneous A-AT20 monoliths.

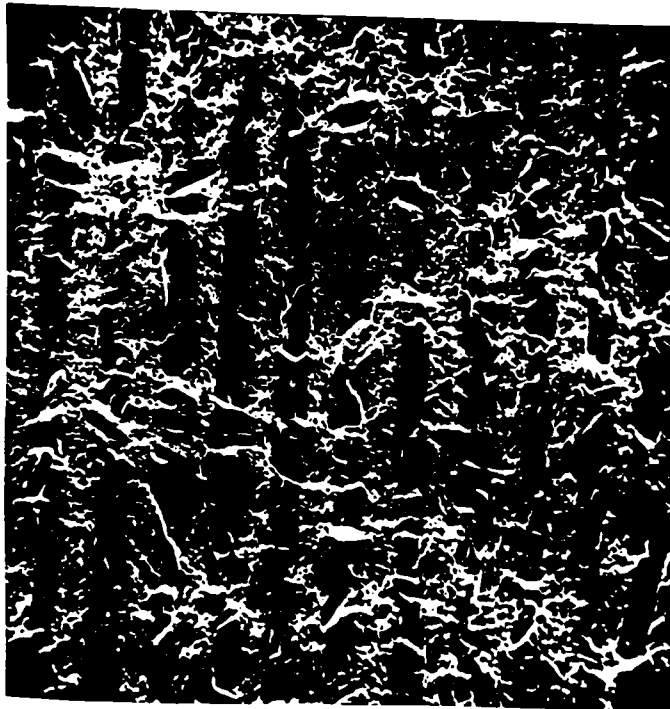


Figure 8. Fracture surface of A-AT20/alumina multilayer composite. The bright stripes are the A-AT20 layers, and the darker stripes are the alumina layers. Layer thickness is 35um. (bar = 75 um)



Figure 9. As-fired surface of A-AT20/alumina multilayer composite, showing the elongated grain structure of the alumina surface layer. (All alumina layers have this structure)(bar = 50 um)

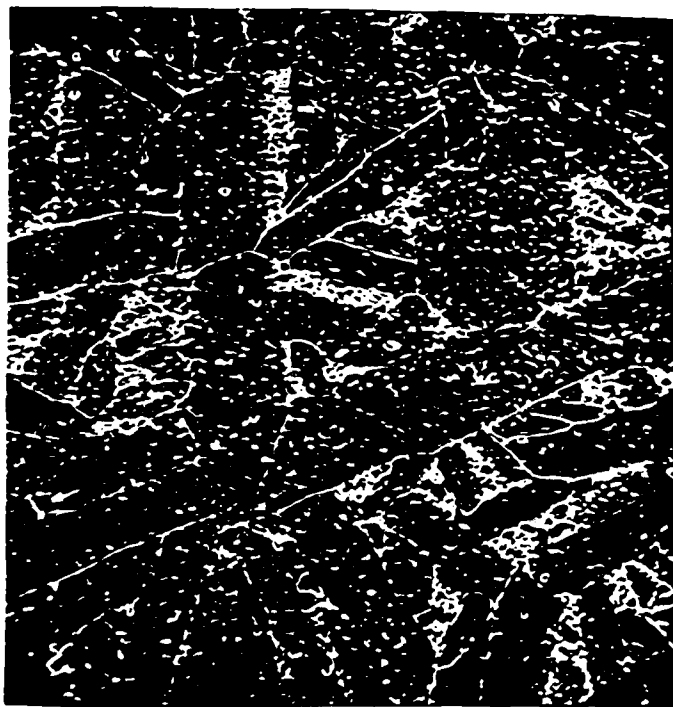


Figure 10. By varying the sintering schedule, it is possible to increase the number density of elongated alumina grains, and thus increase the amount of potential bridging grains.(bar = 50 um)

INFLUENCE OF GRAIN SIZE AND DEGREE OF CRYSTALLIZATION OF  
INTERGRANULAR GLASSY PHASE ON THE MECHANICAL  
BEHAVIOR OF A DEBASED ALUMINA

N.P. Padture and H.M. Chan

Department of Materials Science and Engineering  
Lehigh University, Bethlehem, PA 18015 USA

For Journal of Materials Science

## ABSTRACT

The influence of microstructure on the crack resistance (R-curve) behavior of a commercial debased alumina containing large amounts of glassy phase (28 vol%) has been studied by strength measurements at controlled flaw sizes produced by indentation. Both the individual and combined effects of a) grain size, and b) intergranular second phase (glassy or crystalline) were evaluated. Enhancement of the R-curve behavior was observed when the average grain size was increased from 3 to 18  $\mu\text{m}$  by thermal treatment. However, no effect of the degree of crystallinity of the intergranular second phase on the R-curve behavior, in either small or large grain materials, was observed. These results are discussed with reference to the influence of grain boundary residual stresses on grain bridging across the crack interface.

## 1. INTRODUCTION

In recent years there has been increasing evidence that non-transforming ceramics such as aluminas can exhibit so-called R-curve behavior, i.e. they show increasing toughness with increase in crack size [1-6]. The enhancement of R-curve behavior yields several tangible benefits. Firstly, the ceramic exhibits a range of flaw sizes over which the strength is near-invariant. In turn, this "flaw tolerance" enables the engineer to work with a single (flaw-size independent) design stress. The advantage from the ceramics processing standpoint is that the strength of a ceramic with strong R-curve behavior is relatively insensitive to processing defects. In addition, it has recently been postulated that enhanced R-curve behavior results in an increase in the Weibull modulus [7-9].

Since it has been clearly demonstrated that the extent of R-curve behavior is influenced by microstructure [3], it would seem highly feasible to modify R-curve characteristics through control of microstructural variables. The microstructural parameters evaluated in this study were i) grain size, and ii) degree of crystallinity of intergranular phase. The selection of these particular parameters was based on consideration of a model which assumes grain-localized bridging in the crack wake [1,5,10]. In the afore-mentioned model, represented schematically in Figure 1, the grains bridging the crack are "clamped" in the matrix by compressive residual stresses arising from thermal expansion



anisotropy [11]. These grains thereby exert a restraint across the crack walls, giving rise to increased toughness in a manner analogous to that of fiber-reinforced composites. Without going into the details of the stress-displacement relation for the bridge elements [11,12], it can be appreciated that the degree of enhanced toughening will depend both on the grain size (which determines the length over which the grains must be pulled out), and the residual stresses (which control how tightly the grains are clamped).

A limited number of systematic experimental investigations of these predictions have been carried out, and these confirm a strong dependence on grain size. A study on nominally single phase aluminas showed that coarsening the microstructure results in a stronger R-curve [3]. Similar results were obtained for a debased alumina (containing 18 vol% intergranular phase) [13]. The influence of the intergranular second phases, however, is less well documented, and different studies have produced somewhat conflicting results. Thus several researchers [14-18] have reported significant increases in the toughness values of liquid-phase-sintered aluminas containing 10 to 30 vol% intergranular glass. The toughness improvements resulted from simple heat treatments, and were attributed to crystallization of the glass. However, it should be noted that the toughness measurements in those studies were performed at a single crack length. In contrast to this, work by Bennison et al. [13] showed

that for fine-grained aluminas containing 18 vol% second phase, crystallization of the second phase had very little effect on the crack resistance curve. Powell-Doğan et al. [19] also showed that for 96% alumina, crystallization of the second phase had no effect on either the mechanical properties, or the mode of fracture.

The purpose of this study is to determine experimentally the relative influence of these two variables, grain size and second phase, on the R-curve behavior of a debased alumina. This work differs from that of previous researchers in that both the individual and combined influence of grain size, and crystallinity of the second phase, are determined.

## 2. EXPERIMENTAL

Some 300 specimens of a commercial debased (liquid-phase sintered) alumina<sup>1</sup> in the form of disks (25mm dia x 3mm) were obtained. A series of heat treatments was carefully devised to produce four sets of specimens of differing microstructures. Table I shows the details of the heat treatments and the resulting microstructures. The notation S or L refers to "small" or "large" grain size respectively, and C or G refers to crystalline or glassy second phase respectively.

Specimens for transmission electron microscopy (TEM) were

---

<sup>1</sup> AD85, Coors Ceramics Co., Golden, Colorado, USA.

prepared following standard procedures for ceramic materials. Disks (3mm) were ultrasonically cut from thin sections of the above samples. The disks were then dimpled to a thickness of 20 $\mu$ m in the center and ion-beam milled until perforation. Subsequent investigation on the transmission electron microscope<sup>2</sup> was carried out at an accelerating voltage of 120 keV. The chemical composition of the intergranular glass was determined using energy dispersive spectroscopy of x-rays (EDS) on the same instrument. A "standard" glass<sup>3</sup> of known composition was used to provide the necessary k-factors for compositional analysis. Samples were prepared for scanning electron microscopy (SEM) by polishing sections to 1  $\mu$ m grade followed by thermal etching at 1500 °C for 15 minutes.

Mechanical testing of AD85-S-G, AD85-S-C, AD85-L-G and AD85-L-C was carried out as follows. About 50 disk specimens of each batch were polished to 1  $\mu$ m grade on the prospective tensile side. A Vickers indentation was made at the center of the polished surface with loads varying from 2 to 300 N. Some samples were left unindented. All indentations were made in air and the samples allowed to stand for 10 min. A drop of vacuum grease was then placed on the indentation sites. The specimens were broken in biaxial flexure using the 3-point support and punch fixture [20], and failure times were kept below 20 ms to

---

<sup>2</sup> Philips EM 400T, Mahwah ,New Jersey, USA.

<sup>3</sup> SRM # 2063, N.I.S.T., Gaithersburg, Maryland, USA

minimize effects from static fatigue. Strength values were calculated from the breaking loads and specimen dimensions using thin-plate and beam formulas [21]. Care was taken to examine all specimens after fracture to verify the indentation site as the origin of failure. The specimens that did not fracture from indentations were incorporated into the data pool for unindented controls. Details of this particular method of mechanical testing have been described elsewhere [3].

Preliminary experiments revealed that crystallization of the intergranular glass produced predominantly anorthite ( $\text{CaO} \cdot \text{Al}_2\text{O}_3 \cdot 2\text{SiO}_2$ ). To obtain a comparison between the high temperature mechanical properties of anorthite and alumina, the hardness of bulk anorthite was determined as a function of temperature<sup>4</sup> from 20 to 1200 °C. Bulk anorthite was made by first melting anorthite composition glass from reagent grade  $\text{SiO}_2$ ,  $\text{Al}_2\text{O}_3$  and  $\text{CaCO}_3$ <sup>5</sup> raw materials in a Pt-Rh crucible at 1600 °C for 24 hours. This was followed by crystallization at 1200 °C for 30 minutes.

### 3. RESULTS

#### 3.1 Microstructure

Table II shows the composition of the intergranular glass of

---

<sup>4</sup> Nikon QM high temperature microhardness tester, Nikon, Garden City, New York, USA.

<sup>5</sup> Fisher Scientific Company, Fair Lawn, New Jersey, USA.

AD85-S-G samples after homogenization heat treatment, as determined by x-ray EDS. The values represent an average of ten different spectra obtained from different regions of the sample. The compositions were observed to be consistent within  $\pm 5\%$ , implying that the glassy phase is homogeneous. In addition, the glass composition obtained was found to agree within  $\pm 5\%$  of the values determined by Wiederhorn et al. [22] for AD85 with the same heat treatment. Using this composition as a basis, the heat treatment given in table I was devised in order to obtain anorthite as the major crystalline phase [23].

Figure 2 shows SEM micrographs of AD85-S-G (grain size  $\approx 3 \mu\text{m}$ ) and AD85-L-G (grain size  $\approx 18 \mu\text{m}$ ). Qualitative visual comparison of the two micrographs shows that the heat treatment results in a scaling up of the grain structure as a whole, and that there is no significant change in the distribution of grain sizes about the mean. Figures 3 a) and 3 b) show TEM micrographs of AD85-S-G and AD85-S-C depicting glassy and crystalline intergranular phases respectively. The grain size has not changed appreciably during crystallization heat-treatment. The crystalline intergranular phase in AD85-S-C is observed to be mostly anorthite. With this composition it was not possible to achieve 100% crystallinity; thus pockets of residual glassy phase were observed at many triple points. From TEM examination, the overall degree of crystallinity was estimated to be  $\approx 80\%$ .

### 3.2 Mechanical Behavior

Figure 4 shows indentation load versus failure stress for the four sets of samples. Consider firstly the behavior of the fine-grained material. It can be seen that the data points for AD85-S-G and AD85-S-C lie essentially on the same line. The results for the coarse-grained specimens (AD85-L-G and AD85-L-C), on the other hand, fall on a distinctly separate curve.

The results of the hot-hardness measurements obtained from the bulk anorthite samples are shown in Figure 5. Data for alumina [24] are also plotted for comparison. Although the hardness of anorthite at room temperature is significantly lower than that of alumina, its rate of decrease with increasing temperature is lower. Consequently, at temperatures around 1000 °C, the hardness values of the two phases are similar.

### 4. DISCUSSION

The results depicted in Figure 4 clearly show that R-curve behavior, as evidenced by the flattening of the data in figure 4 at low indentation loads, is enhanced with increasing grain size. This behavior is consistent with the observations of other researchers obtained on both single-phase [3,25] and two-phase aluminas [3,13]. It confirms grain size as a significant parameter in determining the extent of increased toughening with crack extension.

However, the effect of crystallization of the intergranular phase on the R-curve properties of these materials appears to be insignificant. In terms of the grain-bridging model, this null effect may seem surprising, since the bridging processes are thought to be sensitive to residual stresses in the grain boundary regions. To explore the validity of this reasoning further, the magnitude of these grain boundary stresses due to thermal expansion anisotropy between the alumina and the intergranular anorthite can be estimated from the following relation for a spherical inclusion embedded in a matrix [26, 27]:

$$\sigma_r = [(\alpha_{Al} - \alpha_{An}) \Delta T] / [(1 + \nu_{Al})/2E_{Al} + (1 - 2\nu_{An})/E_{An}] \quad (1)$$

(where  $\alpha$  is the linear thermal expansion coefficient,  $\nu$  is the Poisson's ratio,  $E$  is the elastic modulus and  $\Delta T$  is the difference between heat treatment and ambient temperatures). Although the inclusion problem represents an oversimplification of the experimentally observed morphology, it is believed that this relation gives a useful indication of the magnitude of the residual stresses. Taking  $\alpha_{Al} = 9.0 \times 10^{-6} \text{ }^\circ\text{C}^{-1}$  [28],  $\alpha_{An} = 3.7 \times 10^{-6} \text{ }^\circ\text{C}^{-1}$  [29]<sup>6</sup>,  $E_{Al} = 390 \text{ GPa}$  ( $\nu_{Al} = 0.2$ ) [3],  $E_{An} = 250 \text{ GPa}$  ( $\nu_{An} =$

---

<sup>6</sup> It should be noted that alumina and anorthite are non-cubic materials and possess thermal expansion anisotropy along a and c axes. Since the thermal expansion anisotropy within these individual crystals is much less than that between the two phases, the values mentioned here are average and represent the thermal expansion coefficients of polycrystalline materials.

0.25) [30] and  $\Delta T = 1000\text{ }^{\circ}\text{C}$ , we obtain  $\sigma_r = 1.5\text{ GPa}$  for the alumina/anorthite system. For a single phase alumina, taking  $\alpha_{lc} = 8.6 \times 10^{-6}\text{ }^{\circ}\text{C}^{-1}$  and  $\alpha_{nc} = 9.6 \times 10^{-6}\text{ }^{\circ}\text{C}^{-1}$  [28], we obtain  $\sigma_r = 0.35\text{ GPa}$ . Thus the residual stresses induced in the two-phase alumina are greater, by about a factor of four, than in the single phase material.

One could therefore argue that the R-curve in single-phase alumina should be further enhanced in the two-phase alumina with the crystalline second phase. That this was not observed experimentally, suggests that the residual stresses must be at least partially relaxed in AD85-S-C and AD85-L-C. As described previously, TEM examination of these samples revealed that the anorthite was highly twinned. In addition, residual glass was often observed in the intergranular pockets. It is arguable, therefore, that relaxation of the grain boundary residual stresses is taking place at the treatment temperature by deformation of either the anorthite or glassy phase. Because no dislocation activity was observed in the alumina grains, deformation of the alumina grains was disregarded as a possibility. Consideration of Figure 5 shows that deformation of the anorthite appears less likely, because at elevated temperatures the hardness values of alumina and anorthite become comparable, so it is difficult to see why the anorthite would deform in preference to the alumina.



This essentially leaves the role of the residual glass to be considered. Since the approximate composition of the glass is known, it is possible to estimate the value of the glass viscosity from standard data [31]. For comparable glass compositions, the softening temperature, i.e. the temperature at which the glass will deform appreciably under its own weight, is 900 °C. Thus at the level of stresses which have been calculated, the glass would be expected to flow readily. It is therefore suggested that the expected change in mechanical properties does not occur because of relaxation of the induced stresses by viscous flow of the residual glass.

The above discussion represents a highly simplified picture of the deformation processes which take place on cooling of the crystallized AD85 to ambient temperatures. Nonetheless, the postulate that the induced stresses are being relaxed is consistent with the experimental data. Ideally, it would have been desirable to estimate the stress distribution within the microstructure more accurately, by taking into account the morphology of the various phases. Unfortunately, the complexity of the microstructure of the commercial materials studied rendered such analysis intractable. It is envisaged that laboratory-processed specimens with controlled microstructures will be more amenable to theoretical modelling. Work is thus currently under way to process two-phase aluminas where the glass composition is controlled so that virtually 100 % crystallinity

can be achieved.

## CONCLUSIONS

For the commercial liquid phase sintered aluminas examined in this study, the effect of grain size on the R-curve behavior predominates. Crystallization of the intergranular glass had relatively little to no effect on the R-curve behavior. Although significant residual stresses would be expected to be induced due to the differences in thermal expansion between the alumina and the crystallized intergranular phase, these appear to be relaxed by flow of residual glass. The results have interesting implications with respect to the applications of these materials, since they show that prolonged heat-treatment cycles up to 1200 °C do not affect the room temperature mechanical properties.

## ACKNOWLEDGEMENTS

The authors thank S. J. Bennison, B. R. Lawn and M. J. Readey for many stimulating and useful discussions, and B. R. Lawn for valuable suggestions regarding the manuscript. The authors also wish to thank M. J. Readey of Coors Ceramics Co., for providing the starting materials. This work was funded jointly by Coors Ceramics Company and Air Force Office of Scientific Research.

## REFERENCES

1. R. Knehans and R. W. Steinbrech, J. Mater. Sci. Lett. 1 (1982) 327.
2. R. W. Steinbrech, R. Knehans and W. Schaarwachter, J. Mater. Sci. 18 (1983) 265.
3. R. F. Cook, B. R. Lawn and C. J. Fairbanks, J. Amer. Ceram. Soc. 68 (1985) 604.
4. M. V. Swain, J. Mater. Sci. Lett. 5 (1986) 1313.
5. A. Reichl and R. W. Steinbrech, J. Amer. Ceram. Soc. 71 (1988) C299.
6. S. J. Bennison and B. R. Lawn, J. Mater. Sci. 24 (1989) 3169.
7. K. Kendal, N. McN. Alford, S. R. Tan and J. D. Birchall, J. Mater. Res. 1 (1986) 120.
8. R. F. Cook and D. R. Clarke, Acta Metall. 36 (1988) 555.
9. D. K. Shetty and J. S. Wang, J. Amer. Ceram. Soc. 72 (1989) 1158.
10. P. L. Swanson, C. J. Fairbanks, B. R. Lawn, Y-W. Mai and B. J. Hockey, J. Amer. Ceram. Soc. 70 (1987) 279.
11. S. J. Bennison and B. R. Lawn, Acta Metall. 37 (1989) 2659.
12. Y-W. Mai and B. R. Lawn, J. Amer. Ceram. Soc. 70 (1987) 289.
13. S. J. Bennison, H. M. Chan and B. R. Lawn, J. Amer. Ceram. Soc. 72 (1989) 677.
14. N. A. Travitzky, D. G. Brandon and E. Y. Gutmanas, Mater. Sci. Eng. 71 (1985) 65.
15. N. A. Travitzky, D. G. Brandon and E. Y. Gutmanas, Mater. Sci. Eng. 71 (1985) 77.
16. Y. Yeshurun, Z. Rosenburg, N. A. Travitzky and D. G. Brandon, Mater. Sci. Eng., 71 (1985) 71.
17. W. A. Zdaniewski and H. P. Kirchner, Adv. Ceram. Mater., 1 (1986) 99.
18. H. Tomaszewski, Ceramics. Intl. 14 (1988) 93.
19. C. A. Powell-Doğan and A. H. Heuer, J. Amer. Ceram. Soc. to be published.

20. D. B. Marshall, Amer. Ceram. Soc. Bull. 59 (1980) 551.
21. R. J. Roark, in "Formulas for Stress and Strain" (McGraw-Hill, New York, 1965) Ch.7.
22. S. M. Wiederhorn, B. J. Hockey and R. F. Krause Jr., in "Ceramic Microstructures '86", edited by J. Pask and A. G. Evans (Plenum Publishing Company, New York, 1988) p. 795.
23. L. Klein and D. R. Uhlmann, J. Geophys. Res. 79 (1974) 4869.
24. C. P. Alpert, H. M. Chan, S. J. Bennison and B. R. Lawn, J. Amer. Ceram. Soc. 71 (1988) C371.
25. P. Chantikul, S. J. Bennison and B. R. Lawn, J. Amer. Ceram. Soc. to be published.
26. D. Weyl, Ber. Deut. Keram. Ges. 36 (1959) 319.
27. J. Selsing, J. Amer. Ceram. Soc. 44 (1961) 419.
28. G. Bayer, Proc. Br. Ceram. Soc. 22 (1973) 39.
29. M. Czank and H. Schulz, Naturwissenschaften 54 (1971) 94.
30. J. V. Smith and W. L. Brown, in "Feldspar Minerals Vol. 1" (Springer-Verlag, Berlin, 1988) Ch. 12.
31. N. Bansal and R. H. Doremus, in "Handbook of Glass Properties" (Academic Press, Orlando, 1986) Ch. 9.

**Figure Captions:**



1. Schematic representation of grain-localized bridging of the crack (  -active bridges,  -intergranular second phase).
2. SEM secondary electron images of polished and etched sections of AD85 aluminas a) AD85-S-G (fine-grained material), b) AD85-L-G (coarse-grained material).
3. TEM bright field images of AD85 aluminas a) AD85-S-G showing intergranular glassy pockets (A-Alumina, G-Glass), b) AD85-S-C showing crystalline intergranular phase (A-Alumina, An-Anorthite G-Residual glass).
4. Plot of indentation load versus failure stress for four different materials, derived from AD85. The hatched region represents failures from natural flaws. (Representative error bars are included on the end data points.)
5. Comparison of hardness as a function of temperature between alumina [22] and anorthite (present work). (A representative error bar is shown on the end data point.)

Table captions:

I. Heat treatment schedules and microstructures.

II. Average composition of the intergranular glass in AD85.

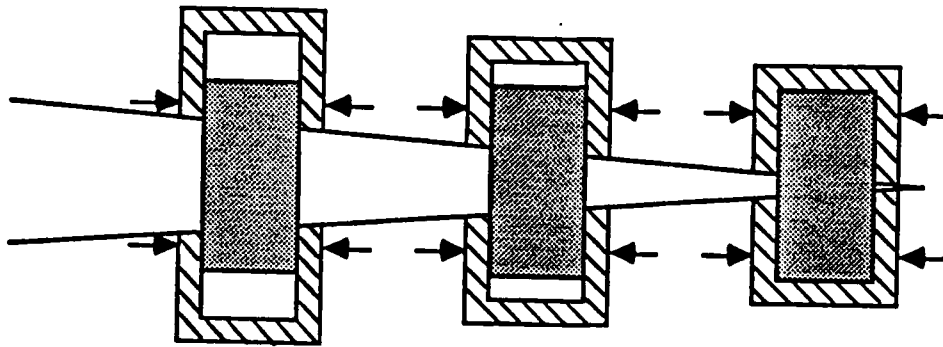
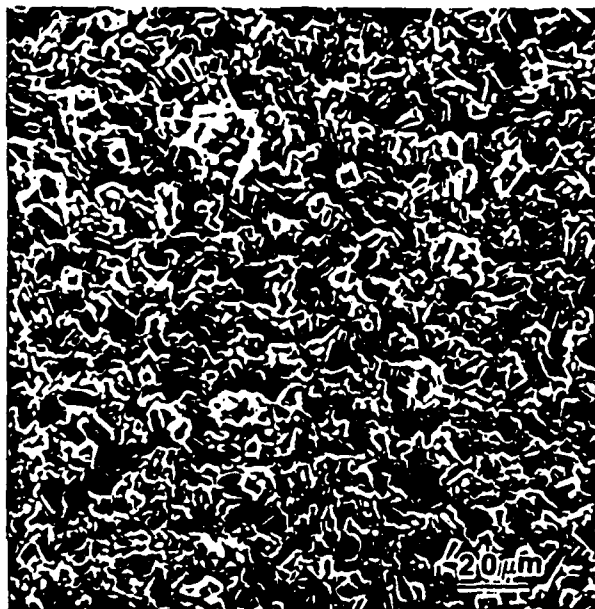


Figure ①

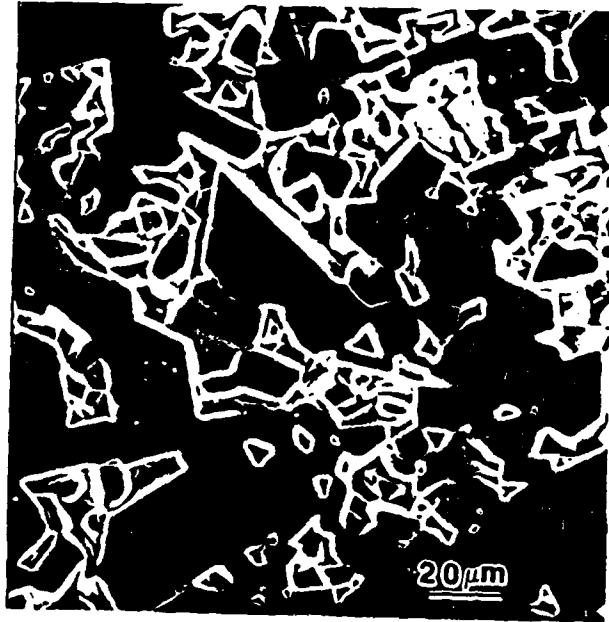
D. Altuve and Chen



(a)

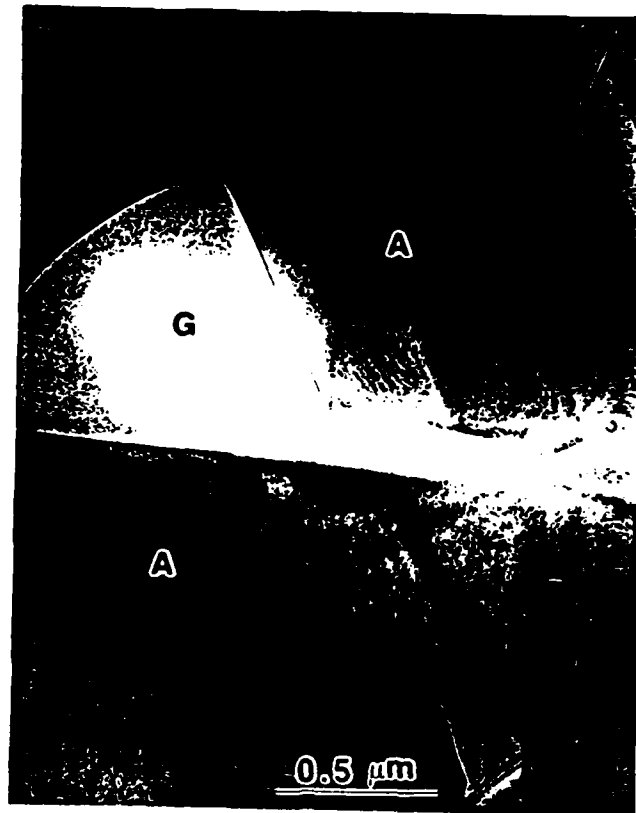
Figure 2 a)  
Padture & Chan





(b)

Figure 2 b  
Padture & Chan



(a)

Figure 3a  
Padtke & Chen.



(b)

Figure 3 b)  
Pasture 4 Chan

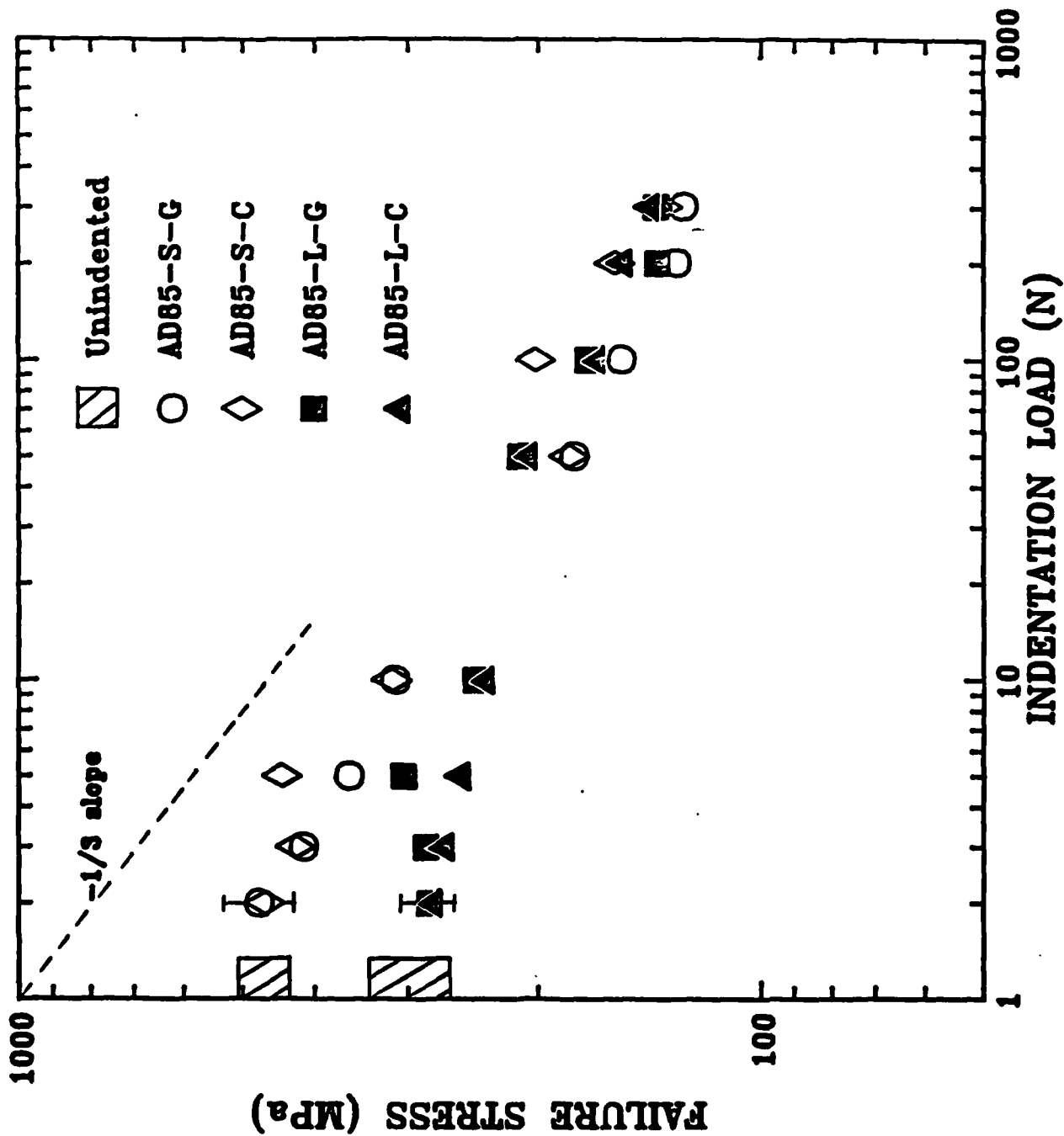


Figure 4

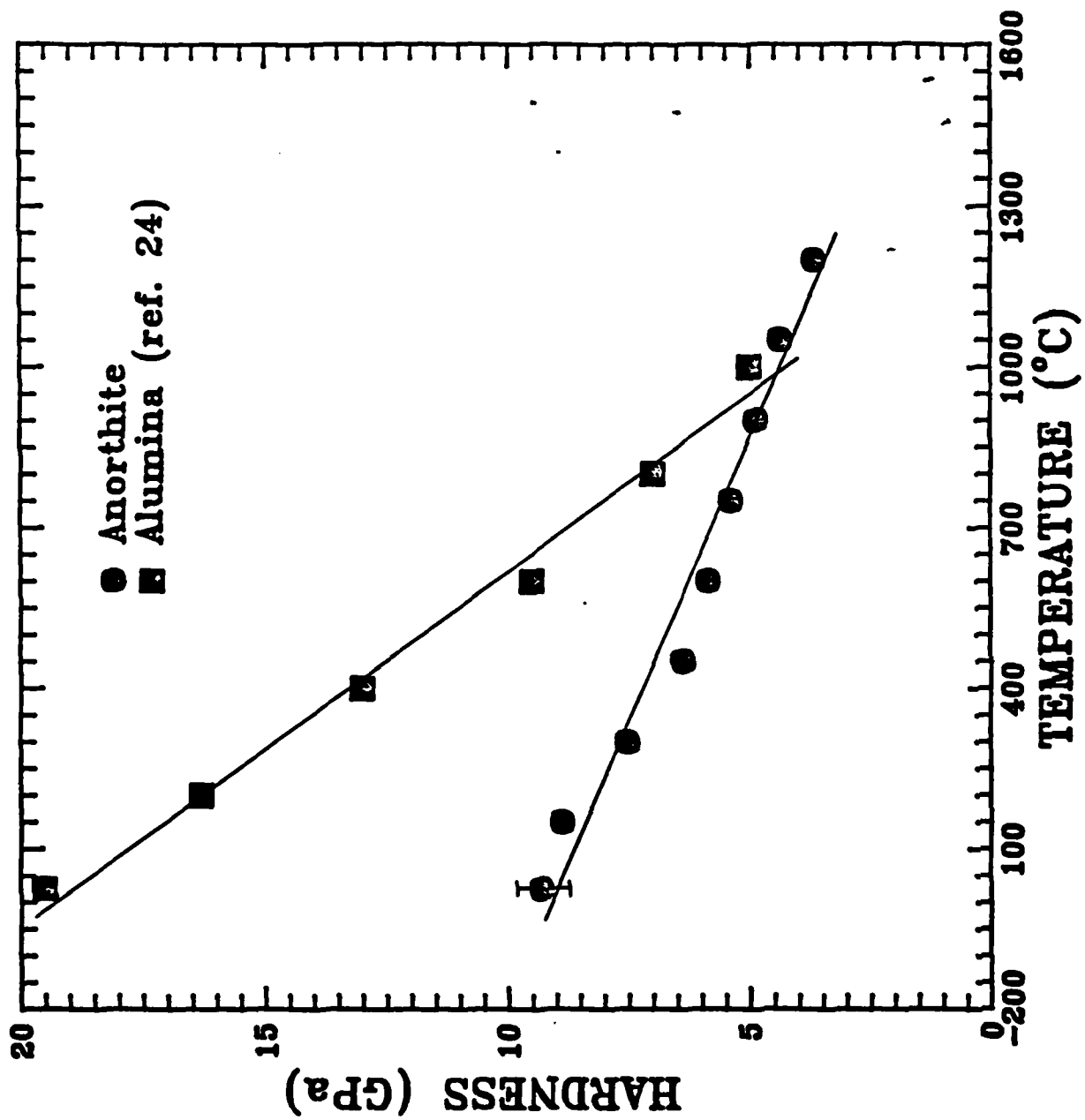


Figure 5  
Padture & Chan

Table I

<u>Material</u>	<u>Heat treatment</u>	<u>Purpose</u>	<u>Resulting microstructure</u>	
			<u>Grain size</u>	<u>Intergranular phase</u>
AD85-S-G	As-received	-	3 $\mu\text{m}$	Glassy
AD85-S-C	a) 1400 °C for 6 hours (quenched)	Homogenize inter- granular glass	3 $\mu\text{m}$	Partially crystalline
	b) 1150 °C for 130 hours	Crystallize inter- granular glass		
AD85-L-G	a) 1550 °C for 250 hours	Increase grain size	18 $\mu\text{m}$	Glassy
AD85-L-C	a) 1550 °C for 250 hours	Crystallize inter-	18 $\mu\text{m}$	Partially crystalline
	b) 1200 °C for 130 hours	granular glass with large grain size		

Table II

<u>Oxide</u>	$\text{SiO}_2$	$\text{Al}_2\text{O}_3$	$\text{MgO}$	$\text{CaO}$	$\text{BaO}$
<u>Wt%</u>	56.5	27.5	2.1	8.6	5.3

**MICROSTRUCTURAL EVOLUTION AND MECHANICAL PROPERTIES IN  
DUAL-PHASE, INTERPENETRATING CERAMIC MICROSTRUCTURES:**

**The  $\text{Al}_2\text{O}_3\text{:c-ZrO}_2$**

**Jonathan D. French**

**Department of Materials Science and Engineering  
Lehigh University, Bethlehem, Pa 18015 USA**

**A thesis submitted for the degree of Master of Science on May 3, 1990.**



## Abstract

This thesis is a study of the microstructural development and mechanical properties of a ceramic system exhibiting a dual-phase interpenetrating microstructure. The  $\text{Al}_2\text{O}_3\text{:c-ZrO}_2$  (8 mol%  $\text{Y}_2\text{O}_3$ ) system was chosen as the model due to the limited mutual solubility of  $\text{Al}_2\text{O}_3$  and c- $\text{ZrO}_2$ , and the absence of intermediate phases. Sintering studies of the composites with high volume fractions of both phases showed the severe grain growth restraint of the interpenetrating network at  $1650^\circ\text{C}$  ( $60^\circ\text{C}$  below the eutectic). The coarsening resistance is attributed to the long diffusion path length for coarsening, the limited mutual solubility, and the high grain coordination number of the phases. Fracture toughness of the composites is shown to follow a series rule-of-mixtures of the single phases. The 5 volume percent c- $\text{ZrO}_2$  composition shows an anomalously high hardness at all temperatures (up to  $1200^\circ\text{C}$ ). The 50 volume percent c- $\text{ZrO}_2$  composition (AZ50) possesses superior hardness to the single phases above  $1000^\circ\text{C}$ . Indentation creep tests show that AZ50 is superior to single phase  $\text{Al}_2\text{O}_3$  for resisting creep deformation, and comparable to single phase c- $\text{ZrO}_2$ . These interpenetrating microstructures, with high volume fractions of second phase, are part of a class of ceramics which possess stable microstructures and reliable mechanical properties at elevated temperatures.

## 2. Publications and Presentations

### Publications

1. J. D. French, H. M. Chan, M. P. Harmer and G. A. Miller, "Mechanical Properties and Grain Growth Inhibition in the System  $\text{Al}_2\text{O}_3\text{:c-ZrO}_2$ ", pp. 239-43 in Mat. Res. Soc. Symp. Proc. vol 170, Tailored Interfaces in Composites, Edited by C. J. Pantano and E. J. H. Chen, Mater. Res. Soc., Pittsburgh, 1990, (reprint attached)
2. J. D. French, M. P. Harmer, H. M. Chan and G. A. Miller, "Strength of a Multi-Layered  $\text{Al}_2\text{O}_3/\text{Al}_2\text{O}_3\text{-ZrO}_2$  Composite" J. Am. Ceram. Soc. 72[10] 2217 (1989).
3. J. D. French, M. P. Harmer, H. M. Chan and G. A. Miller, "Coarsening-Resistant Dual-Phase Interpenetrating Microstructures", J. Am. Ceram. Soc. 73[8] 2508-10, 1990. (reprint attached)
4. J. D. French, M. P. Harmer, H. M. Chan and G. A. Miller, "Creep Resistant Fine Grained Monolithic Ceramics", AFOSR research accomplishments, In Press.
5. J. D. French, H. M. Chan, M. P. Harmer and G. A. Miller, "Mechanical Properties of Interpenetrating Microstructures: the  $\text{Al}_2\text{O}_3\text{:c-ZrO}_2(\text{Y})$  System", J. Am. Ceram. Soc. in preparation.
6. N. P. Padture and H. M. Chan, "Influence of Grain Size and Degree of Crystallization of Intergranular Glassy Phase on the Mechanical Properties of a Debased Alumina", J. Mat. Sci. (in press). (manuscript attached)
7. N. P. Padture, H. M. Chan, B. R. Lawn and M. J. Readey, "The role of Crystallization of an Intergranular Glassy Phase in Determining Grain Boundary Residual Stresses in Debased Alumina", pp. 245-50 in Mat. Res. Soc. Symp. Proc. vol 170, Tailored Interfaces in Composites, Edited by C. J. Pantano and E. J. H. Chen, Mater. Res. Soc., Pittsburgh, 1990, (reprint attached)
8. N. P. Padture, S. J. Bennison, J. L. Runyan, J. Rödel, H. M. Chan and B. R. Lawn, "Flaw Tolerant  $\text{Al}_2\text{O}_3\text{-Al}_2\text{TiO}_5$  Composites", Proc. of Symp. on Composites, 2nd Intl. Ceram. Congress, Amer. Ceram. Soc., Columbus, in press. (manuscript attached)
9. N. P. Padture and H. M. Chan, "Microstructure of Crystallized Synthetic Anorthite ( $\text{CaO} \cdot \text{Al}_2\text{O}_3 \cdot 2\text{SiO}_2$ ): An Electron Microscopy Investigation", J. Mater. Sci. in preparation
10. N. P. Padture, H. M. Chan, S. J. Bennison and B. R. Lawn, "Crack Resistance Properties of Alumina-Aluminum Titanate Composites with Tailored Bimodal Microstructures: I, Processing", J. Am. Ceram. Soc. in preparation.

11. N. P. Padture, H. M. Chan, J. Rödel, S. J. Bennison and B. R. Lawn, "Crack Resistance Properties of Alumina-Aluminum Titanate Composites with Tailored Bimodal Microstructures: II, Mechanical Properties", J. Am. Ceram. Soc. in preparation.

12. N. P. Padture, B. R. Lawn, S. J. Bennison and H. M. Chan, "Crack Resistance Properties of Alumina-Aluminum Titanate Composites with Tailored Bimodal Microstructures: III, Theoretical Fracture Mechanics Model", J. Am. Ceram. Soc. in preparation.

13. J. D. French, "Microstructural Evolution and Mechanical Properties of Dual-Phase, Interpenetrating Ceramic Microstructures: the  $\text{Al}_2\text{O}_3\text{:c-ZrO}_2$  System", Master's Thesis, May 1990.

### Presentations

1. C. J. Russo, J. D. French, M. D. Stuart, M. P. Harmer, H. M. Chan and G. A. Miller, "Strength and Toughness of Tailored Ceramic Microstructures", presented at the 91st Annual Meeting of the Amer. Ceram. Soc. Indianapolis, April 1989.

2. N. P. Padture, H. M. Chan, B. R. Lawn and M. J. Readey, "Effect of Grain Size and Crystallization of the Intergranular Glass on R-Curves in Liquid-Phase-Sintered Aluminas", presented at the 91st Annual Meeting of the Amer. Ceram. Soc., Indianapolis, April 1989.

3. J. D. French, H. M. Chan, M. P. Harmer and G. A. Miller, "The Effect of Residual Grain Boundary Stresses on Mechanical Properties of Alumina-Based Ceramics", presented at the Fall Meeting of the Mater. Res. Soc., Boston, November 1989.

4. N. P. Padture, H. M. Chan, B. R. Lawn and M. J. Readey, "The Role of Crystallization of an Intergranular Glassy Phase in Determining Grain Boundary Residual Stresses in Debased Aluminas", presented at the Fall Meeting of the Mater. Res. Soc., Boston, November 1989.

5. N. P. Padture, H. M. Chan, S. J. Bennison, J. L. Runyan, B. R. Lawn, J. D. French, M. P. Harmer, G. A. Miller, "Crack Resistance and Flaw Tolerance in  $\text{Al}_2\text{O}_3\text{-Al}_2\text{TiO}_5$  Composites: Role of Microstructural Heterogeneity and Internal Stresses", presented at the 92nd Annual Meeting of the Amer. Ceram. Soc. Dallas, April 1990.

6. N. P. Padture, H. M. Chan, B. R. Lawn and M. J. Readey, "The Effect of Nature of Intergranular Phase on Crack Resistance Behavior of Liquid-Phase-Sintered Aluminas", presented at the 92nd Annual Meeting of the Amer. Ceram. Soc. Dallas, April 1990.

7. J. D. French, H. M. Chan, M. P. Harmer and G. A. Miller, "Mechanical Properties of Thermally Stable Ceramic Dual-Phase Microstructures", presented at the 92nd Annual Meeting of the Amer. Ceram. Soc. Dallas, April 1990.

8. S. J. Bennison, N. P. Padture, J. L. Runyan, J. Rödel, B. R. Lawn and H. M. Chan, "Fabrication of Flaw-Tolerant  $\text{Al}_2\text{O}_3$ - $\text{Al}_2\text{TiO}_5$  Composites: I, Role of Microstructural Scale", presented at the Amer. Ceram. Soc. 2nd International Ceramics Congress, Orlando, November 1990.

9. N. P. Padture, H. M. Chan, S. J. Bennison, J. Rödel, J. L. Runyan and B. R. Lawn, "Fabrication of Flaw-Tolerant  $\text{Al}_2\text{O}_3$ - $\text{Al}_2\text{TiO}_5$  Composites: II, Role of Microstructural Heterogeneity", presented at the Amer. Ceram. Soc. 2nd International Ceramics Congress, Orlando, November 1990.

### 3. Awards and Accomplishments

#### Awards

1. Martin P. Harmer received the Lehigh University 1990 Eleanor and Joseph F. Libsch Research Award for outstanding achievement and distinction in research.
2. Helen M. Chan received the Lehigh University 1990 Robinson Award for outstanding performance and promise of professional achievement.
3. Nitin Padture and Helen Chan received the 1990 Rowland B. Snow Award from the American Ceramics Society for the Best of Show entry in the Ceramographic Contest entitled "Crystallization of Synthetic Anorthite".
4. J. D. French received 2nd and 3rd prize awards in the 1990 Ceramographic Contest of the American Ceramic Society for exhibits entitled "Indentation Creep" and "Grain Coarsening in Interpenetrating Microstructures".

#### Accomplishment

Our work on coarsening and creep resistance of alumina-cubic zirconia monolithic ceramic is listed in the 1990 volume of AFOSR accomplishments.

#### 4. Personnel

##### Lehigh University

##### Faculty

Dr. M. P. Harmer  
Dr. H. M. Chan  
Dr. G. A. Miller

##### Graduate Students

Mr. J. D. French  
Mr. C. J. Russo  
Mr. M. D. Stuart  
Mr. N. P. Padture

##### National Institute of Standards and Technology

Dr. B. R. Lawn  
Dr. S. J. Bennison  
Dr. S. Wiederhorn